Characterization of HyNaCs - peptide-gated DEG/ENaCs from *Hydra magnipapillata*

Von der Fakultät für Mathematik, Informatik und Naturwissenschaften der RWTH Aachen University zur Erlangung des akademischen Grades eines Doktors der Naturwissenschaften genehmigte Dissertation

vorgelegt von

Diplom-Biologe

Stefan Johannes Dürrnagel

aus Würzburg

Berichter:

Universitätsprofessor Dr. Stefan Gründer

Universitätsprofessor Dr. Peter Bräunig

Tag der mündlichen Prüfung: 28.05.2013

Teile dieser Arbeit wurden bereits veröffentlicht:

Dürrnagel, S., Kuhn, A., Tsiairis, C. D., Williamson, M., Kalbacher, H., Grimmelikhuijzen, C. J. P., Holstein, T. W., and Gründer, S. (2010).
Three homologous subunits form a high affinity peptide-gated ion channel in *Hydra*. *Journal of Biological Chemistry 285*, 11958–11965.

Dürrnagel, S., Falkenburger, B. H., and Gründer, S. (2012).
High Ca^{2+} permeability of a peptide-gated DEG/ENaC from *Hydra*. *The Journal of General Physiology 140*, 391–402.

Summary

The DEG/ENaC ion channel family comprises a group of phylogenetically related ion channels found in almost all multicellullar animals (metazoa). Common characteristics of DEG/ENaCs are their selectivity for Na^+ and their sensitivity for the inhibitor amiloride. Besides these shared features, the individual DEG/ENaCs display a huge diversity with regard to their expression pattern, stimulus of activation and their physiological function. For example, ASICs are proton-gated channels implied in the perception of pain while ENaCs are constitutively active and facilitate sodium reabsorption across epithelia and FaNaC is the first identified ion channel directly gated by neuropeptides. To obtain a better understanding of the basic properties of this heterogeneous group of ion channels, our group has cloned novel DEG/ENaC subunits from the freshwater polyp *Hydra magnipapillata*. *Hydra* belongs to the phylum Cnidaria, which is considered as the most ancient phylum in which a nervous system has evolved. Therefore, the characterisation of DEG/ENaC channels from *Hydra* will help to identify principal and basic properties, which are shared by all DEG/ENaC members. So far, our group has cloned four DEG/ENaC subunits from *Hydra*, which were named HyNaC1-4. It was already shown that coinjection of the subunits HyNaC2 and -3 leads to expression of a functional ion channel in *Xenopus* oocytes that is directly gated by endogenous neuropeptides from *Hydra*, the HydraRFamides I and II. To date, HyNaCs and related FMRFamide-gated sodium channels (FaNaCs) are the only known peptide-gated ion channels.

In this work HyNaC5, a novel DEG/ENaC subunit from *Hydra,* was investigated. When HyNaC5 was coexpressed together with HyNaC2 and -3, the apparent affinity for the HydraRFamides I and II was increased ≈100-fold. In addition, HyNaC2/3/5 exhibited an increased selectivity for Na^+ and was blocked more potently by the inhibitor amiloride than HyNaC2/3. In summary, the results confirm that the subunits HyNaC2, -3, and -5 together form a heterotrimeric, peptide-gated ion channel. Moreover, the increased current amplitudes, the increased apparent affinity for the HydraRFamides and the enhanced sensitivity for the inhibitor amiloride collectively suggest that the ion channel consisting of HyNaC2/3/5 and not HyNaC2/3 is the physiologically relevant channel in *Hydra.*

In the second part of this thesis it was shown that the channel formed by HyNaC2/3/5 is also highly permeably for Ca^{2+}. This finding is surprising, as all known DEG/ENaCs are Ca^{2+} impermeable or conduct Ca^{2+} only to a minor extend. Indeed, selectivity for Na^+ is a

common and name giving feature of DEG/ENaCs. We estimated a relative Ca^{2+} permeability (P_{Ca}/P_{Na}) of ≈3.8, which places HyNaC2/3/5 into the group of highly Ca^{2+} conductive channels. In *Xenopus* oocytes, the influx of Ca^{2+} through HyNaCs was directly visible by secondary activation of endogenously expressed calcium activated chloride channels (CaCCs). The block of CaCCs revealed the simple, step-like and non-desensitizising current characteristic of HyNaC2/3/5. Moreover, it was shown that Ca^{2+} also blocks HyNaC2/3/5. The block was voltage-dependent and increased at more positive potentials. Furthermore, a conserved aspartate residue situated at the outer entrance of the ion pore that is essential for both, the high Ca^{2+} permeability and the Ca^{2+} block of HyNaC2/3/5 was identified. Substitution of this residue led to a strong reduction of Ca^{2+} permeability and reduced voltage dependent Ca^{2+} block. By an *in situ* hybridisation assay, the expression pattern of *hynac2*, *-3*, and *-5* was localized at the base of the tentacles in *Hydra*. The expression overlapped with the previously reported expression of the HydraRFamides I and II. We therefore speculate that HyNaCs - possibly mediated by their permeability for Ca^{2+} - might play a role in the coordinated movement of the tentacles during feeding in *Hydra*. Indeed, we could show that application of amiloride, a universal inhibitor of DEG/ENaCs, delays the glutathione induced feeding reaction in *Hydra*.

In addition, the identification of a novel DEG/ENaC with high permeability for Ca^{2+} from *Hydra* suggest that selectivity for Na^{+} was not shared by the common ancestor of all DEG/ENaCs and arose later in evolution.

Zusammenfassung

Die DEG/ENaC Ionenkanalfamilie umfasst eine Gruppe phylogenetisch verwandter Ionenkanäle, die in nahezu allen vielzelligen Tieren (Metazoen) zu finden sind. Ein charakteristisches Merkmal aller DEG/ENaC Kanäle ist ihre Selektivität für Natrium sowie die Sensitivität gegenüber dem Inhibitor Amilorid. Neben diesen Gemeinsamkeiten bilden die einzelnen Vertreter der DEG/ENaC Familie hinsichtlich ihrer Expressionsmuster, ihrer Aktivierungsmechanismen und ihrer physiologischen Funktion eine sehr heterogene Gruppe. So sind beispielsweise die durch Protonen aktivierten ASICs an der Schmerzwahrnehmung beteiligt; ENaC vermittelt als konstitutiv geöffneter Kanal die Natriumresorption über Epithelien und FaNaC ist der erste beschriebene Ionenkanal, der durch endogene Neuropeptide aktiviert wird. Um ein besseres Verständnis grundlegender Eigenschaften dieser heterogenen Kanalfamilie zu erhalten und ursprüngliche Funktionsweisen der Kanalfamilie zu erforschen wurden durch unsere Arbeitsgruppe neue DEG/ENaC Untereinheiten aus dem Süßwasserpolypen *Hydra magnipapillata* kloniert. *Hydra* gehört zum Phylum Cnidaria, dem evolutionär ältesten Tierstamm in dem sich ein Nervensystem entwickelte. Die Beschreibung der Eigenschaften von DEG/ENaC Kanälen aus *Hydra* kann somit wichtige Impulse für die Erforschung grundlegender Mechanismen aller DEG/ENaC Kanäle liefern.

Bisher wurden von unserer Gruppe vier neue DEG/ENaC Untereinheiten aus *Hydra* kloniert und HyNaC1-4 genannt. In einer früheren Arbeit konnte bereits gezeigt werden, dass die Untereinheiten HyNaC2 und -3 einen funktionellen Ionenkanal bilden, der durch endogene Neuropeptide aus *Hydra*, die HydraRFamide I und II, direkt aktiviert wird. Bis heute sind HyNaCs und der verwandte FMRFamide-gated sodium channel (FaNaC) die einzigen bekannten peptidaktivierten Ionenkanäle.

In dieser Arbeit wurde HyNaC5, eine weitere DEG/ENaC Untereinheit aus *Hydra,* untersucht. Wird HyNaC5 zusammen mit HyNaC2 und -3 exprimiert, so erhöhte sich die apparente Affinität für die HydraRFamide I und II etwa 100-fach. Zudem zeigte HyNaC2/3/5 im Vergleich zu HyNaC2/3 eine erhöhte Selektivität für Natrium und war stärker durch den Inhibitor Amilorid blockierbar. Zusammenfassend belegen diese Ergebnisse, dass die Untereinheiten HyNaC2, -3 und -5 gemeinsam einen heterotrimeren, peptidaktivierten Ionenkanal bilden. Die nach Koexpression von HyNaC5 vergrößerten Stromamplituden, die erhöhte Affinität für die HydraRFamide sowie die größere Sensitivität für Amilorid deuten zudem darauf hin, dass es sich bei HyNaC2/3/5 und nicht bei HyNaC2/3 um die in *Hydra* physiologisch relevante Kanalform handelt.

In zweiten Teil dieser Arbeit konnte gezeigt werden, dass HyNaC2/3/5 stark permeabel für Kalzium ist. Dieses Ergebnis ist überraschend, da alle bekannten DEG/ENaCs keine oder nur geringe Leitfähigkeit für Kalzium besitzen und Natriumselektivität ein vereinendes und namensgebendes Merkmal der DEG/ENaC Ionenkanalfamilie ist. Die ermittelte Kalziumpermeabilität (P_{Ca}/P_{Na} ≈3.8) zeigt, dass HyNaC2/3/5 in die Gruppe stark kalziumpermeabler Ionenkanäle einzuordnen ist. In *Xenopus* Oozyten führte der Kalziuminflux durch HyNaC2/3/5 zur Aktivierung endogen exprimierter, kalziumabhängiger Chloridkanäle (CaCCs), die den Kalziumeinstrom direkt anzeigten. Durch den Block der CaCCs konnte die einfache, treppenförmige und nicht desensitisierende Stromcharakteristik von HyNaC2/3/5 aufgeklärt werden. Zudem konnte gezeigt werden, dass HyNaC2/3/5 zusätzlich durch Kalzium blockiert wird. Der Block war spannungsabhängig und verstärkte sich bei positiven Potentialen. Es zeigte sich, dass ein konserviertes Aspartat kurz vor dem extrazellulären Poreneingang sowohl für die Kalziumleitfähigkeit als auch für den Kalziumblock von HyNaC2/3/5 essentiell ist. Der Austausch dieser Aminosäure führte zu stark verminderter Kalziumleitfähigkeit und einer Verringerung des spannungsabhängigen Kalziumblocks. Durch eine *in situ* Hybridisierung wurde die Expression von *hynac2, -3* und *-5* an der Tentakelbasis von *Hydra* nachgewiesen werden. Dieses Expressionsmuster überlappt mit der Expression der HydraRFamide I und II. Daher könnten HyNaCs, eventuell vermittelt durch deren Kalziumleitfähigkeit, eine wichtige Funktion bei der Koordination der Tentakelbewegung während der Nahrungsaufnahme spielen. Tatsächlich konnten wir zeigen, dass die durch Glutathion induzierte „feeding reaction“ in *Hydra* durch Applikation des DEG/ENaC Inhibitors Amilorid verlangsamt wird. Die Entdeckung eines DEG/ENaC Kanals mit hoher Kalziumleitfähigkeit aus *Hydra* weist zudem darauf hin, dass Natriumselektivität bei dem gemeinsamen Vorläufer der Kanalfamilie möglicherweise noch nicht ausgeprägt war, sondern sich in der Evolution später entwickelte.

I. Introduction

1.1. Introduction to the DEG/ENaC ion channel superfamily

1.1.1 Discovery and classification

The DEG/ENaC ion channel superfamily forms a group of nonvoltage gated, Na^+-selective and amiloride-sensitive cation channels expressed in multicellular organisms throughout the animal kingdom. The channel family is named after their founding members, the degenerins (DEG) from *C. elegans* and the mammalian epithelial sodium channel (ENaC) (Deval et al., 2003). The DEG/ENaC family is defined by the sequence homology of its members and a phylogenetic tree of the individual family members is shown in Fig. 1. Despite their relationship, the individual family members - that are now shortly introduced- display a large diversity with regard to their physiological function, their expression pattern and their stimulus of activation:

The founding members from *Caenorhabditis elegans*, the degenerins *deg-1* and *mec-4* were identified in a genetic screen for touch-insensitive mutants (Chalfie and Au, 1989; Driscoll and Chalfie, 1991). They are, together with several other degenerins, responsible for touch sensation. Only few years later, the α, β and γ subunits of the rat epithelial sodium channel (ENaC) were cloned in 1993 and 1994 from epithelial colon cells and were functionally expressed in *Xenopus* oocytes (Canessa et al., 1993; 1994). The structural homology to the degenerins led to the classification of both channels to a common family (Kellenberger and Schild, 2002). ENaC is a constitutivley open channel involved in sodium reabsorption across epithelia (Firsov et al., 1996).

The first ligand-gated DEG/ENaC and the first identified ion channel that is directly gated by a neuropeptide was cloned in 1995 from the snail *Helix aspersa* and named FaNaC (FMRFamide-gated sodium channel) (Lingueglia et al., 1995). The FMRFamide (Phe-Met-Arg-Phe) or related mammalian peptides are implied in various physiological functions ranging from control of heart rate in molluscs to pain modulation in mammals (Perry et al., 2001; Lingueglia et al., 2006).

Subsequently, further DEG/ENaC were identified in mammals. They were called acid sensing ion channels (ASICs) as these channels are gated by protons (Waldmann et al., 1997b). ASICs are exclusively expressed in chordates. In mammals four genes code for the isoforms ASIC1a, ASIC2a, ASIC3 and ASIC4 (Waldmann et al., 1997b; Price et al., 1996; Waldmann et al., 1997a; Grunder et al., 2000). Furthermore, alternative splicing gives rise to the isoforms ASIC1b and 2b (Chen et al., 1998; Lingueglia et al., 1997). ASICs are pH-sensors implied in various physiological or pathophysiological functions like the perception of pain after tissue acidosis (Krishtal, 2003), death of neurons under ischemic conditions (Xiong et al., 2004) or learning and memory (Wemmie et al., 2002).

After the genomic sequence of *C.elegans* was resolved, eight putative new DEG/ENaC members, the FLRs were identified. They are characterized by a conserved cysteine-rich domain that is related, but distinct from the *C. elegans* degenerins (Mano and Driscoll, 1999). This lead to the classification of these genes to a new subfamily that is named after *flr-1* (fluoride resistant mutant -1) a gene identified in a screen for fluor-resistance (Katsura et al., 1994) that is involved in the control of defecation rhythm (Take-Uchi et al., 1998).

In 1998, RPK ripped pocket (RPK) and pickpocket (PPK), two novel DEG/ENaC proteins from *Drosophila melanogaster,* were cloned and RPK was functionally expressed in *Xenopus* oocytes, where it generates an amiloride sensitive, sodium selective current (Adams et al., 1998). In total, the genome of *Drosophila* comprises 31 candidate genes related to DEG/ENaC proteins (Ben-Shahar, 2011). Some of these genes have been further characterised and the corresponding channels were shown to be implicated in several physiological functions such as detection of salt (ppk11, ppk19) (Liu et al., 2003) and pheromones (ppk25) (Lin et al., 2005) or mechanosensation (Zhong et al., 2010).

A further family member expressed in mammals was cloned in 1998 from mouse and rat. It was named brain liver intestine Na^+ channel (BLINaC) according to it expression pattern of its mRNA (Sakai et al., 1999). One year later, the human homologue was cloned and named INaC (intestine Na^+ channel) (Schaefer et al., 2000). When expressed in *Xenopus* oocytes, BLINaC and INaC do not generate constitutive currents and their stimulus of activation remained unclear (Wiemuth and Gründer, 2010). Recently, the expression of BLINaC could be specified to cholangiocytes, epithelial cells lining bile ducts. Convenient to these findings, millimolar concentrations of bile acids robustly activated rat BLINaC and human INaC. Therefore, BLINaC and was renamed to BASIC (bile acid sensitive ion channel) (Wiemuth et al., 2012).

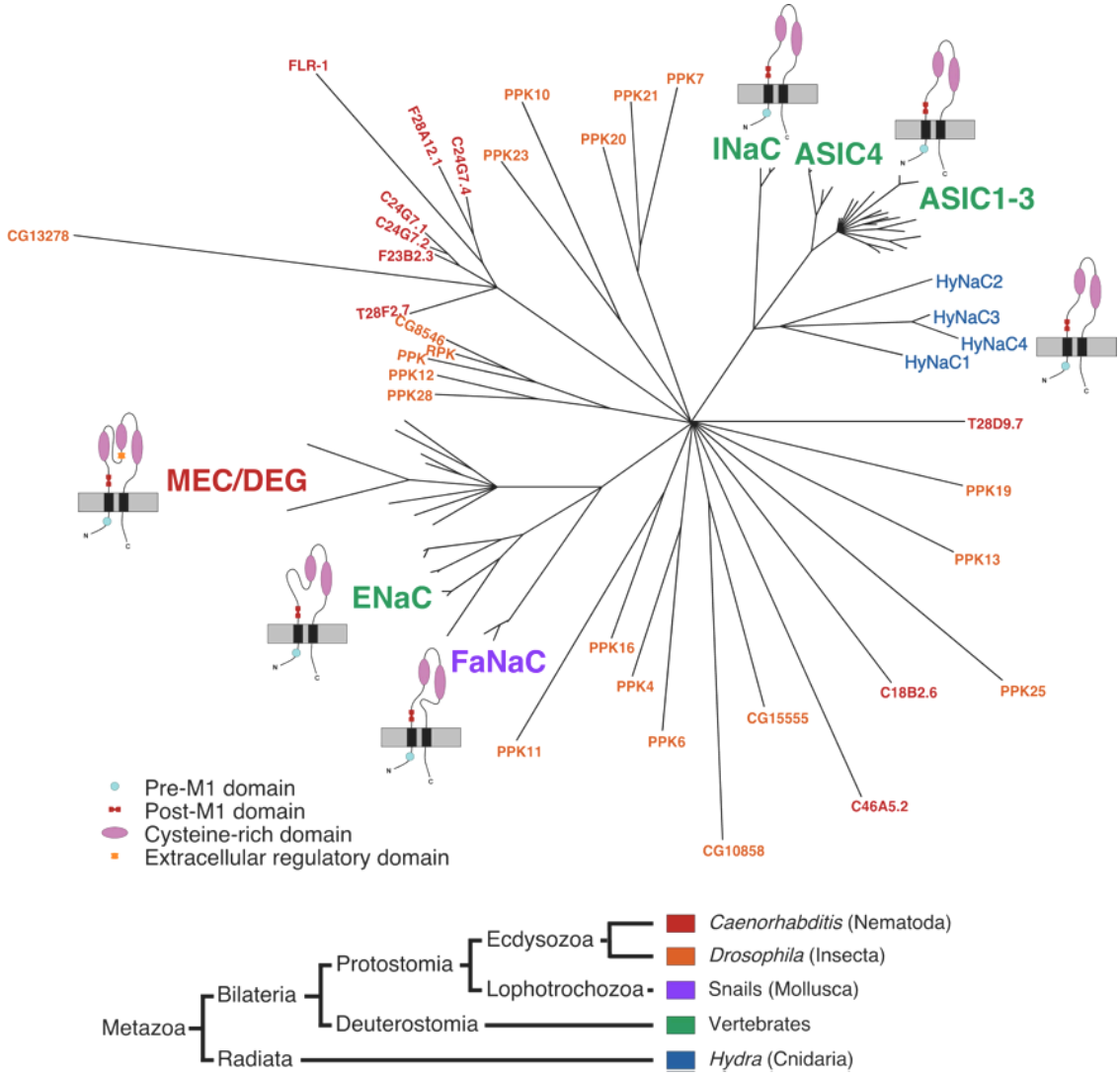

Fig. 1: Phylogenetic tree of the DEG/ENaC ion channel superfamily. The subfamilies in vertebrates comprise ENaCs, ASICs, BLINaC and INaC. The subfamilies in invertebrates consist of the *C. elegans* degenerins (DEG, DEL, MEC, DEL) together with the not directly related FLRs. Further members are the *Drosophila* RPK and PPK channels, FaNaCs from different snail species and the HyNaCs from *Hydra magnipapillata*.
(Adapted from: Golubovic et al., 2007)

Finally, our group has cloned four new DEG/ENaC genes from the Cnidarian *Hydra magnipapillata* that were named *hynac* 1-4 (Hydra sodium channel) (Golubovic et al., 2007). In *Hydra*, expression of *hynac 2-*, *-3* and *-4* was confirmed at the base of the tentacles while *hynac* 1 likely encodes a pseudogene. The coexpression of two subunits, HyNaC2 and 3, in *Xenopus* oocytes lead to expression of an ion channel that is directly gated by two endogenous neuropeptides from the *Hydra* nervous system (see also 1.3 for a detailed

description of the initial characterisation of HyNaC2/3). Until today, HyNaCs and the related FaNaC are the only known ionotropic neuropeptide receptors (Golubovic et al., 2007).

1.1.1 Common features of DEG/ENaCs

With regard to their expression pattern, physiological function and their stimulus of activation the individual DEG/ENaC family members are diverse. However, all known DEG/ENaCs share common characteristics: 1) They are only present in multicellular animals (metazoa), 2) all channels are selective for sodium and 3) can be blocked by amiloride (Kellenberger and Schild, 2002).

DEG/ENaCs are characterized by their high degree of sequence homology. The size of a channel subunit ranges from ≈530 to ≈740 amino acids (Kellenberger and Schild, 2002). Sequence identity between different DEG/ENaC subfamilies is ≈15-30%, the amino acid identity within the subfamilies varies from ≈30-65% (Kellenberger and Schild, 2002). In HyNaCs, the subunits HyNaC3 and 4 are the closest relatives and share 60% identical amino acids; identity between HyNaC2 and subunits 3 or 4 is ≈28%.

Fig. 2 shows a scheme of a typical DEG/ENaC subunit, domains and motifs that are conserved between family members are also depicted. Each subunit consists of two conserved transmembrane domains (M1 and M2) of approx. 20 amino acids length, interconnected via a large extracellular loop typically representing two third of the whole protein (Kellenberger and Schild, 2002). The intracellular N- and C- termini are generally rather short and consist in HyNaC 2-4 of ≈ 20 -70 amino acids (Golubovic et al., 2007). Fully conserved motifs are a HG (His-Gly) motif, located intracellularly close to the M1 region and a FPxxTxC consensus sequence in the post M1 region. The extracellular loop contains two cysteine-rich domains (CRD II and III) conserved in all family members. Other regions are only conserved within subfamilies like the CRD I region, which is unique to the *C.elegans* degenerins or a prolin-rich consensus motif (PY), conserved between ENaC subunits (Kellenberger and Schild, 2002).

In the extracellular domain, in close proximity to M2, the *deg position* is located, a conserved residue harbouring an alanin or glycin. Replacement of this residue by amino acids with larger side chains induces hyperactivation in most DEG/ENaC channels (Kellenberger and Schild, 2002). The mutation was first described for the *C. elegans* degenerins DEG-1 and MEC-4 were it causes degeneration of touch receptor neurons

(Chalfie and Wolinsky, 1990; Driscoll and Chalfie, 1991). Examples for channels that are activated by the “DEG-mutation” are BLINaC (Sakai et al., 1999) and INaC (Schaefer et al., 2000), RPK (Adams et al., 1998), ASIC1a and 2a (Waldmann and Lazdunski, 1998) and HyNaCs (unpublished data).

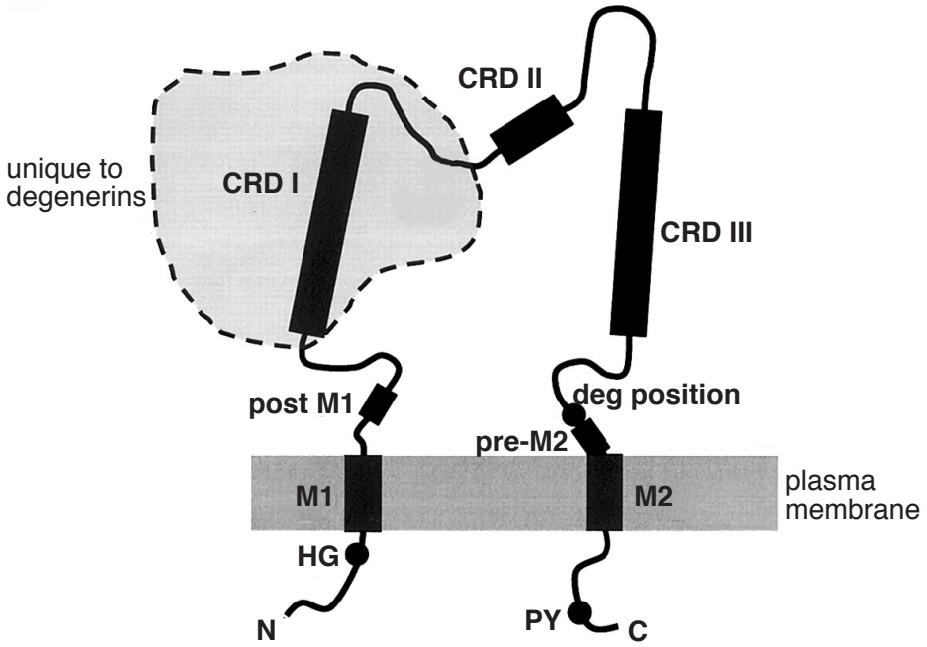

Fig. 2: Scheme of a typical DEG/ENaC subunit showing conserved motifs and regions.
(Adapted from: Kellenberger and Schild, 2002)

As mentioned above, a collective and name giving feature of DEG/ENaCs is their selectivity for Na^+. However, the selectivity for Na^+ over K^+ can vary between individual family members. For example $\alpha\beta\gamma$ENaC almost exclusively conducts Na^+, its P_{Na}/P_K value is >100 (Kellenberger et al., 1999), whereas ASIC1b (Chen et al., 1998) is only slightly selective for sodium with a P_{Na}/P_K value of ≈3 (Chen et al., 1998). In sharkASIC1b (Springauf and Gründer, 2010), ASIC3 (Lingueglia et al., 1997) and BASIC (Wiemuth and Gründer, 2010; Wiemuth et al., 2012) the coexistence of an unselective state and a Na^+-selective state had been reported. A permeability for Ca^{2+} is only described for the mammalian ASIC1a (Bässler et al., 2001) and for MEC-4(d) (Driscoll and Chalfie, 1991), a mutant DEG/ENaC channel from *C.elegans*. For both channels, the permeability for Ca^{2+} is very weak (Bianchi et al., 2004; Samways et al., 2009) and the wildtype MEC-4 is not Ca^{2+} permeable (Goodman et al., 2002; O'Hagan et al., 2005).

The discovery of the crystal structure of ASIC 1a shows that DEG/ENaCs assemble as trimers (Jasti et al., 2007). Moreover, the crystal structure confirmed several older studies suggesting the second transmembrane domain as selectivity filter and pore lining domain of DEG/ENaCs (Jasti et al., 2007; Gonzales et al., 2009; Gründer and Chen, 2010).

1.1.2 The crystral structure of ASIC1 reveals the trimeric structure of DEG/ENaCs

In 2007, the first crystal structure of chicken ASIC1 was resolved at 1.9 Å resolution (Jasti et al., 2007). Although the first structure brought an invaluable progress for the further research on ASICs and related channels, the exact architecture of a functional channel remained elusive as the crystal was obtained from a non-functional deletion mutant lacking the intracellular N- and C-termini. Subsequently, the crystal structure of a functional, sodium selective chicken ASIC1 was obtained at 3 Å resolution that still missed most residues of the C-terminus but contained the N-terminus which is known to be important for channel gating (Gonzales et al., 2009). The main advancement of the second crystal structure was a more precise insight in the arrangement of the transmembrane domains. ASIC1 desensitizes at acidic pH values. As both crystals were obtained at low pH, they provide a snapshot of the desensitized state of the channel. Recently, the structures of ASIC1 in complex with psalmotoxin for two open state conformations were resolved (Baconguis and Gouaux, 2012). Psalmotoxin is a peptide toxin derived from the South American tarantula. It acts on ASIC1a by increasing the channels apparent affinity for protons (Chen et al., 2006a) and has either agonistic or antagonistic effects depending on species and splice variant of ASIC1(Baconguis and Gouaux, 2012). Depending on the pH at which the crystals were derived, two different open state conformations were resolved: One sodium selective state (obtained at low pH) and one unselelective state (obtained at neutral pH). To date, the sum of all available structures allow the reconstruction of the transitions occurring between channel opening and desensitisation. The structure of the closed and non-desensitized state is still unknown.

Before the first ASIC structure was resolved, the subunit stoichiometry of DEG/ENaCs was controversially discussed with authors postulating tetrameric (Firsov et al., 1998; Coscoy et al., 1998; Dijkink et al., 2002) or even nonameric assemblies (Snyder et al., 1998). However, the first crystal structure proofed the trimeric assembly of ASIC1a (Jasti et al.,

2007) and, by extension, this stochiometry is most likely valid for all DEG/ENaCs (Gonzales et al., 2009). Fig. 3A shows the trimeric structure of chicken ASIC1a in complex with psalmotoxin and in Fig. 3B the schematic drawing sketches the composition of a single subunit together with individual subdomains and important regions.

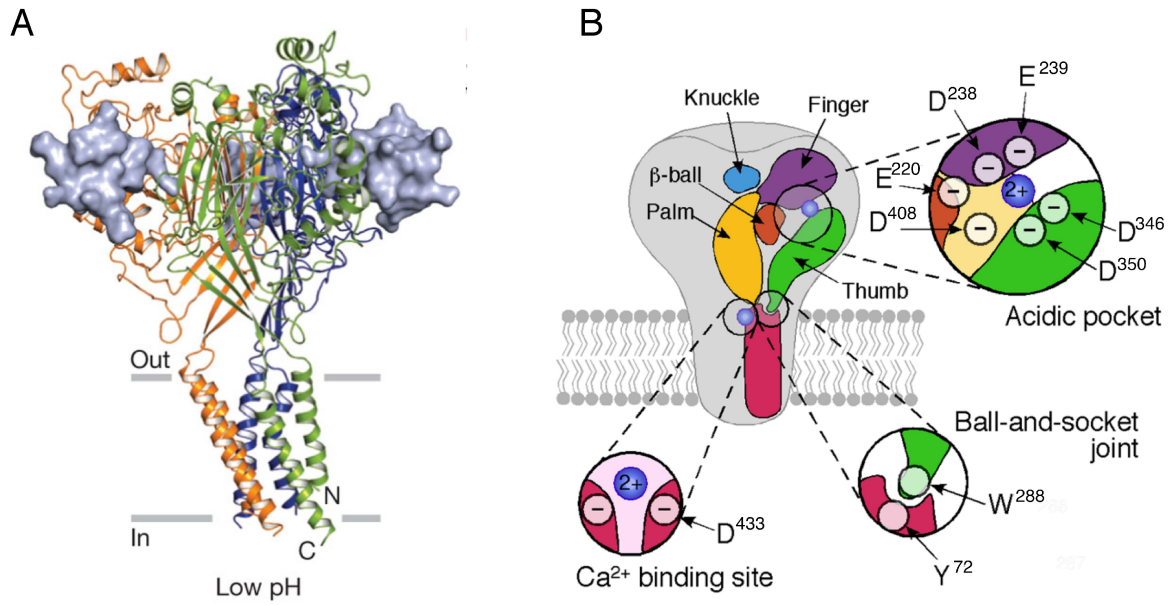

Fig. 3: (A) Crystal structure of ASIC1 at pH 5.5 in complex with psalmotoxin viewed parallel to the membrane. Each of the three subunits is in a different colour and psalmotoxin is shown in purple in solvent-accessible surface representation (from: Baconguis et al.; 2012). (B) Model of the transmembrane topology of an individual ASIC1 subunit based on the crystal structure from Jasti et al., 2007. The insets highlight the individual domains of the extracellular loop, the acidic pocket, the putative Ca^{2+} binding site and the ball-and-socket joint. The residues are numbered according to the chicken ASIC1 sequence (from: Gründer and Chen, 2010).

Each subunit resembles an upright forearm (formed by TM1 and TM2) and a clenched hand (formed by the ECD). The hand is subdivided in a palm, finger, thumb, knuckle and β-ball domain. Both TM-domains directly connect to the palm domain which spans the entire height of the ECM and also connects to the thumb domain (Jasti et al., 2007). As many disulphide bonds localize to the thumb, it has a rigid structure. The thumb domain is implicated in transferring conformational changes to the transmembrane ion pore via an aromatic interaction between Trp 288 (thumb) and Tyr 72 (TM1) by forming a molecular "ball-and-socket joint" (Li et al., 2009; Gründer and Chen, 2010). As binding site for protons, the natural ligands of ASIC1, a region clustering several acidic residues has been proposed. This "acidic pocket" is formed by intersubunit contacts between the thumb, β-ball and finger domains together with residues from the palm domain (Jasti et al., 2007 see Fig. 3B).

Consistent with this, the acidic pocket forms a cavity which is also the binding spot of psalmotoxin (Baconguis and Gouaux, 2012). In the desensitized state of the channel, the α-helices of the transmembrane segments are symmetrically arranged and the TM1 helices make most contacts with the lipid bilayer while the TM2 helices line the ion pore (Gonzales et al., 2009). The ion conduction pathway is occluded by a constriction formed by the crossing of the TM2 helices at about halfway of the membrane bilayer (Fig. 4A).

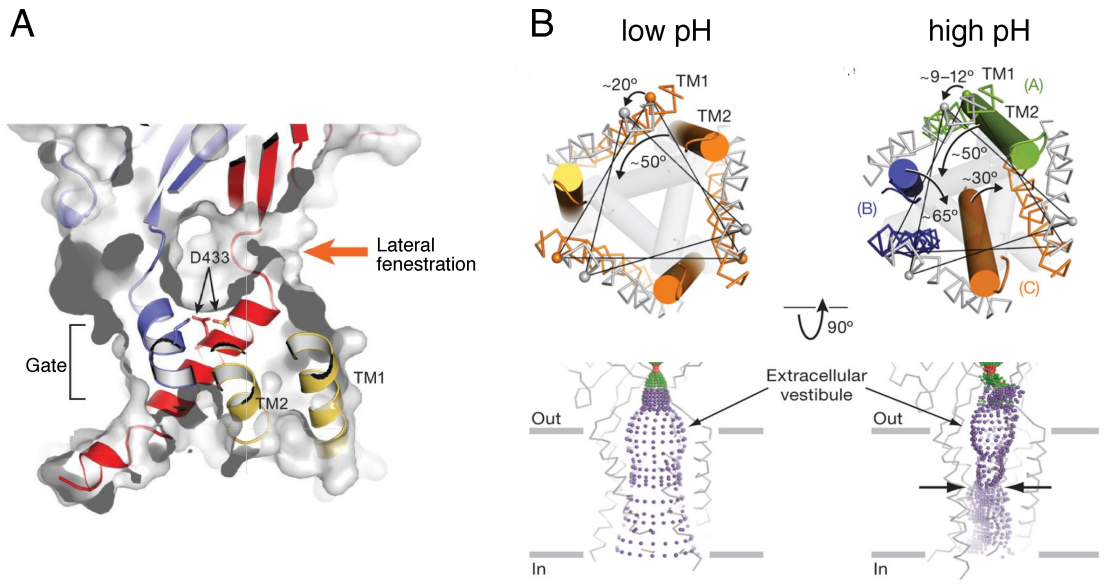

Fig. 4: (A) Structure of the TM-region of chicken ASIC1 in the desensitized state. The ion conduction pathway is occluded by the crossing of the three TM2 domains. Asp 433 is the position of the desensitisation gate. The arrow illustrates one of the three putative entry sites for cations (adapted from: Gonzales et al., 2009). (B) *Top,* comparison of the transmembrane domains from the high pH (*left*) and low pH (*right*) state structures. The desensitized states are shown in *grey.* Transmembrane domains are shown from the extracellular site. *Bottom,* mapping of a solvent accessible pathway along the threefold axis for the high- and low pH states. *Arrows* indicate the constriction of the pathway in the low pH state (adapted from: Baconguis et al., 2012).

This constriction forms the desensitisation gate which is defined on the extracellular side by Asp 433 (Gonzales et al., 2009). Asp 433 is conserved among DEG/ENaCs and is implicated in open channel Ca^{2+} block of ASIC1a - possibly by tight binding of Ca^{2+} to this residue thereby occluding the ion pore. Substitution of this residue by cysteine almost completely abolishes the blocking effect of Ca^{2+} in ASIC1a (Paukert et al., 2004). According to this, a Cs^{+} ion can bind Asp 433 in the desensitized and in the open conformation of the channel (Gonzales et al., 2009; Baconguis and Gouaux, 2012). Directly above Asp 433, the structure reveals three lateral fenestrations trough witch ions might enter the ion pore (Fig. 4A).

The structure of ASIC1a in complex with psalmotoxin revealed two different open channel conformations (Fig. 4B). At high pH, ASIC1a is unselective for monovalent cations and forms a large, threefold symmetric pore lined by both TM-domains of each subunit. The pore has its smallest diameter of 10 Å near the conserved Asp 433 and conducts cations as large as $NMDG^+$. In contrast to this, at low pH the ion pore of ASIC1a selects for sodium and the second transmembrane domain of one subunit is shifted by ≈4 residues to the extracellular side relative to the other subunits conferring axial asymmetry onto the pore (Gründer and Augustinowski, 2012). The three TM2 domains together with the TM1 of one subunit line the ion conduction pathway. Na^+ is supposed to pass the pore in a fully hydrated state (Baconguis and Gouaux, 2012). At low pH, the ion pore has an elliptical shape with its narrowest constriction of ≈5-7 Å at Leu 440 which is close to the conserved "GAS motif" that has been previously identified as selectivity filter of many DEG/ENaCs (Kellenberger and Schild, 2002; Li et al., 2011; Baconguis and Gouaux, 2012).

In summary, the available crystal structures nicely demonstrate the different conformations between the desensitized and the two open states of ASIC1a. For a more complete understanding of the transitions during channel gating, it would be interesting to resolve the structure of ASIC1a also in the closed and non-desensitized state.

1.1.3 Identification of FaNaC - the first peptide-gated ion channel

Most effects of neuropeptides in the nervous system of vertebrates and invertebrates are either of modulatory nature, or slow and frequently depend on G-protein coupled receptors (GPCRs) (Cottrell, 1997). The first evidence for an ion channel that is directly gated by neuropeptides came from outside-out patch-clamp experiments in C2 neurons *from Helix aspersa*. In these experiments, application of FMRFamide elicited unitary Na^+ inward currents that were insensitive to inhibitors of GPCRs but could be blocked by amiloride (Cottrell et al., 1990; Green et al., 1994; for review see Cottrell, 1997). Subsequently, the FMRFamide-gated sodium channel (*Ha*FaNaC) was cloned from *Helix aspersa* by homology to known DEG/ENaC subunits (Lingueglia et al., 1995). When expressed in *Xenopus* Oocytes, HaFaNaC is directly gated by micromolar concentrations of FMRFamide (Fig. 5) and shows large, partly desensitizising Na^+ selective currents, which can be blocked by amiloride. Hence, HaFaNaC is the first identified peptide-gated ion channel. Its ligand, FMRFamide (Phe-Met-Arg-Phe-NH_2) belongs to a class of neuropeptides present in the nervous system of many invertebrates. In addition to activate FaNaC, FMRFamide has

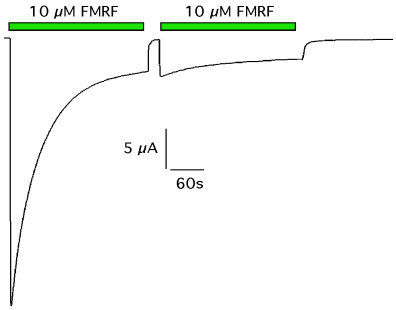

Fig. 5: Characteristic current trace of HaFaNaC recorded from *Xenopus* occytes.

been implicated to participate in several physiological functions which are mediated, in most instances, by binding to GPCRs (Askwith et al., 2000a).

To date, further FaNaCs have been cloned and functionally expressed from the molluscs *Lymnea stagnalis* (Perry et al., 2001), *Heliosoma trivolis* (Jeziorski et al., 2000) and *Aplysia kurodai* (Furukawa et al., 2006). All known FaNaCs are closely related and share about 60% amino acid identity and highly conserved regions within the extracellular loop and transmembrane regions (Furukawa et al., 2006). Apparent affinities for the ligand FMRFamide range from ≈2 μM for *Ha*FaNaC (from *Helix aspersa*) (Lingueglia et al., 1995) to ≈70 μM for HtFaNaC (from *Heliosoa trivolis*) (Jeziorski et al., 2000). These differences in the apparent affinity were used in a chimeric approach to identify the ligand-binding site of FaNaCs. Although the exact binding site could not be determined, it was postulated that an important region which controls the apparent affinity for the peptide is situated in the N-terminal region of the extracellular loop close to the first transmembrane domain (Cottrell et al., 2001). To this day, the physiological role of FaNaCs is unknown.

1.1.4 Physiological roles of RFamides and related peptides in the vertebrate nervous system

In general, the release and subsequent binding of a neurotransmitter to an ionotropic or metabotropic receptor mediates the chemical signal transduction in the nervous system. Ionotropic receptors are ion channels that typically get activated by binding one of the classical small molecule transmitters like acetylcholine, GABA or glutamate. Due to the direct propagation of ligand-binding to channel-gating, ionotropic receptors are especially suited to transmit fast and short-lasting signals. On the other hand, metabotropic GPRCs activate second-messenger cascades and typically transmit slow, modulatory and long-lasting signals. As general rule of thumb, the classical small molecule neurotransmitter can bind and activate both, ionotropic and metabotropic receptors, while neuropeptides activate metabotropic receptors but have only modulatory impact on ionotropic receptors (Pierobon, 2012).

However, as mentioned before, two invertebrate ionotropic receptors from the DEG/ENaC family form an exception from this rule, as they are directly gated by neuropeptides: The FMRFamide-gated FaNaC from molluscs (Lingueglia et al., 1995) and the HydraRFamide gated HyNaCs from *Hydra* (Golubovic et al., 2007).

The discovery of peptide-gated FaNaCs stimulated the research for mammalian peptide-gated ion channels but until now, no such receptor has been identified. However, FMRFamides and HydraRFamides modulate mammalian ASICs, which are closely related to FaNaCs and HyNaCs. For example Askwith et al. demonstrated that application of FMRFamide slowed the desensitization time-constant of ASIC1a, 1b and 3 (Fig. 6A) (Askwith et al., 2000a). A similar effect was reported for the HydraRFamides I-IV on ASIC 3 currents (Fig. 6B), (Golubovic et al., 2007).

FMRFamide and HydraRFamides are not present in the mammalian nervous system (Lingueglia et al., 2006). However, related RFamide peptides, the neuropeptide FF (NPFF), the neuropeptide AF (NPAF) and neuropeptide SF (NPSF), which all derive from a common precursor, were identified in mammals by their similarity with FMRFamide (Perry et al., 1997; Vilim et al., 1999). These neuropeptides have been implicated in participating in various processes like pain modulation, opiate perception, cardiovascular regulation and neuroendocrine function (Panula et al., 1996; 1999; Roumy and Zajac, 1998).

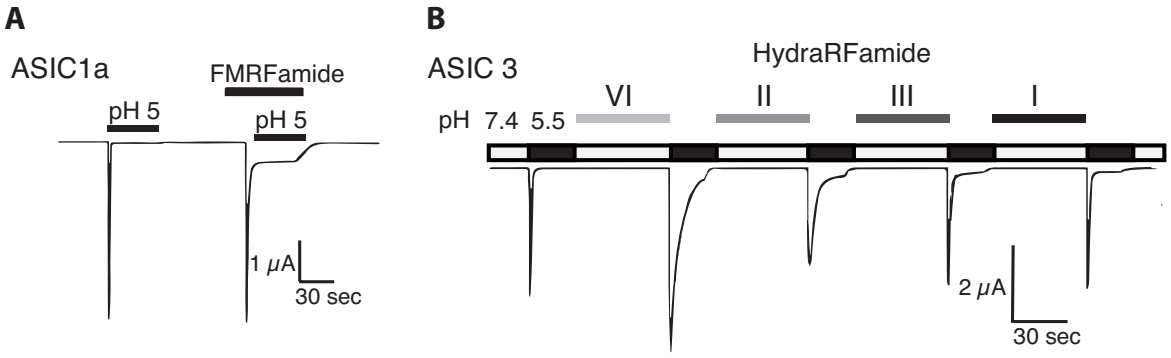

Fig. 6: (A) Application of 50 μM FMRFamide slows desensitization of ASIC1a (from: Askwith et al., 2000). (B) Similarly, application of 50 μM HydraRFamides I-VI modulates ASIC3 currents (from: Golubovic et al., 2007). Both measurements show recordings from *Xenopus* Oocytes expressing ASIC1a and ASIC3, respectively.

Most of the observed effects seem to rely on G-protein coupled receptors but for NPFF and NPSF a direct modulation of ASIC3 currents, which is similar to the effect of FMRFamide, has been reported (Askwith et al., 2000b; Deval et al., 2003). These findings are in agreement with the participation of NPFF, NPSF and ASIC3 in the response to painful

stimuli and correlate with reports of increased expression of these proteins during chronic inflammation in mammals (for review see Lingueglia et al., 2006).

Besides the neuropeptides mentioned above, further peptides with modulatory effects on ASICs were discovered. For example the opioid peptide dynorphin, which is abundantly expressed in the CNS, was shown to enhance activity of ASIC1a by the inhibition of steady-state desensitization (Sherwood and Askwith, 2009). Recently, it was proposed that mutations around the acidic pocket (i.e around H173) are involved in this modulation by dynorphin (Frey et al., 2012).

Furthermore, an interaction of ASIC1a with the painful tarantula peptide toxin psalmotoxin1 was reported (Escoubas et al., 2000). It was shown that the toxin shifts the steady-state desensitisation of ASIC1a to lower H^+ concentrations (Chen et al., 2006a).

1.2. The Hydra nervous system

Hydra belongs to the phylum Cnidaria, which is considered as the earliest phylum in which a nervous system has evolved. The features and mechanisms of function of this evolutionary old nervous system are considered as basic, fundamental features of higher developed brains. Therefore Cnidarians became a model system in the study of the evolution of the nervous system (for reviews see Kass-Simon and Pierobon, 2007; Pierobon, 2012).

From the anatomical point of view, the Cnidarian nervous system is very simple. The neurons are connected to one another forming a nerve net which is composed of two distinguishable cell types: (1) sensory neurons which posses an apical cilium and project to the surface of the epithelial cell layer and (2) the ganglion or interneuronal cells which lie parallel to muscle processes and are located at the basal end of epithelial cells (Pierobon, 2012). In *Hydra,* the nerve net is not homogenously diffuse but exhibits condensed structures especially in the head and foot region. For example, a concentration of neurons is observed at the apex of the hypostome region of *Hydra oligactis* and, in addition, a nerve ring is formed that runs circumferentially in the lower hypostome (Fig. 7) (Koizumi, 2007). An unusual property of the Cnidarian nervous system is its dynamic structure. Neurons differentiate continuously from the multipotent stem cells among the interstitial cells along the entire length of the animal (Bode, 1992). They become integrated into the existing nerve

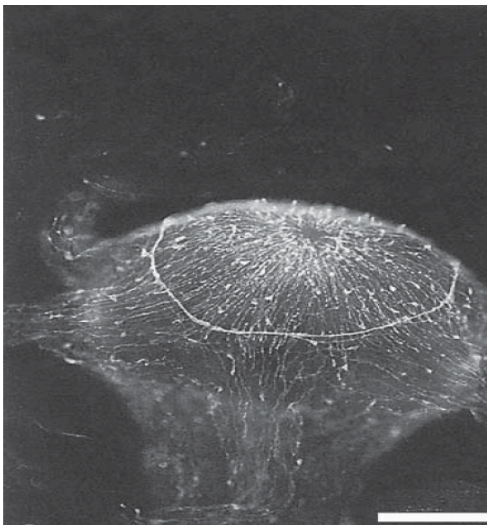

Fig. 7: Concentration of neurons in the hypostome region and formation of a nerve ring in *Hydra oligactis.* Whole mount staining with RFamide antiserum. (From: Koizumi, 2007)

net at the rate of epithelial cell division and migrate towards the extremities were they get finally lost together with the epithelial tissue. By this mechanism, the mash size as well as the number of neurons remains constant (Heimfeld and Bode, 1986; Bode, 1992) .

Although the Cnidarian nervous system is regarded as evolutionary old and simple, there is accumulating evidence that the simplicity of the nervous system is rather on the anatomical than on the biochemical level (Pierobon, 2012). The analysis of genomic data and the recent publication of the genome of *Hydra* and *Nematostella* revealed the complexity of the Cnidarian genomic repertoires and striking similarity to bilateria (Putnam et al., 2007; Anctil, 2009; Chapman et al., 2010). Cnidarian neurons have been shown to be electrically excitable, they can exhibit action potentials and are connected by chemical synapses, gap junctions or synaptic bridges (Pierobon, 2012).

One main interest in the study of the Cnidarian nervous system is the identification of the neurotransmitters this evolutionary old nervous system is using. Numerous studies employing histochemical, biochemical, immunocytochemical and behavioural approaches indicate that all classical small molecule neurotransmitter, involved in fast synaptic transmission in vertebrates, seem to be present in the Cnidarian nervous system as well (Kass-Simon and Pierobon, 2007). In Table 1, the body of evidence for the presence of these neurotransmitters is shown together with the individual detection method. Although the evidence for the existence of the classical transmitters is compelling and electron microscopic images document the presence of small clear vesicles in Cnidarians, many studies failed to proof that the identified substances really work as neurotransmitter. So far, in no instance it has been shown that a candidate transmitter meets all the traditionally accepted criteria for a neurotransmitter (Anderson and Trapido-Rosenthal, 2009).

Summary of experimental evidence for the various substances in Cnidaria

	Vesicles	ACH	Glutamate	GABA	Glycine	Taurine	Catecholamines	E/NE	5HT	NO	Eicosanoids
Hydra spec.	CD	HPM	IBPM	IBPM	BP	B	IBPMS	HBP	HBP	BP	BP

C=Clear vesicles, D=Dense cored vesicles, I= Immunicytochemistry, H= Histochmeistry, M= Molecular biology, P=Pysiological/Behavioral effects, S=Synaptic localistaion

Table 1: Experimental evidence for small melucule tranmitter in *Hydra* spec.
(Adapted from: Kass-Simon and Pierobon, 2007)

Similarly, the search for the receptors of these small molecule neurotransmitters has been intensively pursued (reviewed by Kass-Simon and Pierobon, 2007). For example, hints for the presence of both, ionotropic $GABA_A$ and metabotropic $GABA_B$ receptors were found in membrane preparations of *Hydra vulgaris* (Pierobon et al., 1995; Scappaticci and Kass-Simon, 2008) and immunocytochemical studies localised $NMDAR_1$ immunoreactivity in nerve cells, epitheliomuscular cells and nematocytes (Scappaticci et al., 2004; Scappaticci and Kass-Simon, 2008). In behavioural studies on *Hydra vulgaris*, application of glutamate, AMPA and kainate had excitatory effects in the ectodermal pacemaker systems providing hints for the presence of the corresponding receptors (Kass-Simon et al., 2003). However, molecular evidence for the existence of these receptors is still lacking.

Recently, large progress in the search for classical chemical neurotransmission in Cnidarians was made with the sequencing of the genome of *Nematostella vectensis* (Anctil, 2009). A subsequent genomic analysis suggests the presence of 12 apparent nicotinic acetylcholine receptors together with 5 genes coding for apparent acetylcholinesterases and 3 genes for choline-acetyltransferases. Similar, genes with homology to AMPA (6), Kainate (2) and NMDA (4) receptors were identified. In addition, the genome comprises genes with homology to $GABA_A$ (12) and $GABA_B$ (9) receptors. Furthermore, the analysis suggested the presence of purinergic P2X (2) receptors and the presence of receptors for biogenic amines, adenosine and NO (Anctil, 2009). In *Hydra*, the sequencing of the genome revealed the presence of nicotinic acetylcholinreceptors and other genes that are present at the neuromuscular junction in bilaterians. However, as other genes are missing it is unclear weather the neuromuscular junction in *Hydra* is really cholinergic (Chapman et al., 2010). Another recent study identified TRPA1 in sea anemones in the hair bundles of sensory

neurons that are associated with cnidocyst discharge and TRPA1 is also encoded in the genome of *Hydra* (Mahoney et al., 2011; Holstein, 2012). This suggests a possible role of TRPA1 in the discharge of nematocysts and is in accordance with the function of TRPA1 as mechanosensor in vertebrates (Holstein, 2012).

Besides the accumulating evidence for the role of small molecule transmitters in both, fast and slow synaptic transmission, there is evidence for the ubiquitous presence of neuropeptides in the Cnidarian nervous system. Pioneering work in the identification of these Cnidarian neuropeptides came from Grimmelikhuizen and his co-workers in the early 1980´s. In a series of studies using immuocytochemical approaches, they identified substance-P-like, neurotensin-like, bombesin-like, vasopressin/ocytocin-like and FMRFamide-like immunoreactivity in *Hydra* and other Cnidarians (Grimmelikhuijzen et al., 1981a; 1981b; 1981c; 1982; Grimmelikhuijzen, 1983). Further studies led to the identification and resolution of the structure of numerous neuropeptides from different Cnidarian species (Fujisawa and Hayakawa, 2012).

So far, all isolated neuropeptides share some structural hallmarks: They posses a C-terminal amide group and frequently their N-termini contains protection groups like pyro-Glu residues or X-Pro sequences (Hansen et al., 2002). The biosynthetic pathways of Cnidarian neuropetides was also identified. Similar to mammalians, the neuropeptides are synthesized from precursor proteins, which are called preprohormones. By post-translational cleavage they give rise to different neuropeptides that all share the same dipeptide-amide ending (Grimmelikhuijzen et al., 1996; Leviev et al., 1997; Darmer et al., 1998). Table 2 shows a list of the known preprohormones together with their neuropeptides from *Hydra*.

The HydraRFamides I-IV which were used in this work arise from the preprohormones A, B and C (Darmer et al., 1998). While preprohormones A gives rise to HydraRFamides I-IV preprohormone B codes for HydraRFamide I and II and preprohormone C only codes for seven copies of RFamide I (Darmer et al., 1998). A whole mount *in situ* hybridization with cRNA probes against the preprohormones A-D revealed that the individual preprohormones are expressed in different subsets of the *Hydra* nervous system. For example preprohormone A expression was localised in the hypostome, gastric region and peduncle whereas preprohormone C staining was only observed in tentacles (Hansen et al., 2002).

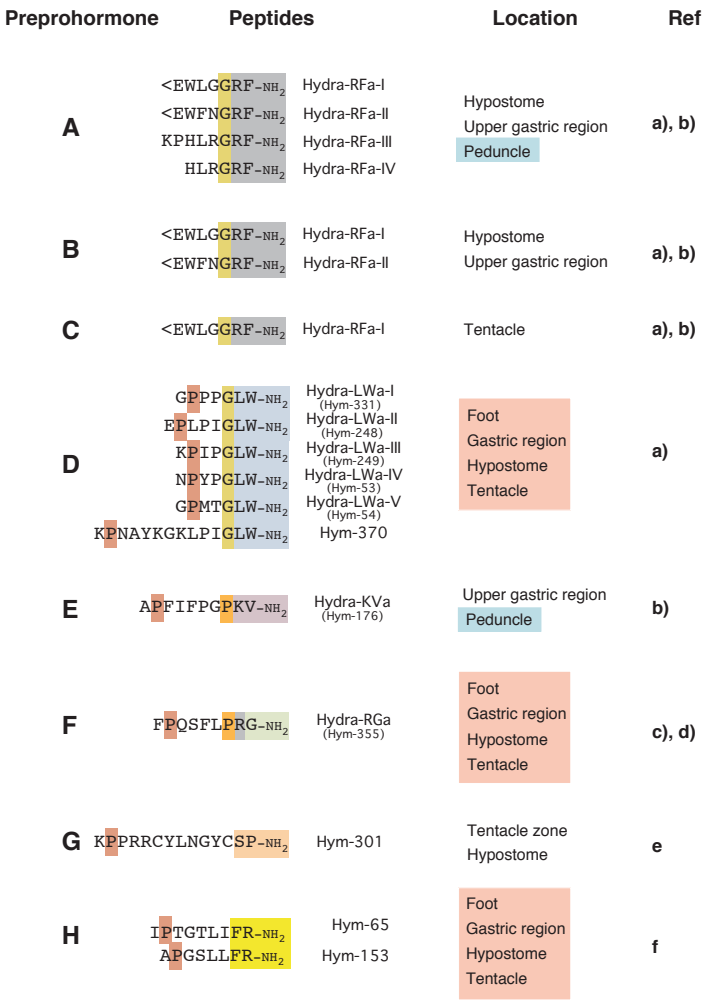

Table 2: Summary of the identified preprohormones together with their neuropeptides and localisation in *Hydra*. <Q designates C-terminal pyroglutamate. References: a) Mitgutsch et al., 1999; b) Hansen et al., 2000; c) Takahashi et al., 2000; d) Hansen et al., 2002; e) Takahashi et al., 2005; f) Hayakawa et al., 2007.

In addition, colocalisation of preprohormone A and E was found in the peduncle but not in other body regions. In summary, these findings suggest the presence of at least six neurochemical different classes of neurons in *Hydra* (Hansen et al., 2002).

The HydraRFamides and several other neuropeptides were identified in dense-core vesicles associated with synaptic and non-synaptic release sites (Koizumi et al., 1989; Grimmelikhuijzen and Westfall, 1995). Although the physiological function of many Cnidarian neuropeptides remains elusive, behavioural effects have been reported for some of them. For example in sea anemones an either agonistic (AnthoRW-amides I and II), or antagonistic (Antho-KAamide and AnthoKIamide) effect on muscle contractions was observed (McFarlane et al., 1991; 1993). In another study, the anthozoan neuropeptide

AnthoRWamide was shown to excite muscle contractions and simultaneous recordings from myoepithelial cells documented that the peptide increases an inward Ca^{2+} current (Cho and McFarlane, 1996). For the HydraRFamides and HydraLWamides behavioural and developmental effects in the Hydrozoan *Hydractinia echinata* were reported. Thereby, the two classes of neuropeptides seem to have antagonistic effects. HydraLWamides induced the metamorphosis of planula larvae into adult polyps and HydraRFamides inhibited it (Katsukura et al., 2003). Similarly, the migration of planula larvae is stimulated by HydraLWamides and suppressed by HydraRFamides (Katsukura et al., 2004). To date, the receptors of most Cnidarian neuropepides are unkown. However, the identification of ligand-gated ion channels directly gated by HydraRFamides (Golubovic et al., 2007) and the presence of more than 100 putative genes coding for GPCRs (Fujisawa, 2008) suggest that the Cnidarian neuropeptides work by binding and activating both, ionotropic and metabotropic receptors.

1.3. Identification of a peptide-gated DEG/ENaC from *Hydra*

To identify evolutionary conserved features of the DEG/ENaC channel family, our group cloned four novel DEG/ENaC subunits from the freshwater polyp *Hydra magnipapillata.* These new subunits have been characterized previously in our group by Andjelko Golubovic (see Golubovic et al., 2007). A short summary of this characterisation is given below:

The new DEG/ENaC members were named HyNaC1-4 (*Hydra* sodium channel). The subunits HyNaC3 and 4 are most closely related and share 60% identical amino acids; identity between HyNaC2 and subunits 3 or 4 is ≈ 28%. One of the cloned genes, *hynac1,* is most likely a pseudogene as it is lacking both, a methionine to initiate translation and a conserved N-terminal HG-motif common to all DEG/ENaC channels. Using an *in situ* hybridisation assay, the expression of *hynac2-4* transcripts was detected at the base of the tentacles in adult *Hydra* polyps most likely in epitheliomuscular cells. Moreover, *hynac2* and *3* transcripts were observed in the budding region of growing polyps, whereas expression of HyNaC4 was observed at a later developmental stage, when buds detached from the mother polyp. The new HyNaC subunits were also investigated by TEVC measurements in *Xenopus* oocytes. Coexpression of HyNaC2 and 3 gave raise to an ion channel that is directly gated by two endogenous neuropeptides from Hydra, *the* HydraRFamides I and II

(Fig. 8A). Application of the HydraRFamides I and II induced inward currents (1-10 μA) that consisted of a transient peak and a non-desensitisizing sustained current component (Fig. 8A). The HydraRFamides I and II activated the channel with an apparent affinity of 34 ± 9 and 28 ± 4 μM, respectively (Fig. 8B). The related HydraRFamides III and VI failed to open the channel (Fig. 8A). Further characterisation revealed that repeated activation with HydraRFamides I and II led to a decrease in current amplitudes (Fig. 8C).

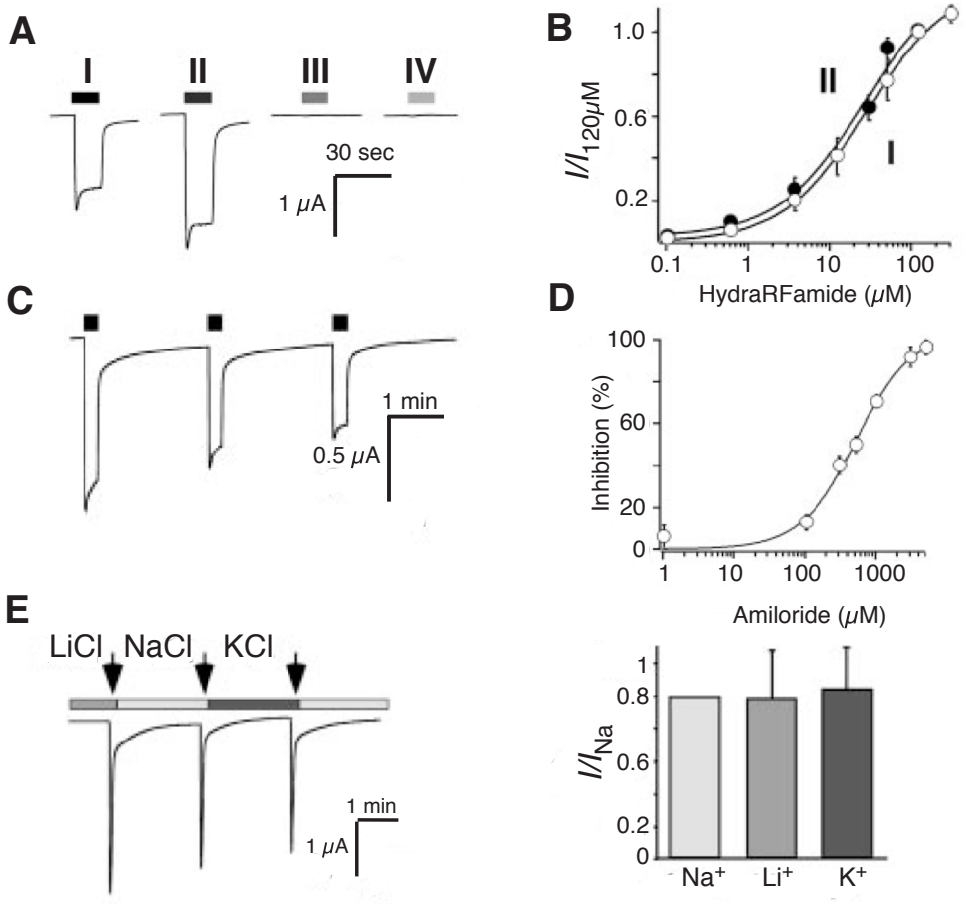

Fig. 8: (A) Currents elicited by HydraRFamides in *Xenopus* ocytes injected with HyNaC2 and 3. (B) Concentration-response curves for the HydraRFamides I and II. (C) Repeated application of HydraRFamides lead to a decreased response. (D) Concentration-response curve for the inhibition of HyNaC2/3 by amiloride. (E) Replacement of Na^+ by K^+ and Li^+ did not significantly alter the current amplitudes.
(From: Golubovic et al., 2007)

A similar effect had been reported previously for the related DEG/ENaC channel ASIC1a where the "run-down" of currents was named tachyphylaxis (Chen and Gründer, 2007). Similar to other DEG/ENaCs, HyNaC2/3 is blocked by amiloride but the efficacy of block was low (IC_{50}= 540 ± 40 μM) (Fig. 8D). When extracellular Na^+ was replaced by K^+ or Li^+, the current amplitudes were not significantly changed (Fig. 8E) suggesting that HyNaC2/3 is

an unselective ion channel, which is an atypical feature within the DEG/ENaC family as other members are selective for Na^+ (Kellenberger and Schild, 2002).

Taken together, these results confirmed HyNaC2/3 as a new DEG/ENaC family member that is directly gated by endogenous neuropeptides. These findings were surprising as neuropeptides usually only have modulatory functions on ion channels. Indeed, HyNaCs and the related FaNaCs are the only known peptide-gated ion channels.

However, the low affinity for amiloride and the lack of selectivity for sodium are unexpected findings as all known DEG/ENaC are sodium selective and sensitive for amiloride. This indicates that these features are either not evolutionary conserved among DEG/ENaC channels or that another subunit of the HyNaC2/3 heteromer might still be missing.

II. Materials and Methods

2.1 Materials

2.1.3 Chemicals

All standard chemicals were purchased from Sigma-Aldrich (St. Louis, MO, USA), Merck (Darmstadt, Germany) and Roth (Karlsruhe, Germany) if not stated otherwise.

2.1.3 Materials for molecular biology

Ready to use materials:

100 bp DNA-ladder	New England Biolabs, Ipswich, MA, USA
1 kB GeneRuler DNA-ladder	Fermentas, St. Leon-Rot, Germany
DEPC H_2O	Carl Roth, Karlsruhe, Germany
RedSafe DNA-staining dye	Chembio, Medford, NY, USA
Super Signal ELISA Femto Maximum Sensitivity Substrate	Thermo Fisher Scientific, Rockford, IL, USA
dNTPs	Carl Roth, Karlsruhe, Germany
Fura2-AM	Invitrogen, Carlsbad, CA, USA

Enzymes:

Restriction endonucleases	New England Biolabs, Ipswich, MA, USA
Taq DNA-polymerase	New England Biolabs, Ipswich, MA, USA
KAPA HiFi DNA-polymerase	Peqlab, Erlangen, Germany
Alkaline phosphatase	New England Biolabs, Ipswich, MA, USA

Collagenase from *Clostridium histolyticum,* Type II	Sigma-Aldrich, St. Lois, MO, USA
HydraRFamides I and II	Genemed Synthesis, San Antonio, TX, USA

Plasmid-vectors

All constructs used for expression in *Xenopus leavis* oocytes were cloned into the custom-made oocyte expression vector pRSSP-6009. The vector has a size of ≈3000 bp and carries an ampicilin resistance gene for positive selection of transformed *E. coli* cells. To facilitate robust expression of foreign genes in oocytes, the vector carries the 5´-untanslated region of the *Xenopus* ß-globin gene 5´-upstream of the multiple cloning site and a poly-A sequence ≈50 bp downstream of the cloning site.

The probes for the *in situ* hybridisation assay (3.1.3) were cloned in the vector pBluescript from Stratagene (now AgilentTechnologies, Santa Clara, CA, USA)

Top10 chemically competent E. coli

Top10 competent cells (Invitrogen, Carlsbad, CA, USA) were used for all transformation reactions performed in this work. The phenotype of Top10 cells is similar to the DH10B strain and cells have a high transformation efficacy of 10^9 cfu/μg.

Kits:

Ligate-IT Rapid Ligation Kit	USB, Cleveland, OH, USA
High Pure PCR Product Purification Kit	Roche, Mannheim, Germany
High Pure PCR Cleanup Micro Kit	Roche, Mannheim, Germany
High Pure Plasmid Isolation Kit	Roche, Mannheim, Germany
mMESSAGE mMACHINE SP6 RNA Transcription Kit	Ambion, Carlsbad; CA, USA

Antibodies:

Anti-HA High Affinity Clone 3F10, rat IgG1 monoclonal	Roche, Mannheim, Germany
Peroxidase-AffiniPure F(ab')2 Fragment Goat Anti-Rat IgG (H+L)	Jackson ImmunoResearch West Grove, PA, USA

2.1.3 Solutions and buffers for molecular biology

Agarose-Gels: 30 ml or 90 ml TAE-buffer
Add x g agarose

LB-media
10 g tryptone
5g yeast extract
10 g NaCl
Add ddH_20 to 1l; pH 7.5
Sterilized by autoclaving

Agar-plates:
15g/l agarose
1 ml ampicilin (100 mg/ml)
Add LB-media to 1 l
Sterilzed by autoclaving, after cooling add ampicilin

SOC-media:
20g tryptone
5 g yeast extract
2.5 ml of 1 M KCl
10 ml of 1M $MgCl_2$
10ml of 1M $MgSO_4$
Sterilized by autoclaving
Add 20ml of 1M glucose
Add ddH_20 to 1 l

50 X TAE-buffer: 242 g Tris-Base
57.1 ml glacial acid (100%)
100 ml 0.5 M EDTA
Add ddH_2O to 1 l

2.1.3 List of primers

All PCR primers were ordered from MWG-Biotech AG, Ebersberg, Germany. Working concentration was 10 pmol/μl. The primers used in this work are listed below:

Name	Sequence	Purpose
Hy2-HA-up	5´-CGT ACG ACG TTC CAG ATT ATG CCG ATA TTC AAG GAG AAG AAC-3´	To insert a HA-epitope in the extracellular loop of HyNaC2.
Hy2-HA-lo	5´-AAT CTG GAA CGT CGT ACG GAT AGA ATC CTG GAT TTT CTA AAT TG-3	
Hy2-430_D-C-QC-up	5´-GAT TTT TAC AAG CTT ATT GGT TGT GTC GGA GGT CAA CTT GGT TTG C-3´	Quick-Change primer for HyNaC2_D-C
Hy2-430_D-C-QC-lo	5´-GCA AAC CAA GTT GAC CTC CGA CAC AAC CAA TAA GCT TGT AAA AAT C-3	
Hy3_D-C-Fl-up	5´-CAA CAC TAT GAA TAC TAT AGA G-3	Flanking primer for HyNaC3_D-C
Hy5-437_D-C-up	5´-GTT TCT TGG TTG TAT GGG AGG TGA AAT TG-3	Mutagenesis primer for HyNaC5_D-C
Hy5-437_D-C-lo	5´-CCT CCC ATA CAA CCA AGA AAC TG-3´	
Hy5_D-C-FL-up	5´-GGG GAA AAG ATG TCC AGT AG-3´	Flanking primer for HyNaC3_D-C
Hy3-432_D-C-up	5`-GGC TAG GAT GTG TTG GTG GTC AGA TAG-3	Mutagenesis primer for HyNaC3_D-C
Hy3-432_D-C-lo	5´-CCA CCA ACA CAT CCT AGC CAC ACC-3´	
SP6-upper	5´-AGG TGA CAC TAT AGA AAT AC-3´	Primers, flanking the MCS of the oocyte expression vector pRSSP-6009
PSP3-lower	5´-CTC AGA GAT TCG ATG TAT-3´	

Table 3: List of primers used in this thesis.

2.2 Molecular biological methods

2.2.1 Agarose gel electrophoresis

Agarose gel electrophoresis was used to analyze DNA- and RNA-fragments according to their size and concentration. Moreover, preparative agarose gels were used to isolate individual DNA-fragments. Depending on the size of the analyzed DNA or RNA, gels with 0.8-2% agarose solved in 1x TAE-buffer were used. The mixture was boiled in a microwave to dissolve the agarose and 1.5 μl "Red Safe" staining dye per 30 ml gel was added. Wells were formed with plastic combs of appropriate size. After cooling, the gels were placed in running chambers (Bio-Rad) filled with 1x TAE as running buffer. Before loading the gel, samples were mixed with 6x gel-loading buffer and RNA probes were additionally incubated at 65°C for 10 min to minimize formation of secondary RNA structures. A 100 bp or 1 kb DNA-ladder was used as molecular weight standard. Gel chambers were connected to a power supply (Power Pac 300; Bio-Rad) and run at 80-120 V for 20-45 min. Probes were visualized under a UV-transilluminator (Gel Doc XR, Bio-Rad) and analyzed using the software Quantitiy-One 4.6.1 (Bio-Rad).

2.2.2 Purification of DNA

The purification of DNA from agarose gels, PCR products and restriction enzyme digests was carried out with the "High Pure PCR Product Purification Kit" (Roche) according to the manufacturers instructions. DNA from PCR reactions and restriction enzyme digests were purified directly with the provided columns. For the recovery of DNA from agarose gels, bands of the expected size were excised with a scalpel under UV-light and transferred into 1.5 ml reaction tubes. To solubilise the agarose, a threefold (w/w) excess of the provided solubilisation buffer was added and the gel slices were incubated at 65°C for 10 min in a shaking incubator (Thermo Mixer, Eppendorf). After this solubilisation step, the extracted DNA was loaded on the columns and purified according to the manufactures manual.

2.2.3 Restriction digest of DNA

All restriction digests were carried out with restriction endonucleases (New England Biolabs) according to the manufacturer's recommendations using the provided buffers and solutions. 10 U of enzyme were used to digest 1 μg of DNA. Restriction digests were carried out at the recommended temperature for 1-2 hours in a shaking-incubator (Thermo Mixer, Eppendorf). The DNA was subsequently checked for complete digestion by agarose gel electrophoresis.

2.2.4 Polymerase chain reaction (PCR)

Polymerase chain reaction (PCR) was used to generate all HyNaC mutants and for the identification of positive clones after transformation of heat-competent *E. coli* bacteria. PCR reactions were performed with a T 3000 thermocycler (Biometra).

2.2.4.1 Inserting mutations by recombinant PCR

All HyNaC mutants except HyNaC2_D-C were generated by recombinant PCR. With the recombinant PCR technique, a site directed mutagenesis or a site directed insertion of a custom DNA sequence was performed in three PCR reactions:

In the first step of recombinant PCR, two individual PCR reactions were performed. For each PCR of the first step, a primer-pair consisting of a gene-specific primer and a mutagenic primer was used. While the exact binding site of the gene specific primer was arbitrary, the mutagenic primers had two features: 1) they carried the desired mutation; 2) the primer design gave rise to PCR products with overlapping sequences at the mutation site.

With this primer design, the two PCR products from the first step hybridized at mutation site. This feature was used in a third PCR reaction in which both PCR products from the first step were corporately used as template. The gene specific primers from the first two rounds of PCR were used to amplify the final PCR fragment that was flanked by the gene specific primers and carried the desired mutation. Subsequently, the mutated PCR fragment was inserted into the vector carrying the *wt* construct by cutting vector and PCR fragment with the same two restriction enzymes to facilitate site directed ligation of the fragment into the

vector. Afterwards, the PCR fragment was inserted into the target vector in a ligation reaction (see 2.2.5).

PCR (50 µl reaction volume) was performed with the proofreading "KappaHiFi polymerase" (Peqlab). PCR products from the first step were loaded on a preparative 1% agarose gel and fragments of expected size were excised with a scalpel under dimmed UV-light and purified with the "High Pure PCR Product purification Kit" (Roche) (see 2.2.2). 1 µl purified DNA from each PCR reaction was used as template for the third PCR. The PCR product was again loaded on an agarose gel and the DNA-fragment of expected size was excised and purified.

To insert the mutated PCR fragment into the vector carrying the wildtype construct, 0.5 µg vector and the PCR fragment were cut with two different restriction enzymes creating sticky ends. Both restriction digests were loaded on a preparative agarose gel and bands of expected size were excised and purified. Following this step, both products were ligated (see 2.2.5) and the ligation product was subsequently used for transformation of competent Top10 *E. coli* cells (see 2.2.6). The success of mutagenesis was verified by DNA-sequencing (see 2.2.8).

Pipetting scheme for recombinant PCR mutagenesis:

5x KAPAHiFi polymerase buffer	10 µl
Template DNA ≈ 10 ng	1 µl
Forward primer (10 pmol/µl)	1.5 µl
Reverse primer (10 pmol/µl)	1.5 µl
dNTPs (10 mM/µl each)	1µl
KAPAHiFi polymerase (1 U/µl)	1 µl
ddH_2O	34 µL
Reaction volume:	50 µl

PCR protocol for recombinant PCR mutagenesis:

Step	Temperature	Time	Cycles
Initial denaturation	95°C	180 s	1
Denaturation	98°C	20 s	16-20
Annealing	T_m ±10°C	30 s	
Elongation	72°C	30 s/kb	
Final elongation	72°C	180 s	1

2.2.4.2 Quick-Change mutagenesis

In this work, the Quick-Change mutagenesis was used to create the HyNaC2_D-C mutant. Quick-Change was originally invented by the company Stratgene as an *in vitro* method to induce site directed point mutations or single amino acid changes into a plasmid in just one PCR reaction.

For Quick-Change mutagenesis, complementary primers of 25-50 bp length that have a T_m ≥ 75°C and carry the desired mutation in the middle of their sequence are used (see 2.1.3). The whole plasmid is amplified in a single standard PCR reaction with a proofreading polymerase. By this procedure a “new”, nicked plasmid containing the desired mutation is synthesized. The “new” PCR-generated plasmid is unmethylated, whereas the DNA from the template plasmid is methylated as it orginates from *E. coli* cultures. In the next step, the template plasmid is removed by means of the restriction enzyme Dpn I, which selectively digests methylated and hemimethylated DNA. Subsequently, the nicked mutated plasmid is transformed into competent TOP10 *E. coli* cells that repair the nick in the mutated plasmid.

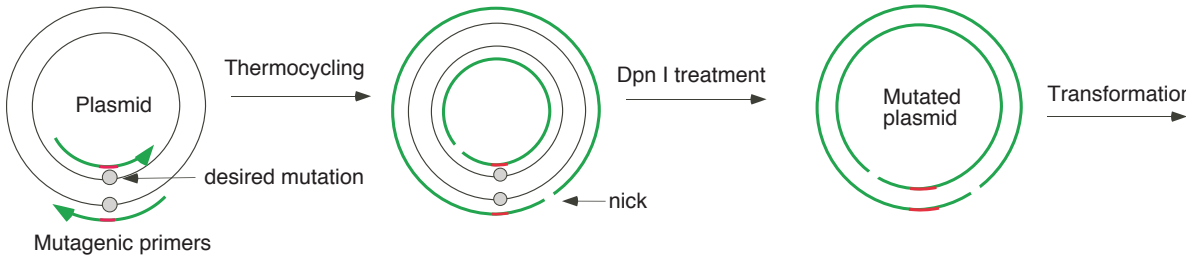

Fig. 9: Principle of the Quick-Change mutagenesis. (Adapted from: Stratagene™ Quick-Change manual)

Pipetting scheme for the Quick-Change mutagenesis:

5x KAPAHiFi polymerase buffer	10 µl
Template plasmid DNA (5-, 10- or 20 ng)	x µl
Mutagenesis Primer A (125 ng)	x µl
Mutagenesis Primer B (125 ng)	x µl
dNTPs (10 mM each)	1 µl
ddH_2O	x µL
Reaction volume:	50 µl

PCR protocol for the Quick-Change mutagenesis:

Segment	Cycles	Temperature	Time
1	1	95°C	120 s
2	16	98°C	20 s
		55°C	60 s
		72°C	1min/kb plasmid length

After thermocycling, 1 µl Dpn I (10 U/µl) was directly added to the PCR reaction. Dpn I treatment was for 1 h at 37°C. Subsequently, 1 µl of the Dpn I treated DNA was used for transformation of competent Top10 *E. coli* cells (see 2.2.6). The success of Quick-Change mutagenesis was verified by DNA-sequencing (see 2.2.8).

2.2.5 Ligation of PCR fragments into plasmid vectors

In the ligation reaction, the enzyme ligase catalyzes the ATP-depended formation of two phosphodiester bonds between the free 3´-hydroxy and 5´-phosphate endings between vector and insert. To ligate a PCR fragment (insert) into a plasmid vector, ≈0.5 µg vector and insert were cut with two restriction endonucleases creating „sticky ends“ for 2 hours. To prevent self ligation of the vector, 5 U of alkaline phosphatase was added to the restriction enzyme digest for 20 min. Subsequently, the digested vector and insert were loaded on a preparative agarose gel and bands of expected size were cut out with a scalpel and purified with the “High Pure DNA Purification Kit” (Roche) (see 2.2.2). For the ligation reaction, approx. 100 ng vector was mixed with a 3-fold molar excess of insert. This mixing ratio was estimated by analytical agarose gel electrophoresis. The ligation reaction was carried out with the “Ligate IT Rapid Ligation Kit” (USB Cooperation) for 10 min according to the manufacturers instructions. Subsequently, the ligated plasmid was used for transformation of chemically competent TOP10 *E. coli* cells (see 2.2.6).

2.2.6 Transformation of chemically competent *E. coli*

To amplify DNA-plasmids, chemically competent TOP10 *E. coli* cells were used (Invitrogen) that were stored in aliquots of 50 µl at -80°C. For transformation, the cells were carefully thawed on ice for 10 min. Either 50 ng of plasmid DNA or 10 µl of a ligation reaction (see 2.2.5) were carefully added to the cells followed by further incubation on ice for 30 min. After a heat shock (42°C for 45 s), 250 µl of SOC-media (preheated to 37°C) was added and the cells were incubated at 37°C for 60 min in a shaking-incubator at 220 rpm. The cells were then centrifuged (5000 x g, 5 min at room temperature) and the supernatant was removed. The cells were resuspended in 100 µl LB-media and spread on agar plates containing ampicilin for selective growth of transformed bacteria. The plates were incubated at 37°C for ≈12 hours. Ampicilin resistant colonies were then screened for the expression of the plasmid by colony-PCR. Further verification of positive clones was carried out by DNA-Miniprep, followed by restriction enzyme analysis or DNA-sequencing. Positive clones were stored either as gylcerol stocks (LB-medium containing 25% (v/v) glycerol) or purified by DNA-Miniprep and stored as plasmid-DNA at -20°C.

2.2.7 Isolation of plasmid-DNA

The isolation of plasmid-DNA from transformed cells was carried out by DNA-Miniprep. In the first step, 3 ml LB-medium containing 3 µl ampicilin (100 mg/ml) was inoculated with a single bacterial colony carrying the desired plasmid. The culture was incubated over night at 37°C at 220 rpm in a shaking incubator. The cultures were then pelleted by centrifugation (5000 x g for 5 min) and the plasmid preparation was performed with the "High Pure Plasmid Isolation Kit" (Roche) according to the manufacturers instructions. Finally, concentration and purity of the DNA was analyzed by UV-Vis spectroscopy.

2.2.8 Sequencing of DNA

All HyNaC constructs were entirely sequenced prior to cRNA synthesis. DNA-sequencing was carried out by MWG-Biotech, Ebersberg, Germany. As sequencing probes 1 µg purified DNA, diluted in 15 µl ddH_2O, was sent to the company. As sequencing primers SP6 and PSP3, which bind up- and downstream of the multiple cloning site of the oocyte expression vector pRSSP-6009, were used. Results were downloaded from the company's website and analyzed using the software Lasergene Ver. 8.0 (DNASTAR, Madison, WI, USA).

2.2.9 Determination of surface expression

To quantify the surface expression of different HyNaC subunit combinations, a bioluminescence assay was performed. The principle of this assay is based on the insertion of a hemagglutinin (HA) epitope of the influenca virus into the extracellular loop of the membrane protein of interest. By means of this, the incorporation of the tagged protein in the extracellular membrane can be detected with an anti-HA monoclonal antibody. Subsequently, a second horseradish-peroxidase-coupled antibody is applied which detects the primary antibody. The horseradish-peroxidase from the secondary antibody enzymatically activates a chemiluminescent substrate and the evoked luminescence is measured with a luminometer. The luminescence is, in theory, proportional to the amount of bound secondary antibody and therefore proportional to the surface expression of the tagged protein.

To quantify surface expression, the (HA) epitope (YPYDVPDYA) was inserted in a non-conserved region in the extracellular loop of HyNaC2 between residues Phe_{124} and Asp_{125} by recombinant PCR (see 2.2.4.1). Oocytes were injected with a total of ≈3 ng cRNA. Two days after injection, the follicular membrane surrounding the oocytes was removed manually with forceps. The chemiluminescence measurement was performed four days after injection directly after immunollabeling. All of the following steps were carried out on ice: To block unspecific binding, oocytes were first incubated for 30 min in ND96 with 1% BSA. ND96 solution contained (in mM): 96 NaCl; 2 KCl; 2 MgCl; 1.8 CaCl; 10 HEPES; pH: 7.4 adjusted with 1 NaOH. After block, oocytes were incubated for 60 min with 0.5 µg/mg rat monoclonal anti-HA antibody (Roche, Germany). Following incubation, six washing steps in ND96 with 1% BSA removed unbound primary antibody. Subsequently, oocytes were incubated with 2 µg/ml horseradish-coupled secondary antibody (goat anti-rat F (ab´) 2 fragments, Jackson ImmunoResearch) for 60 min. After incubation, oocytes were washed six times with ND96 with 1% BSA followed by three washing steps in ND96 without BSA. Oocytes were then placed individually in wells of microplates and luminescence was quantified in an “Orion II microplate luminometer” (Berthold Detection Systems; Pforzheim). The chemiluminescent substrate (50 µl of Super Signal ELISA; Thermo Fisher) was added automatically and luminescence was measured after 2 s for 5 s. Relative light units per second (RLUs/s) were calculated as a measure of surface expressed channels. The results are from two independent experiments from two different frogs. Eight oocytes were analyzed for each experiment and each condition.

2.2.10 Synthesis of capped cRNA

For expression of HyNaCs in *Xenopus* oocytes, 5´-capped cRNA was synthesized from plasmid DNA by *in vitro* transcription with the SP6 “mMessage mMachine Kit” (Ambion). As template for transcription, HyNaCs cloned in the oocyte expression vector pRSSP 6009 were used. The vector carries a SP6 polymerase-binding site 5´-upstream of its multiple cloning site. Synthesis of cRNA was done according to the manufactures manual. In short, 2 µg of template DNA was linearized by restriction enzyme digest with Mlu I. The linearized DNA was purified from proteins and contaminations by phenol/chloroform extraction and then precipitated at -80°C with 550 µl 100% ethanol and 20 µl 3M NaAc. After centrifugation at 4 °C for 12 min, the DNA was dried in a centrifugal evaporator and resuspended in 6 µl DEPC H_2O. The cRNA synthesis was performed with 5 µl of the purified DNA template for 2

hours according to the manufacturers instructions. After cRNA synthesis, the reaction-mix was precipitated by adding 30 µl DEPC H_2O and 30 µl precipitation solution containing 7 M LiCl and 50 mM EGTA. The precipitated RNA was centrifuged at 4°C for 15 min to pellet the cRNA. The supernatant was removed, the pellet was washed with 1 ml 70% EtOH and again centrifuged at 4°C for 15 min. The supernatant was removed again and the cRNA pellet was resuspended in 20 µL DEPC H_20. Finally, the concentration of cRNA was adjusted to ≈200 ng/µl by running samples on an agarose gel against RNA standards with known concentration. The cRNA was separated into aliquots and stored at -80°C.

2.3 Electrophysiological methods

2.3.1 Preparation and handling of oocytes

Stage V to VI oocytes (Eppig and Dumont, 1974) were surgically removed from *Xenopus leavis* frogs that had been anaesthetized for 30 min in tap water containing 1% (w/w) ethyl 3- aminobenzoate methanesulfonate salt (Sigma) prior to surgery. After anaesthetisation, the frog was placed on ice and a ≈1cm long cut along the body axis into the abdominal skin and subcutaneous musculature layer was made in order to remove a sufficient number of oocytes. After removal of oocytes the cuts of skin and muscle layer were stitched separately with absorbable yarn. Frogs were operated several fold; the interval between individual surgeries was at least 3 month.

The freshly removed oocytes are agglutinated in “bags” consisting of connective tissue and blood vessels. To isolate single oocytes, the bags were roughly reduced to small pieces with forceps. Afterwards, oocytes were separated enzymatically by shaking in OR-2 medium containing 1mg/ml collagenase type A (Sigma) for approx. 2 hours. After incubation, oocytes were extensively washed in OR-2 to completely remove the collagenase. Healthy looking oocytes were manually selected for injection.

2.3.2 Injection of oocytes

For injection of cRNA, EGTA or Fura2-AM into oocytes, pulled glass capillaries (Order ID 4878; World Precision Instruments) were used. Capillaries were pulled with an automatic puller (Flaming/Brown Micropipette Puller Model P-97; Sutter Instrument Co.) in two pulling

steps. Before the capillaries were mounted to the microinjector, the tips were manually broken under a stereomicroscope to enlarge the tip diameter. Afterwards, the capillaries were backfilled with paraffin oil and mounted on a hand driven microinjector (Nanoliter 2000, World Precision Instruments). The oocytes were placed on a petri-dish containing boreholes to fixate the oocytes and filled with OR-2 solution The petri-dish containing the oocytes and the microinjector were mounted on a custom made coarse manipulator driven table to facilitate the injection.

2.3.2.1 Concentrations and volumes used for injection

Injection volume of cRNA was 41.6 nl. If cRNA was injected undiluted, the total amount of RNA per oocyte was ≈8 ng. To adjust the expression level of the individual ion channels, cRNA was diluted with DEPC H_20, if necessary. If not stated otherwise, the following dilutions were used: HyNaC2/3 undiluted; HyNaC2/3/5_D-C undiluted; HaFaNaC undiluted; HyNaC2/3/5 1:25; for the bioluminescence assay, a total amount of ≈2.8 ng was injected for each condition. After injection, oocytes were incubated in OR-2 2-4 days at 19°C before measurements.

To suppress the calcium activated chloride channels (CaCCs), 50 nl EGTA or BAPTA solution was injected 30-120 min before the experiments. EGTA solution contained (in mM): 20 EGTA, 5 HEPES, pH was adjusted to 7.4 with NaOH. For the BAPTA solution, EGTA was replaced by an equimolar amount of BAPTA.

For photometric calcium measurements, oocytes were injected with 50 nl Fura2-AM (1 mM) 30-120 min prior to the recording. The AM ester form was used solely due to availability.

2.3.3 Production of glass electrodes for the TEVC-measurements

As electrodes for the TEVC, borosilicate capillaries with filament (1.05 mm ID, 1.5 mm OD) were used. They were pulled with an automatic puller (Flaming/Brown Micropipette Puller Model P-97; Sutter Instrument Co.) in two pulling steps. Capillaries were filled with 3M KCl solution and had a resistance in the range of 0.5-1.5 MΩ.

2.3.4 Setup for TEVC-measurements:

Electrophysiological recordings were performed with the software-controlled, semi-automated OTC-20 system (npi Electronics). This system consists of a rotary table, a recording chamber and a control interface. The recording chamber is equipped with holders for fixation and movement of the two electrodes as well as adapters for the voltage and current grounding electrodes. It is situated above the rotary table that carries the individual recording solutions. During measurement, the oocyte is fixed in the chamber via suction on a glass electrode. Recording solutions are applied via the rotary table that can be loaded with up to 20 different petri-dishes. Thereby, the solution in the petri-dish situated under the recording chamber is, controlled by a valve, sucked into the recoding chamber. The turntable and the valve are controlled by the OTC-20 interface. Due to the small chamber volume, this setup allows the exchange of 80% solution within 300 ms (Chen et al., 2006b). The whole setup was made up of a TurboTec03X amplifier (npi Electronics), an oscilloscope HM 507 (Hameg Instruments) and a computer equipped with the AD/DA interface PCI 1200 (Texas Instruments). Data acquisition and control of the OTC-20 interface was managed with the software Cellworks 6.2.2 (npi electronic).

2.3.5 Solutions used for TEVC-measurements

OR-2 solution (Oocyte ringer solution 2):

NaCl	82.5 mM
KCl	2.5 mM
Na_2HPO_4	1 mM
Polyvinylpyrroldione (PVP)	0.5 g/l
$MgCl_2$	1 mM
$CaCl_2$	1 mM
HEPES	5 mM
	pH: 7.3; adjusted with 1M NaOH

Standard bath solution:

NaCl	1mM
$CaCl_2$	1mM
HEPES	10 mM
	pH: 7.4; adjusted with 1 M NaOH

2.3.6 Analysis of electrophysiological data

Data were recorded with the software Cellworks 6.2.2 (npi Electronics) with a sampling frequency of 0.1-1kHz, filtered at 20 Hz and stored on hard drive. Analysis of data was done either using Cellworks or the software IgorPro 6.02 (Wave Metrics). Statistical analysis and determination of significance was done with Excel for Mac 12.3.2. (Microsoft) using Student´s paired or unpaired *t*-test, as appropriate. Figures were created using the software Canvas 10.6.8 (ACD Systems).

If not stated otherwise, voltage was clamped at -70 mV and measurements were performed at room temperature (20-25°C).

Results are reported as means ± SEM unless stated otherwise. They represent the mean of *n* individual measurements on different oocytes.

Concentration response curves were determined by fitting data to the *Hill* function (Hill, 1910):

$$I = a + \frac{\left(I_{\max} - a\right)}{\left[1 + (EC_{50}/[c])^{n}\right]} \qquad (1)$$

Where I_{max} is the maximal current, *a* is the residual current, [c] is the concentration of the ligand, EC_{50} is the concentration at which half maximal activation occurs and *n* is the Hill coefficient.

For determination of reversal potentials E_{rev}, all current-voltage relationships were corrected for background conductivities by subtracting the currents measured at a given voltage without agonist application. For calculation of reversal potentials and calculation of relative permeabilities (in Figs. 23; 24D; 25A and B), oocytes were additionally injected with EGTA (20 mM) to minimize the influence of CaCCs. All I-V relationships were corrected for

background conductances by subtracting the currents measured without agonist application.

Ionic permeability ratio for monovalent cations P_{Na}/P_K (see 3.2.3) was calculated from the shift in E_{rev} when NaCl in the standard bath solution was replaced by an equimolar amount of KCl, according to the following equation derived from the Goldman-Hodgkin-Katz equation (Hille, 2001):

$$\frac{P_{Na}}{P_K} = \frac{\left[K^+\right]_o}{\left[Na^+\right]_o} e^{\left(\frac{\Delta E_{rev} * F}{R * T}\right)} \qquad (2)$$

Where $\Delta E_{rev} = E_{Na} - E_K$, R is the gas constant, F is the Faraday constant, and T is the temperature. It was assumed that the intracellular concentrations of Na^+ and K^+ are constant within one batch of oocytes.

Assuming additionally that $[Ca^{2+}]$ is very small, P_{Ca}/P_{Na} can be calculated from the shift in E_{rev} when Na^+ was replaced by Ca^{2+} in the application solution, according to the following equation (Lewis, 1979; Bässler et al., 2001):

$$\frac{P_{Ca}}{P_{Na}} = \frac{\left[Na^+\right]_o \left(1 + e^{\frac{E_{Ca} * F}{R * T}}\right)}{4\left[Ca^{2+}\right]_o e^{\frac{\Delta E_{REV} * F}{R * T}}} \qquad (3)$$

Where $\Delta E_{rev} = E_{Na} - E_{Ca}$; R, T and F have the same meaning as above. The solution used to determine E_{Ca} contained (in mM): $CaCl_2$ 10, NMDG-Cl 126.5, HEPES 10, pH 7.4; the solution used to determine E_{Na} contained: NaCl 140, $CaCl_2$ 1, HEPES 10, pH 7.4. The minor amount of Ca^{2+} in this solution was considered negligible.

Activity of ions was used in all terms of [*c*]. Activity coefficients f_i of single ions *i* of valence *z* were calculated for Na^+ and Ca^{2+} with a modified *Davies* equation (Davies, 1962; Bässler et al., 2001):

$$\log_{10} f_i = -0.509 z^2 \left(\frac{\sqrt{I}}{1 + \sqrt{I}} - 0.2 I\right) \qquad (4)$$

Where I is the ionic strength, which is defined as (Bässler et al., 2001):

$$I = 0.5 \Sigma \; c_i z_i^2 \qquad (5)$$

In all figures of this work showing voltage ramps and in the bioluminescence assay, the individual conditions were were measured with different oocytes of the same batch (except measurements for the P_2X_4 receptor in Fig. 23B, which were performed on separate batches of oocytes). Furthermore, batches of oocytes were identical between Fig. 21 and Fig. 24D and between Fig. 23A and Fig. 25A.

2.4 Photometric calcium measurements

Oocytes were injected with 50 nl Fura2-AM (1 mM) 30-120 min prior to the recording and were placed with the animal pole facing away from the objective on a 35mm petri dish that was filled with 4.5 ml standard bath solution and had a drilled hole to fixate the oocyte. Measurements used a BX51WI upright microscope (Olympus) with a 40x water immersion objective (NA 0.8) and a TILL photometry system (TILL Photonics, Gräfelfing, Germany). The region of interest chosen for recording included most of the upper surface of the cell. The penetration depth of the optics into the oocyte was unknown but is estimated not to be more than a few micrometers. Fura-2 was excited every 2 seconds with a 100 ms pulse of 340 nm light and a 50 ms pulse of 380 nm light using a Polychrome 5 light source (TILL Photonics). Emission was collected by a Photodiode (TILL Photonics) behind a 535/30 nm bandpass filter, digitized at 5 kHz by a LIH8+8 interface run by Patchmaster software (HEKA, Lambrecht, Germany). Emission during the 340 nm pulse and the 380 nm pulse was averaged and the F340/F380 ratio determined for each time point (emission with 340 nm excitation / emission with 380 nm excitation). As emission was generally lower with 340 nm than with 380 nm excitation, a longer recording was taken for the 340 nm excitation to increase the signal-to-noise-ratio. Currents were recorded simultaneously with a TurboTec03X amplifier (npi Electronics) filtered at 20 Hz and digitized at 100Hz also using the LiH8+8 interface and Patchmaster software. To activate HyNaCs, 500 μl HydraRFamide I (10μM) was manually applied to the petri dish to achieve a final concentration of ≈1 μM.

Data were analyzed offline using IGOR Pro (WaveMetrics, Lake Oswego, USA). The fluorescence changes induced by HyNaC agonists were reproducible and large compared to the signal-to-noise-ratio (Fig. 22A). On average, they were 47 ± 9 % of baseline F340/F380 ratio and small compared to the variation between cells in resting F340/F480 ratio (Fig. 22B). Therefore no calibration and conversion of the F340/380 signal into absolute intracellular concentrations of Ca^{2+} could be performed.

III. Results

3.1 Part I - Three homologous subunits form a high affinity peptide-gated ion channel in *Hydra*

3.1.3 Aims of the first study

The diverse physiological roles and gating mechanisms of DEG/ENaCs raise the question of the primordial functions of these channels in their common ancestor. Which features arose early in evolution and can be considered as basic and evolutionary conserved and which features developed later and are only found in individual subgroups of the channel family? This question can be addressed by comparative analysis of DEG/ENaCs from evolutionary separated groups of animals. Animals from the phylum Cnidaria are especially suited to answer this question, as they are the most basic group in which a nervous system has evolved. *Hydra magnipapillata* belongs to the phylum Cnidaria and is an important model organism for the evolution of the nervous system and developmental processes. Therefore, our group has cloned new DEG/ENaC members from *Hydra* and named them HyNaCs (*Hydra* sodium channels). It was already shown in a previous study that HyNaC2 and 3 together form an ion channel directly gated by endogenous neuropeptides (Golubovic et al., 2007; 2007) .

The aim of the first part of this thesis was the characterisation of HyNaC5, a novel DEG/ENaC subunit from *Hydra*. Therefore, HyNaC5 was heterologously expressed in *Xenopus* oocytes to identify possible ligands, interaction partners and current characteristics of the novel subunit by TEVC-recordings. Moreover, the specific expression pattern of HyNaC5 in *Hydra was* revealed with an *in situ* hybridisation assay. Finally, in a behavioural assay, we attempted to figure out putative physiological functions of HyNaCs in the living animal.

3.1.3 Cloning of HyNaC5 from *Hydra magnipapillata*

A new partial sequence with high homology to HyNaC2-4 from *Hydra magnipapillata* was identified by screening an on-line *Hydra* Expressed Sequence Tag data base and used to design primers for rapid amplification of 5´ and 3´-cDNA ends (RACE). From these 5´- and 3´-RACE products, a new full-length cDNA was cloned in our group by Stefan Gründer. The corresponding protein was named HyNaC5 and was kindly provided for further characterisation (see Appendix for methods). The predicted amino acid sequence of HyNaC5 is shown together with the sequences of HyNaC2–4 in Fig. 10A.

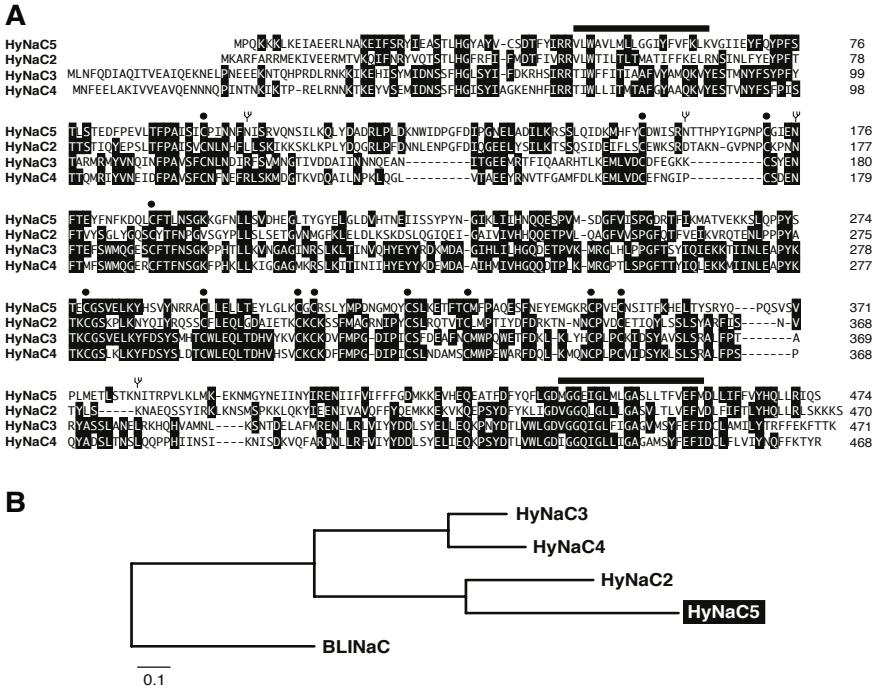

Fig. 10: (A) Sequence alignment of HyNaC5 with HyNaC2–4. Amino acids showing a high degree of identity are shown as *white letters* on a *black background*. The putative positions of transmembrane domains are indicated by *bars*, conserved cysteines are indicated by *circles*, and consensus sequences for N-linked glycosylation in HyNaC5 are indicated by *branched symbols*. Accession numbers are as follows: HyNaC2, AM393878; HyNaC3, AM393880; HyNaC4, AM393881; and HyNaC5, FN257513. (B) *Phylogram* illustrating the relationship of HyNaCs. Amino acid sequences of HyNaC2–5 and rat BLINaC were aligned, and the tree for the phylogram was established by Neighbor Joining with ClustalX; highly divergent sequences at the N- and C-termini had been deleted. Branch lengths are proportional to the evolutionary distance. BLINaC is a related channel (Golubovic et al., 2007) that was included for comparison; the accession number of rat BLINaC is Y19034.

(From: Dürrnagel et al., 2010)

The degree of amino acid sequence identities between HyNaC5 and HyNaC2–4 ranges from 28–44%; the closest relative is HyNaC2 (Fig. 10B). Thus, sequence identities between different HyNaCs are similar to sequence identities between the three subunits of the

epithelial Na^+ channel, ENaC (Canessa et al., 1994). The open reading frame of the HyNaC5 cDNA codes for a protein of 473 amino acids with a predicted molecular mass of ≈55 kDa. HyNaC5 shows the structural hallmarks of the DEG/ENaC gene family: two hydrophobic transmembrane domains, short N- and C-termini, and a large extracellular loop containing 12 conserved cysteines between the two hydrophobic domains (Fig. 2). A topology with two transmembrane domains, a large ectodomain, and short intracellular termini is common to all DEG/ENaC subunits (Jasti et al., 2007).

3.1.3 Expression pattern of HyNaC5

To investigate the expression pattern of *hynac5* in *Hydra,* a 1435 bp fragment from the coding part of HyNaC5 cDNA was cloned into the vector pBluescriptKS and used as probe for whole mount *in situ hybridization* (ISH). The ISH was carried out by Anne Kuhn in the lab of T.W. Holstein, Heidelberg, Germany (see Appendix for methods). It revealed strong expression of *hynac5* at the base of the tentacles (Fig. 11A), most likely in epitheliomuscular cells. During budding, *hynac5* is expressed at the sites of tentacle formation, immediately before the first tentacle bumps appear (Fig. 11G). Thus, the expression pattern of *hynac5* is very similar to the expression patterns of *hynac2* and *hynac3* (Fig. 11) (Golubovic et al., 2007), suggesting that the three genes are coexpressed in *Hydra* cells.

A more careful comparison, however, reveals subtle differences in the expression pattern of the three genes. Although *hynac2* and *hynac3* are uniformly expressed at the tentacle base (Fig. 11, B and C), *hynac5* expression is strongest at the oral site of each tentacle base with a gradient toward the aboral site (Fig. 11 and Fig. 12A).

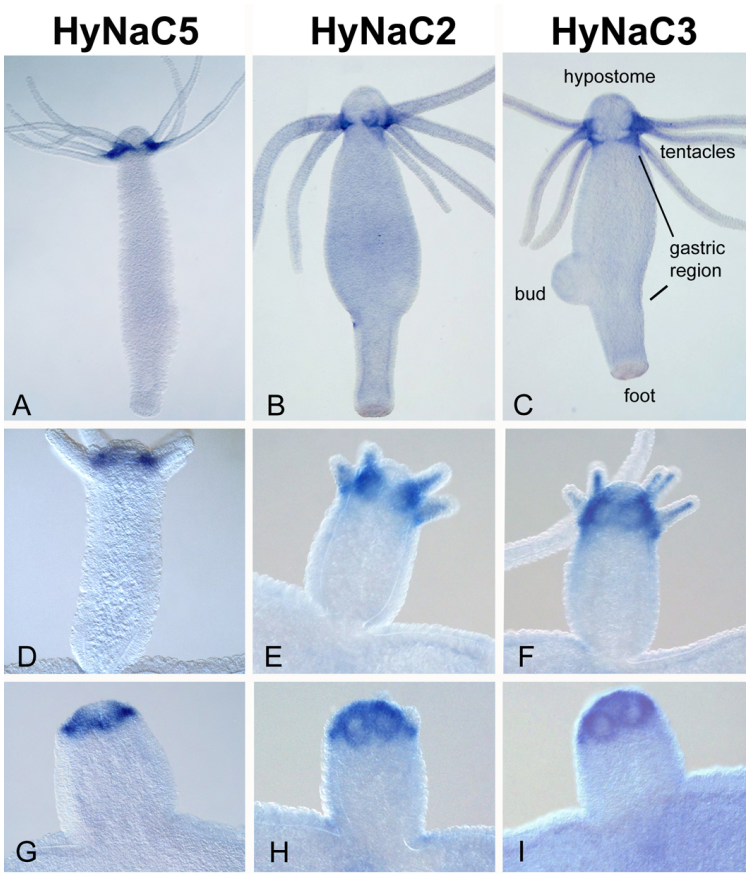

Fig. 11: *hynac5* is expressed at the base of the tentacles. Whole mount *in situ* hybridization reveals strong expression of *hynac5* transcripts at the tentacle base in adult animals (A) and buds (D and G). By comparison, *hynac2* and *hynac3* transcripts are uniformly distributed (B and C). During bud formation, *hynac5* transcripts appear as soon as tentacles begin to appear (G) similar to *hynac2* and *hynac3* (E and F, and H and I). Expression of *hynac5* is strongest at the *upper side* (oral) of the tentacles (A); primary magnifications are 4 × (A–C) and 20 × (D-I).

(From: Dürrnagel et al., 2010)

By comparison, *hynac4* expression exhibits a strong restriction to the aboral site of the tentacles (Fig. 12B) (Golubovic et al., 2007). The mutually exclusive expression patterns of *hynac4* and *hynac5* at the base of the tentacles suggest a different function for HyNaC4 and HyNaC5. Previously, it was speculated that activation of HyNaCs leads to tentacle contractions during the “feeding reaction” of Hydra (Golubovic et al., 2007). The feeding reaction is induced by physical contact with a prey animal and characterized by an upward movement and contraction of the tentacles, which brings the prey close to the mouth (Loomis, 1955). Perhaps HyNaC4 and HyNaC5 have distinct roles in the coordination of this feeding behavior.

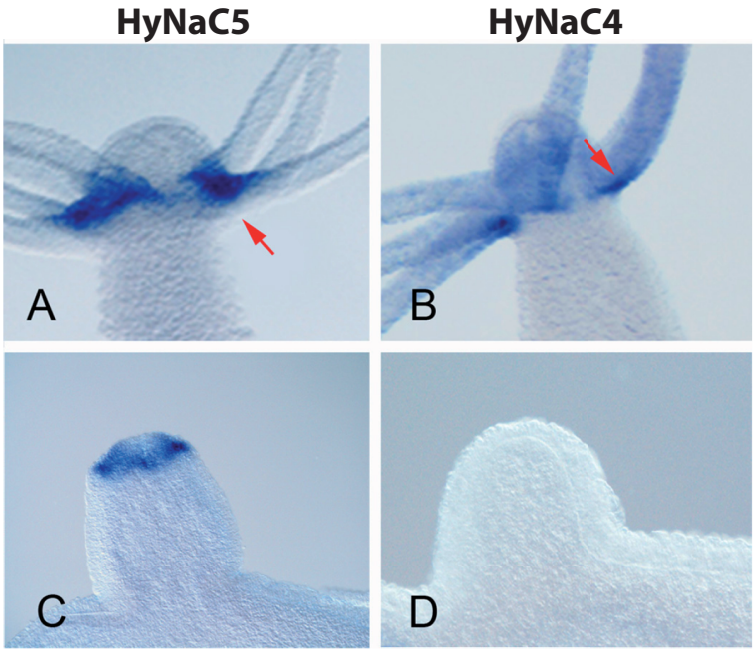

Fig. 12: *hynac5* and *hynac4* show complementary expression patterns. *hynac5* is expressed at the oral site of the tentacle bases (A) and in early bud (C), whereas *hynac4* is expressed at the aboral site of the tentacles (B); it also lacks any expression in early bud stages. *Arrows* indicate the different expression zones of both genes; primary magnifications are 20 × (A–C).

(From: Dürrnagel et al. 2010)

3.1.3 HyNaC5 strongly increases the current amplitude of the HyNaC2/3/5 heteromer

The functional properties of HyNaC5 were investigated by expression in *Xenopus* oocytes; cRNAs coding for HyNaC2–5 were injected in oocytes either alone or in combination. Oocytes expressing HyNaC5 alone or in combination with one other HyNaC subunit (2, 3, or 4) could not be activated by any of the four HydraRFamides (I–IV; data not shown). In contrast and as previously reported (Golubovic et al., 2007), oocytes coexpressing HyNaC2 and -3 exhibited a robust current after stimulation with HydraRFamide I (Fig. 13A) and II (data not shown); current amplitudes were usually in the range of a few μA. Oocytes expressing HyNaC5 in addition to HyNaC2 and -3 could also be activated by RFamides I and II and showed dramatically increased current amplitudes compared with oocytes coexpressing only HyNaC2 and -3: current amplitudes of oocytes expressing HyNaC2, -3, and -5 were so large (<50 μA) that they were above the capacity of the used TEVC-amplifier

(Fig. 13A, *left panel*). A quantitative comparison with oocytes, which had been injected with 25-fold diluted RNA, and half-maximal peptide concentrations (see below) revealed a 16-fold increase in the peak current amplitude of HyNaC2/3/5 compared with HyNaC2/3 ($p \leq 0.01$; Fig. 13A, right panel), strongly suggesting that HyNaC5 was incorporated in the channel complex to form a HyNaC2/3/5 heteromer.

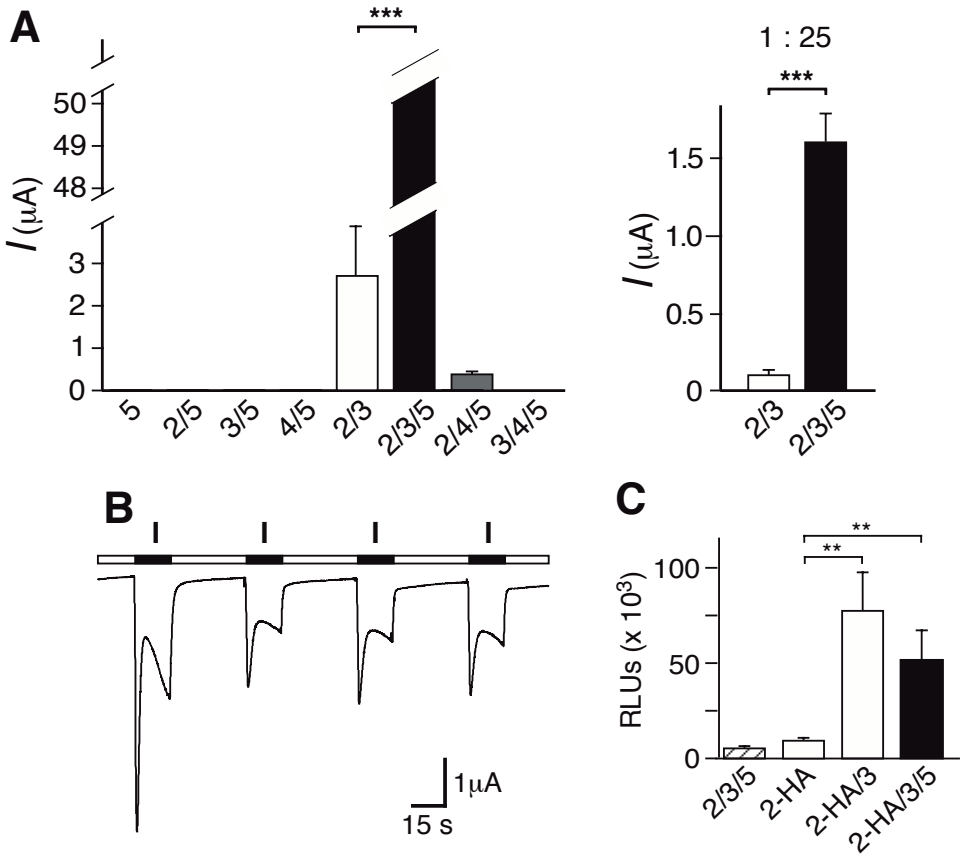

Fig. 13: (A) HyNaC5 potently increases the current amplitude of the HyNaC2/3 heteromer. *Left*, *bar graphs* illustrating the whole oocyte current amplitude after coexpression of different combinations of HyNaC subunits; HyNaCs were activated with 30 μM HydraRFamide I. For each condition, a total of ≈8 ng cRNA had been injected in oocytes. Note that the amplitude for HyNaC2/3/5 was > 50 μA and therefore only a lower limit of the amplitude can be given. *Error bars* represent S.E.; for HyNaC2/3/5, the S.E. could not be calculated. n =10 oocytes. *Right*, bar graphs illustrating current amplitude of oocytes coexpressing HyNaC2/3 or HyNaC2/3/5; a total of ≈0.3 ng cRNA had been injected. Both channels were activated with a concentration of HydraRFamide II eliciting half-maximal response: HyNaC2/3 with 33 μM and HyNaC2/3/5 with 0.35 μM. ***, $p \leq 0.001$. (B) representative current traces for the HyNaC2/3/5 heteromer. Repeated activation of HyNaC2/3/5 with Hydra-RFamides led to decreased response between the first and second application; in the example shown, 30 μM HydraRFamide I was used. cRNA for HyNaCs 2, 3, and 5 was diluted 25-fold (a total of 0.3 ng/oocyte). (C) HyNaC5 does not increase surface expression of the HyNaC2/3 heteromer. Surface expression of HyNaC2 and HyNaC2/3 in comparison to HyNaC2/3/5 (mean ± S.E.); only the HyNaC2 subunit was HA-tagged. Oocytes injected with untagged HyNaC2/3/5 served as a control (*first column*). The results are expressed as *relative light units* (*RLUs*)/oocyte/s (n = 16). **, $p \leq 0.01$.

(From: Dürrnagel et al., 2010)

The crystal structure of an ASIC1 - a related acid-sensing ion channel - revealed a number of three subunits in the functional channel (Gonzales et al., 2009; Baconguis and Gouaux, 2012). Because acid-sensing ion channels are close relatives of HyNaCs in the DEG/ENaC gene family (Golubovic et al., 2007), it is reasonable to assume that functional HyNaCs are also composed of three subunits, suggesting a 1:1:1 ratio for the HyNaC2, -3, and -5 subunits in the functional complex.

In the remainder of this study, 25-fold diluted cRNAs of HyNaC2/3/5 were usually injected to get current amplitudes in the range of 1–30 μA. Oocytes coexpressing HyNaC5 together with HyNaC2 and -4 could also be activated by HydraRFamides I and II; current amplitudes were much smaller than for the HyNaC2/3/5 heteromer, however (Fig. 13A), suggesting that although HyNaC4 is closely related to HyNaC3 (Fig. 10B) it cannot efficiently replace it in the heteromeric complex. Fig. 13B shows representative current traces of oocytes expressing HyNaC2, -3, and 5. Similar to HyNaC2/3 channels (Golubovic et al., 2007), HyNaC2/3/5 currents exhibited a biphasic morphology when measured in *Xenopus* oocytes: A rapid declining peak amplitude was followed by a sustained current. A second application of the ligand induced currents with significantly smaller amplitudes than the first application. Further applications of the ligand induced currents with amplitudes comparable with the second application. In previous reports, this current characteristic was stated as an intrinsic property of HyNaC channels (Golubovic et al., 2007; Dürrnagel et al., 2010). However, these conclusions were wrong. HyNaC 2/3/5 and most likely also HyNaC 2/3 are highly permeable for Ca^{2+} (see 3.2 and Discussion). The influx of Ca^{2+} through HyNaCs leads to strong activation of Ca^{2+} activated chloride channels (CaCCs), which are endogenously expressed in *Xenopus* oocytes. Therefore, all current traces shown in the first part of the results are the sum of two current components: The HyNaC current and the current that rises from secondary activation of CaCCs. When CaCCs are blocked by injection of the Ca^{2+} chelators EGTA or BAPTA, the simple, step-like, non-desensitizing current characteristic of HyNaC2/3/5 is revealed (Fig. 19). The reduction of current amplitudes after repeated activation is mediated by run-down of CaCC currents.

3.1.3 HyNaC5 strongly increases the current through surface-expressed HyNaCs

Increased current amplitudes of the HyNaC2/3/5 heteromer compared with the HyNaC2/3 heteromer (Fig. 13A) can be due to increased surface expression and/or increased current through surface-expressed channels. To differentiate between these possibilities, the expression level of the two heteromers at the oocyte surface was compared. Therefore an HA-epitope was inserted into the extracellular loop of HyNaC2 and by use of a monoclonal anti-HA antibody and a luminescence assay the surface expression of HA-tagged channels was compared (Chen and Gründer, 2007). Luminescence was not significantly different (p = 0.3) between oocytes expressing the HyNaC2/3/5 heteromer and oocytes expressing the HyNaC2/3 heteromer (Fig. 13C). For oocytes expressing the heteromers, luminescence was, however, significantly larger than for oocytes expressing HyNaC2-HA alone ($p \leq 0.01$), for which luminescence was not significantly above background (p = 0.2; Fig. 13C). Assuming a number of three subunits in a functional HyNaC (Gonzales et al., 2009), in the 2/3/5 channel only one subunit per channel was tagged, whereas in the 2/3 channel either one or two subunits were tagged, depending on the subunit stoichiometry (2/3/3 or 2/2/3). Therefore, in the case of a 2/2/3 channel, the assay would underestimate the surface expression of the 2/3/5 channel relative to the 2/2/3 channel by a factor of two. Even in this case, however, the difference in surface expression (at most 2-fold) cannot account for the 16-fold difference in current amplitude (Fig. 13A). Thus, HyNaC5 predominantly increases the current through surface-expressed channels. This result suggests that the HyNaC2/3 heteromer either has a small single channel amplitude or that HydraRFamides are partial agonists at this channel, leading to a low open probability.

3.1.3 HyNaC5 changes the properties of the HyNaC2/3 heteromer

Similar to HyNaC2/3, HyNaC2/3/5 was activated by HydraRFamides I and II. For both peptides, the affinity of HyNaC2/3/5 was increased ≈100-fold compared with HyNaC2/3 (Fig. 14): half-maximal activation was obtained with 4.8 ± 2.0 μM (n = 8) HydraRFamide I and 0.34 ± 0.08 μM (n = 8) HydraRFamide II compared with 326 ± 108 μM and 38 ± 13 μM (n = 4, each), respectively, for HyNaC2/3. In each case, the concentration response curve could be well fitted assuming a single population of channels, suggesting that most of the

channels in oocytes coexpressing HyNaC2, -3, and -5 were of a single type (2/3/5). Hill coefficients were similar for HyNaC2/3/5 and HyNaC2/3 (0.9 ± 0.1 compared with 0.8 ± 0.1 for HydraRFamide I, $p = 0.6$, and 1.8 ± 0.2 compared with 1.7 ± 0.4 for HydraRFamide II, $p = 0.8$, respectively; $n = 8$ for HyNaC 2/3/5 and $n = 4$ for HyNaC 2/3).

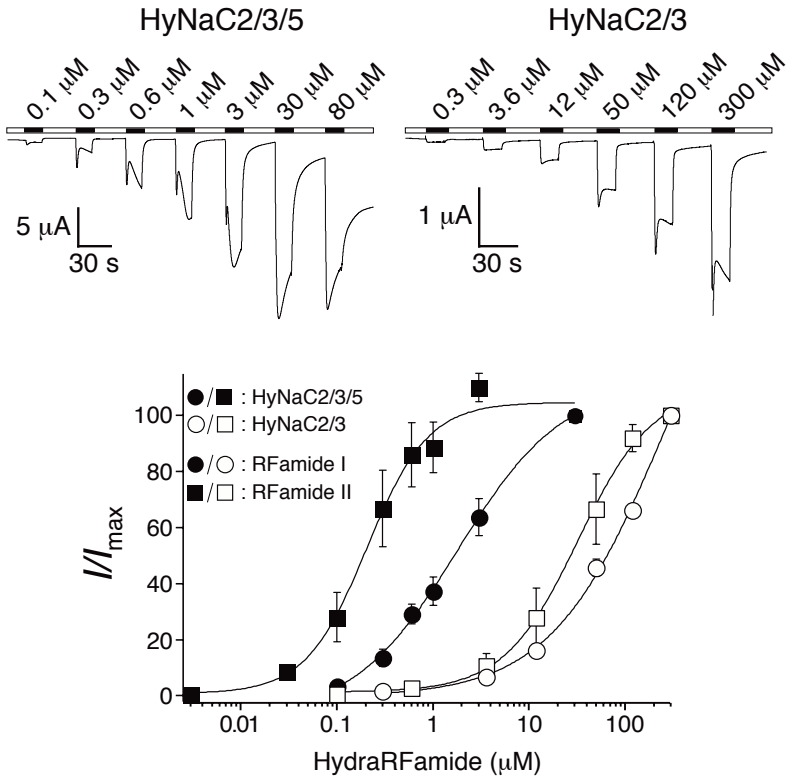

Fig. 14: HyNaC5 strongly increases apparent affinity for HydraRFamides. *Top*, representative current traces of whole oocytes either expressing HyNaC2 and -3 or HyNaC2, -3, and -5; channels were activated with HydraRFamide I. *Bottom*, concentration-response curves for HyNaC2/3 (*open symbols*) and HyNaC2/3/5 (*closed symbols*), each with HydraRFamides I (*circles)* and II (*squares*). *Error bars* represent S.E., and lines were fitted to the Hill function. Current amplitudes were normalized to the amplitude obtained with the highest concentration of the ligand (I_{max}) ($n = 8$ for HyNaC2/3/5 and $n = 4$ for HyNaC 2/3).

(From: Dürrnagel et al., 2010)

It is important to mention that the apparent affinities were measured without block of secondary activated CaCCs. Therefore, the EC_{50} values and Hill coefficients should be considered as rough estimate. However, concentration response curves recorded for HyNaC2/3/5 that had been injected with EGTA to block contaminating CaCC currents yielded comparable EC_{50} values (Marc Assmann, personal communication).

Previous evidence suggested that HydraRFamides activate HyNaC2/3 directly and not by a second messenger cascade (Golubovic et al., 2007). Activation of HyNaC2/3/5 with a strongly increased affinity for HydraRFamides further confirms that the binding sites for HydraRFamides are on HyNaCs and that these peptides directly activate HyNaCs. In

oocytes expressing the HyNaC2/3/5 heteromer (dilution, 1:25), high concentrations (50 μM) of HydraRFamides III and IV also elicited a tiny current (≈0.1 μA; data not shown), suggesting that these peptides are agonists at this channel with a very low affinity. HydraRFamides III and IV did not activate other subunit combinations, also containing HyNaC4. One might speculate that a related channel, perhaps containing HyNaC4 in combination with other HyNaC subunits not yet identified, is the high affinity receptor for HydraRFamides III and IV.

Reversal potentials in standard bath solution were not significantly different between HyNaC2/3/5 and HyNaC2/3 (10.1 ± 1.2 mV compared with 8.6 ± 3.5 mV; n = 8; p = 0.69; Fig. 15A), indicating that both HyNaC2/3 and HyNaC 2/3/5 are unselective channels. The inward rectification of HyNaC2/3/5 suggests that for HyNaC2/3/5 outward K^+ currents are less well conducted than for HyNaC2/3.

However, due to secondary activation of CaCCs in consequence of the Ca^{2+} permeability of HyNaC2/3/5 and HyNaC2/3 channels, the reversal potentials are likely contaminated by chloride currents. Assuming an intracellular concentration of 33 mM intracellular chloride (Barish, 1983), the calculated equilibrium potential of chloride in standard bath solution is ≈ -38 mV. This would cause an artificial leftward shift of reversal potentials. Therefore, a more precise measurement of P_{Na+}/P_{K+} values of HyNaC 2/3/5 is given in chapter 3.2.3.

To further investigate the ion permeability, all extracellular Na^+ was replaced by Li^+ or K^+ and the current amplitude of inward currents at –70 mV was measured. In the case of HyNaC2/3/5, inward currents with K^+ and Li^+ as the main charge carrier were significantly smaller than Na^+ currents ($p < 0.01$; Fig. 15B). This relative current reduction was especially prominent for K^+ and indicates that HyNaC2/3/5 is more selective for Na^+ over K^+ and Li^+ than HyNaC2/3. In the case of HyNaC2/3, amplitudes of inward K^+ and Li^+ currents were also significantly smaller than Na^+ currents, but the reduction in relative amplitude was smaller than for HyNaC2/3/5 ($p < 0.01$; Fig. 15B). Together, these results show that the ion pore of HyNaC2/3/5 has slightly different permeability properties than the HyNaC2/3 pore.

In addition to a low selectivity for Na^+, the HyNaC2/3 pore is characterized by a low apparent affinity for the open channel blocker amiloride (Golubovic et al., 2007), which is also uncommon for DEG/ENaC channels.

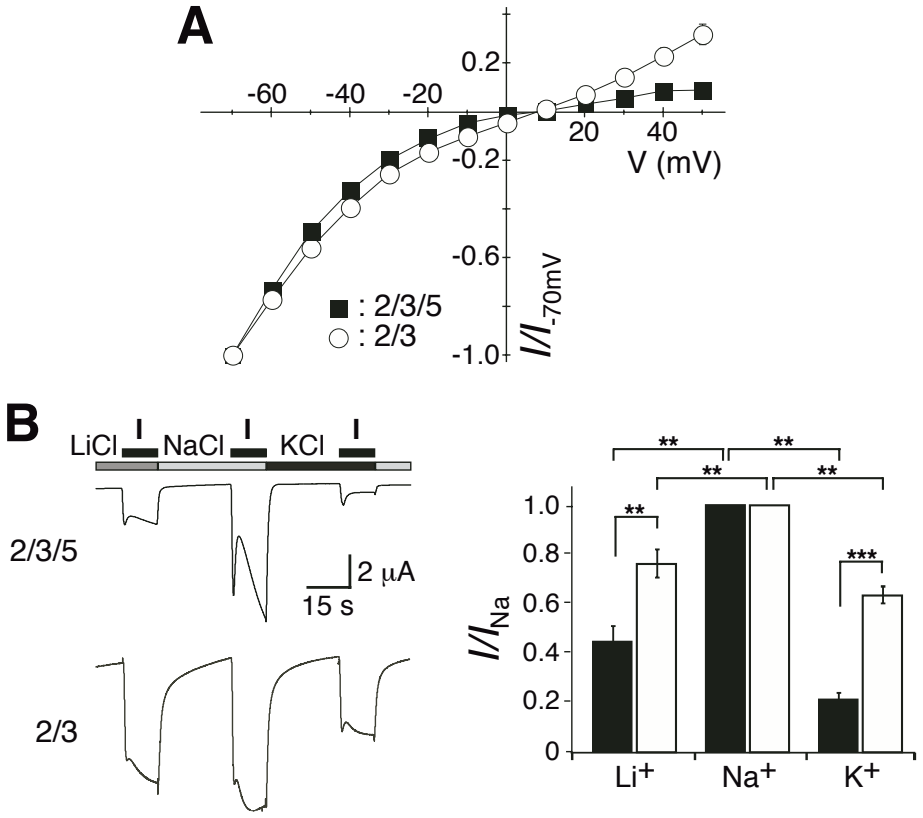

Fig. 15: Ion selectivity of HyNaC2/3/5. (A) the HyNaC5 subunit does not change reversal potentials. Channels were activated with 30 μM (HyNaC2/3) or 0.3 μM HydraRFamide I (HyNaC2/3/5), respectively, and reversal potentials measured by stepping to the indicated holding potentials for 3 s. (B) the HyNaC5 subunit decreases currents carried by K^+. *Left*, representative current traces of whole oocytes either expressing HyNaC2 and -3 or HyNaC2, -3, and -5. Channels were activated in the presence of different monovalent cations. *Right, bar graphs* illustrating the amplitude of the Li^+ and K^+ current relative to the Na^+ current; black bars represent HyNaC2/3/5, white bars HyNaC2/3. Error bars represent S.E. (12 oocytes); HyNaCs were activated with 30 μM (HyNaC2/3) or 0.3 μM HydraRFamide I (HyNaC2/3/5), respectively. In the presence of HyNaC5, amplitudes of Li^+ and K^+ currents were significantly reduced relative to the amplitude of the Na^+ current. **, $p < 0.01$; ***, $p < 0.001$, two-tailed *t* test.

(From: Dürrnagel et al., 2010)

According to previous findings, it was confirmed that for HyNaC2/3 the IC_{50} for amiloride is ≈500 μM (540 ± 160 μM; $n = 5$; Fig. 16A). In contrast, for HyNaC2/3/5 the IC_{50} for amiloride was significantly reduced (122 ± 9 μM; $p < 0.02$; $n = 6$; Fig. 16A). As FaNaC is not only activated but also blocked by its peptide ligand, FMRFamide (Green and Cottrell, 1999), it was tested whether the low apparent amiloride affinity of HyNaCs might be due to a competition with HydraRFamides at the rather high peptide concentrations (30 μM) used to determine amiloride affinity. However, even with a 100-fold lower concentration of the

peptide (0.3 μM), apparent amiloride affinity of HyNaC2/3/5 was not significantly increased (IC_{50} = 98 ± 18 μM; p = 0.2; n = 6; Fig. 16A), showing that HydraRFamides do not strongly compete with amiloride. Of note, at low concentrations (1 μM) amiloride slightly increased HyNaC current amplitudes.

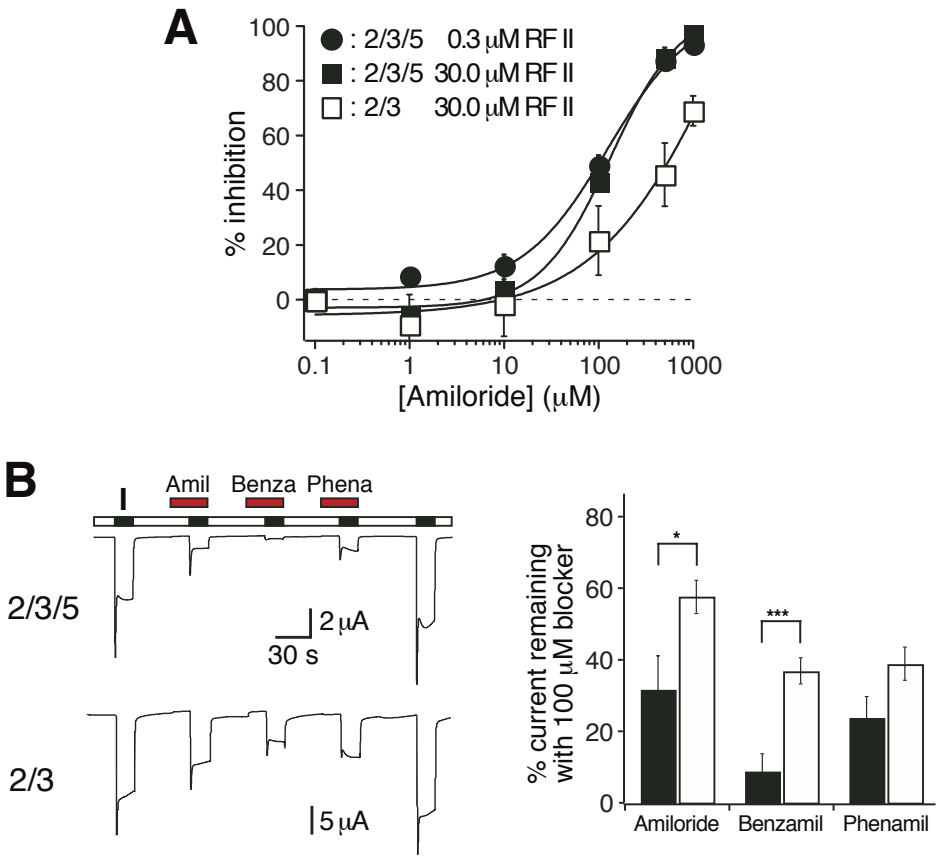

Fig. 16: HyNaC5 increases the apparent affinity for amiloride and amiloride analogs. (A), concentration response curve for the inhibition of HyNaC currents by amiloride. Curves were determined with 0.3 μM (HyNaC2/3/5) and 30 μM HydraRFamide II (HyNaC2/3 and HyNaC2/3/5), respectively (n = five oocytes for HyNaC2/3 and n = 6 oocytes for HyNaC2/3/5). (B), *left*, representative current traces of oocytes either expressing HyNaC2 and -3 or HyNaC2, -3, and -5. Channels were activated in the presence of different blockers (100 μM). *Right*, *bar graphs* illustrating the current remaining in the presence of the respective blockers; *black bars* represent HyNaC2/3/5, *white bars* HyNaC2/3. Before and after application of the blockers, channels were activated without blockers; the mean value of these two measurements was used to normalize the currents obtained in the presence of the blockers. *Error bars* represent S.E. (six oocytes); HyNaCs were activated with 30 μM (HyNaC2/3) or 1 μM HydraRFamide I (HyNaC2/3/5), respectively. In the presence of HyNaC5, amiloride (Amil) and benzamil (Benza) blocked significantly more current, suggesting an increased affinity for these blockers. *, $p < 0.05$; ***, $p < 0.001$, two-tailed t test. Phena, phenamil.

(Adapted from: Dürrnagel et al., 2010)

An increased open probability by amiloride has previously also been noted for FaNaC (Jeziorski et al., 2000; Green and Cottrell, 2002). Finally, the inhibition of HyNaC2/3 and

HyNaC2/3/5 by 100 μM of the two amiloride analogs benzamil and phenamil was investigated. Both blockers more potently blocked HyNaC2/3/5 than HyNaC2/3 ($p < 0.05$; Fig. 16B). This increased apparent affinity was highly significant for benzamil, for which 100 μM blocked almost 90% of the current. The increased apparent affinity for open channel blockers further support the conclusion that HyNaC5 is incorporated into the HyNaC2/3 channel complex and contributes to its ion pore.

3.1.3 Amiloride delays the feeding reaction of *Hydra*

In situ hybridization suggested that HyNaCs might contribute to the feeding reaction of *Hydra*. We tried to support this hypothesis by investigating the feeding reaction in the presence of amiloride in the medium. This experiment was carried out in collaboration with C. D. Tsiairis in the lab of T. W. Holstein, Heidelberg, Germany (see Appendix for methods).

The feeding reaction can be induced by glutathione (Loomis, 1955). After addition of glutathione (10 μM final concentration), *Hydras* responded quickly by moving their tentacles, contracting them, and bringing them to their mouth.

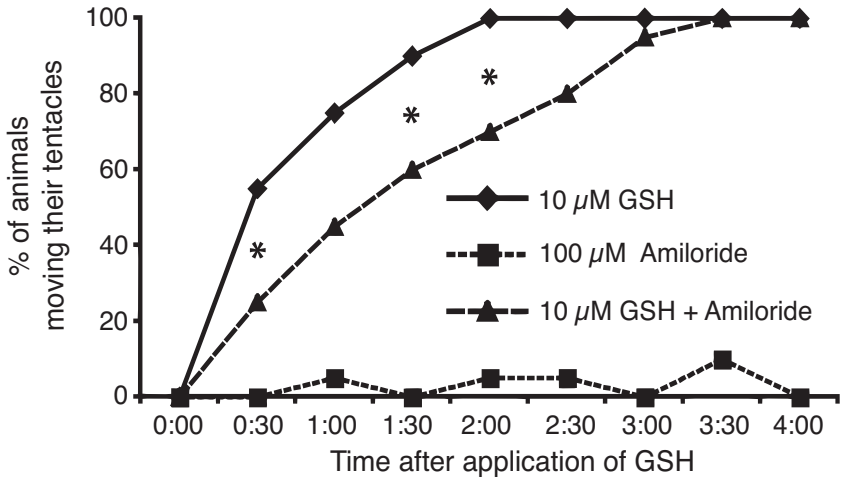

Fig. 17: Amiloride delays the glutathione induced feeding response. *H. magnipapillata* were relaxed in plain medium or medium containing 100 μM amiloride. At time 0, glutathione was added to a final concentration of 10 μM. Every 30 s, the number of animals moving their tentacles was recorded. A statistically significant delay in the response to glutathione (*GSH*) was detected in the presence of amiloride. The calculated p value is < 0.05 as indicated (by an *asterisk*), whereas it is 0.06 for the time point 1:00.
(From: Dürrnagel et al., 2010)

When the animals were in a medium containing 100 μM amiloride, however, the initiation of tentacles movement was significantly delayed ($p < 0.05$; Fig. 17). Moreover, the movements

did not lead to the characteristic contraction of the tentacles pointing them to the mouth. Similarly, the natural catching reaction after exposing *Hydra* to *Artemia* shrimps was inhibited by 100 mM amiloride (data not shown). These effects of amiloride were reversible; when animals were brought back to a medium without amiloride, they could feed on *Artemia* like the untreated ones and responded properly to glutathione by initiating the feeding reaction. Amiloride did not affect the general behavior of the animal; animals were still able to contract and move in the medium. However, they were unable to perform the coordinated movements of the tentacles associated with feeding reflex, suggesting the potential importance of amiloride-sensitive ion channels for the feeding reaction.

3.2 Part II - High Ca^{2+} permeability of a peptide-gated DEG/ENaC from *Hydra*

3.2.3 Aims of the second study

The aim of the first part of this work was the basic characterisation of HyNaC5. It was shown that coexpression of HyNaC2, -3 and -5 forms an ion channel that is directly gated by HydraRFamides and has different properties than the channel made of HyNaC2 and -3. HyNaC2/3 or 2/3/5 expressing oocytes exhibit a biphasic current consisting of a transient peak and a sustained component. In the first part of this work and in a previous study (Golubovic et al., 2007) the measured currents were entirely attributed to currents passing through the HyNaC pore. However, this assumption was wrong. HyNaC2/3/5 is permeable for Ca^{2+} and this Ca^{2+} influx through HyNaCs activates CaCCs, which are endogenously expressed in *Xenopus* oocytes. Therefore, the measured currents consist of a HyNaC and a CaCC fraction. This finding is surprising, as all known DEG/ENaC channels are Na^{+} selective and Ca^{2+} impermeable or conduct Ca^{2+} only to a minor extend. Therefore, this unique feature of HyNaCs was investigated in detail in the second part of this work. One main focus was to quantify the relative Ca^{2+} permeability and to compare it to other known Ca^{2+} permeable channels. Furthermore, the contaminating Cl^{-} currents in previous measurements demanded re-evaluation of some basic properties of HyNaC2/3/5 when CaCCs were blocked. Finally, we aimed to identify conserved amino acids that are crucial for the high Ca^{2+} permeability of HyNaC2/3/5.

3.2.3 The transient current in HyNaC-expressing oocytes is carried by Cl^-

Fig. 18A illustrates the typical biphasic currents elicited by HydraRFamide I (Moosler et al., 1996) in oocytes expressing HyNaC2/3/5 (named HyNaC in the remainder of the results, for simplicity). A fast transient current was followed by a slower sustained current; the ratio of transient and sustained currents was variable. Typically, a second peptide application elicited a similar response but of smaller amplitude (72 ± 8% of the first amplitude, $n = 11$, $p < 0.01$; Fig. 18A and Fig. 19A). A third application elicited a response of similar amplitude as the second (74 ± 9% of the first amplitude, $n = 11$, $p < 0.01$; Fig. 18A and Fig. 19A). The basis for this inactivation between first and second application has remained unclear.

In the first part of the results, E_{rev} of the sustained current was determined by stepping to different voltages during long agonist applications (Fig. 15A); E_{rev} was around +10 mV, indicating a relatively unselective cation current. Now, E_{rev} of the peptide-activated currents was determined by repeatedly activating HyNaC at different holding potentials between -70 and +20 mV. Notably, the transient and sustained components had different E_{rev}s (Fig. 18B and C). While at -20 mV the transient current was clearly outward, the sustained current was inward, showing that both currents had different ion selectivity. Although the strong rectification rendered a precise determination of E_{rev} of the sustained current difficult, it was estimated to be 2 ± 3 mV ($n = 6$; Fig. 18C), similar to the results in Fig. 15B. In contrast, E_{rev} of the transient current was -22 ± 2 mV ($n = 6$; Fig. 18C). Thus, the transient current clearly had different ion selectivity than the sustained current ($p < 0.001$). The leftward shift of the reversal potential, however, was not compatible with an increased Na^+-selectivity of the transient current. In addition, it is notable that at more depolarized potentials the amplitude of the transient outward current decreased rather than increased in amplitude (Fig. 18B and C). This decreased amplitude can now be attributed to a block by Ca^{2+} that inhibits flux of ions at more depolarized potentials (see below).

Assuming an intracellular Cl^- concentration of 33 mM, as reported for immature oocytes (Barish, 1983), in standard bath solution the Cl^- equilibrium potential was -38 mV, close to E_{rev} of the transient current. Therefore it was tested, whether Cl^- contributed to the transient current and E_{rev} was determined in Cl^--free solutions. Under these conditions, outward currents due to influx of Cl^- were abolished (Fig. 18D). While E_{rev} of the sustained current was not changed (E_{rev} = 0.6 ± 2.8 mV, $n = 5$, $p = 0.8$), no transient outward currents were

observed, strongly suggesting that the transient outward current in Cl^--containing solutions was carried by Cl^-.

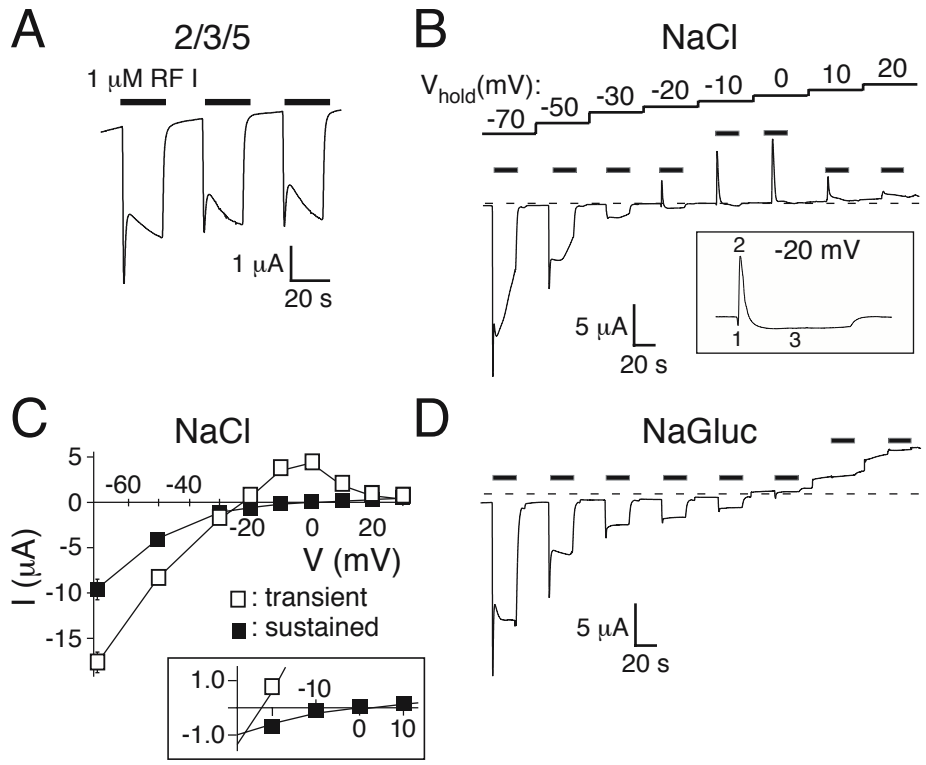

Fig. 18: Transient peptide-activated currents depend on Cl^-. (A) Representative current trace showing activation of HyNaC2/3/5 in standard bath. HyNaC was activated with 1 *μ*M HydraRFamide I (black bars). (B) Repeated activation of HyNaC at different holding potentials (V_{hold}) reveals the different reversal potentials of the transient and the sustained current component. A representative current trace in standard bath solution is shown. Note that the transient current changes to outward at more negative potentials than the sustained current. The inset highlights the three current phases (initial inward, transient outward, sustained inward) at a holding potential of -20 mV. (C) *I/V* plot revealing the different reversal potentials of the transient (*open squares*) and sustained current components (*filled squares*) in standard bath (*n* = 6). Note the strong inward rectification of both components. The inset shows the *I/V* relations close to the reversal potentials on an expanded scale. (D) Representative current trace in bath solution lacking Cl^- (NaCl replaced by NaGluconate). Note the absence of transient outward currents.

(From: Dürrnagel et al., 2012)

Xenopus oocytes contain a Ca^{2+}-activated Cl^- channel (CaCC) in their plasma membrane, which is activated by increases in intracellular Ca^{2+} concentration (Miledi, 1982; Barish, 1983). Activation of the CaCC leads to biphasic currents: an initial transient Cl^- current (Miledi, 1982; Barish, 1983; White and Aylwin, 1990) is followed by sustained Cl^- currents (Boton et al., 1990; Wu and Hamill, 1992; Schroeder et al., 2008), resembling the appearance of peptide-activated currents in HyNaC expressing oocytes. Moreover, repeated activation of the CaCC leads to reduced responses (Boton et al., 1990; Wu and

Hamill, 1992), akin to the reduced amplitude of peptide-activated currents with repeated peptide application (Fig. 18A and Fig. 19A). It was therefore considered that HyNaC is permeable to Ca^{2+} and that HyNaC activated the CaCC of oocytes. Closer inspection of measurements at a holding potential slightly positive to the Cl^- equilibrium potential (-20 mV) indeed revealed a current with three phases (Fig. 18B, inset): an initial inward current, which could reflect an initial influx of cations through HyNaCs, was followed by a transient outward current, presumably carried by the influx of Cl-, and a third sustained inward current, again dominated by influx of cations through HyNaCs.

3.2.3 The transient current is mediated by the endogenous Ca^{2+}-activated Cl^--channel.

To test for the activation of the CaCC, oocytes were injected with either EGTA or BAPTA to chelate Ca^{2+} and prevent a rise in intracellular [Ca^{2+}] and activation of the CaCC. Under these conditions, transient currents were indeed completely abolished and peptide-activated currents had a step-like appearance with no strong desensitization (Fig. 19A). Moreover, a second peptide application elicited a current of similar amplitude as the first application (for EGTA, 96 ± 5 % of the first amplitude, $p = 0.7$, and for BAPTA, 94 ± 2 % of the first amplitude, $p < 0.01$, paired t test, $n = 11$, Fig. 19A). In addition to the disappearance of transient currents, sustained currents had significantly smaller amplitudes after injection of EGTA or BAPTA (for EGTA, 43 ± 6 % of the sustained current amplitude without EGTA injection, $p < 0.01$, and for BAPTA, 47 ± 6% of the sustained current amplitude without BAPTA injection, $p < 0.01$, $n = 11$; Fig. 19A), suggesting that the CaCC current may contribute not only to the transient but also to the sustained component of the peptide-activated currents. There were no significant differences in oocytes injected with EGTA or BAPTA. Therefore, in the remainder of this study, EGTA was used to prevent a rise in intracellular [Ca^{2+}].

To further test for the activation of the CaCC, extracellular Ca^{2+} was replaced by Ba^{2+}, which does not activate CaCCs (Barish, 1983). Indeed, in the presence of Ba^{2+}, peptide-activated currents had a step-like appearance like after chelation of intracellular Ca^{2+} (Fig. 19B). Furthermore, CaCCs were pharmacologically blocked by 5-nitro-2-(3-phenylpropylamino)-benzoate (NPPB) (Wu and Hamill, 1992). 100 μM NPPB reduced the amplitude of transient currents by about half and of sustained currents by 28% ($p < 0.05$; $n = 8$; Fig. 19B),

indicating partial block of CaCCs by 100 μM NPPB, which is similar to previous reports (Wu and Hamill, 1992; Schroeder et al., 2008).

To exclude the possibility that NPPB had a direct effect on HyNaC those experiments were repeated with EGTA-injected oocytes. The amplitudes of currents in the presence of Ba^{2+} were now ~2-fold increased compared to currents in the presence of Ca^{2+} ($n = 8$, $p < 0.001$), suggesting either that Ba^{2+} potentiated HyNaC currents or that Ca^{2+} blocked HyNaCs. NPPB slightly reduced the amplitude of HyNaC currents from 0.88 ± 0.1 to 0.75 ± 0.09 μA ($n = 8$, $p = 0.2$, paired *t* test; Fig. 19C), indicating that NPPB has no strong direct effect on HyNaC.

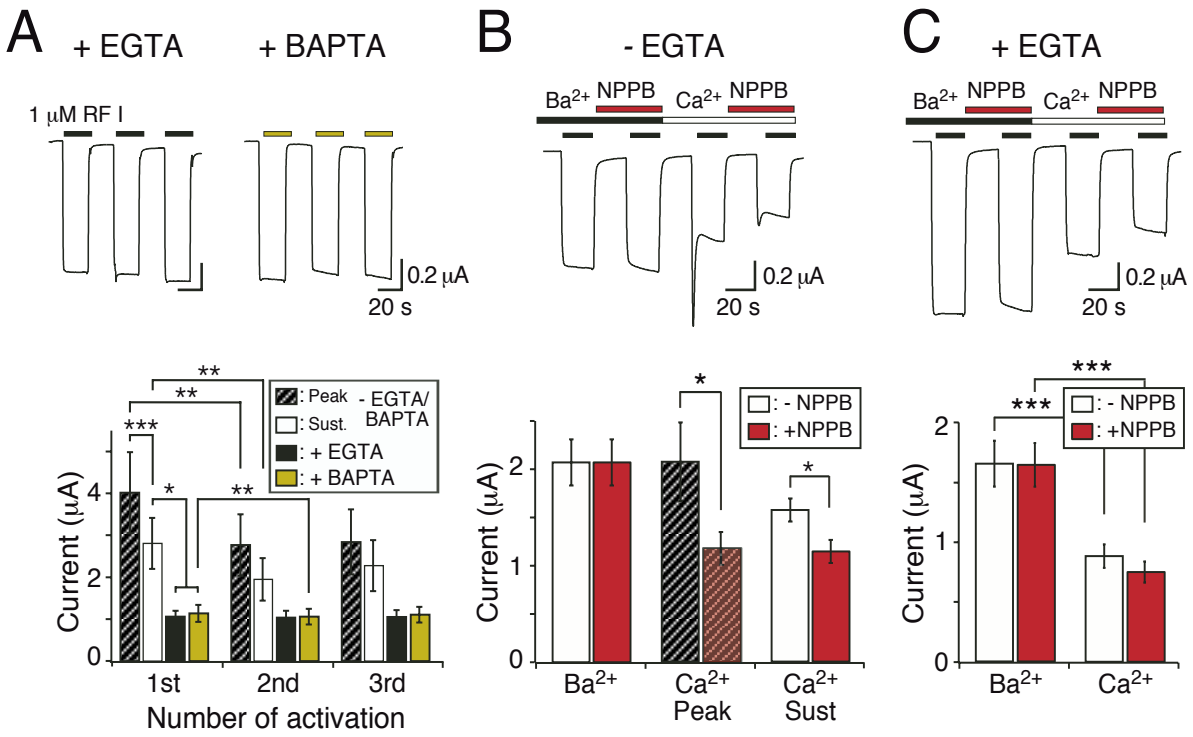

Fig. 19: Chelation of Ca^{2+}_i abolishes transient peptide-activated currents. (A) *Top*, representative HyNaC2/3/5 currents in oocytes injected with EGTA or BAPTA. Note the absence of a transient current and the step-like appearance of the currents. *Bottom,* bar graphs comparing the peak (*hatched bars*) and sustained (*white bars*) current amplitudes of oocytes expressing HyNaC and of oocytes expressing HyNaC and injected with EGTA (*black bars*) or BAPTA (*green bars*) (n = 11). (B) *Top,* representative current trace comparing peptide-activated currents in standard bath and in standard bath, in which $CaCl_2$ was replaced by an equimolar amount (1.8 mM) of $BaCl_2$. Currents were measured either in the presence or the absence of 100 μM NPPB. Oocytes were pre-incubated for 20 s in the corresponding test solutions prior to activation by 1 μM RFamide I. *Bottom,* bar graph comparing the current amplitudes in the absence of NPPB (*white or hatched bars*) and in the presence of 100 μM NPPB (*red bars*) for the indicated conditions. In the presence of Ba^{2+}, no transient current was discernible. The application sequence of the individual solutions was shuffled (n = 8). (C) As in (B), for oocytes that had been injected with EGTA. Note the absence of peak currents. *Bottom,* bar graph comparing the current amplitudes in the absence of NPPB (*white bars*) and in the presence of 100 μM NPPB (*red bars*) for sustained currents. *, $p < 0.05$; ***, $p < 0.001$.

(Adapted from: Dürrnagel et al., 2012)

So far, these results strongly argue for an activation of the endogenous CaCC by HyNaCs. Peptide-activated inward currents of HyNaC-expressing oocytes apparently are the sum of a Na^+ current flowing through HyNaCs and a Cl^- current flowing through CaCCs, with CaCCs being responsible for the biphasic kinetics of the currents. To directly test this interpretation, HyNaCs were activated in the absence of extracellular Na^+ (Fig. 20A).

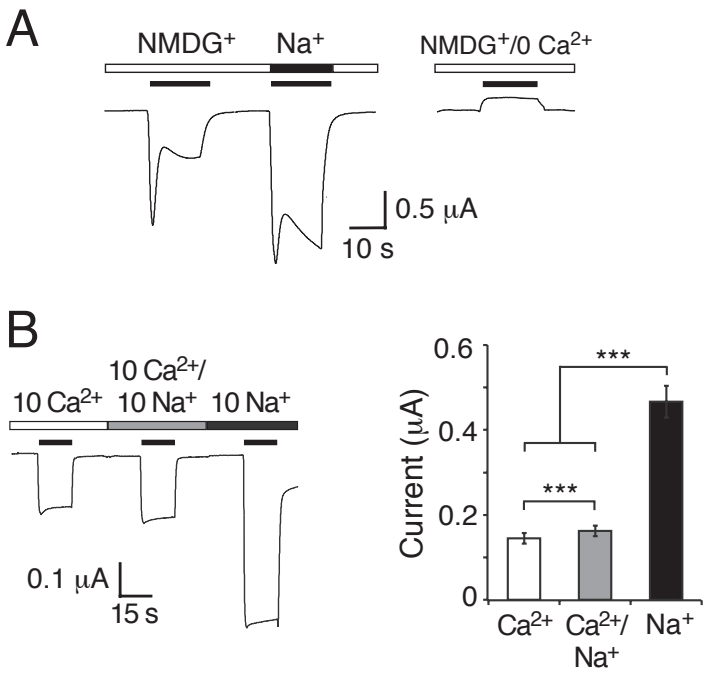

Fig. 20: Peptide-activated currents in the absence of Na^+_e. (A) *Left*, representative current trace for HyNaC2/3/5 in solutions containing 1 mM Ca^{2+} together with either 140 mM $NMDG^+$ or Na^+. 1 μM RFamide I was used for activation. *Right,* control experiment in $NMDG^+$ solution nominally free of Ca^{2+}. Similar results were observed in 4 out of 4 oocytes. (B) *Left*, representative current trace for HyNaC2/3/5 in solutions containing 10 mM Ca^{2+}, 10 mM Ca^{2+} and 10 mM Na^+, or 10 mM Na^+ (nominally free of Ca^{2+}). Solutions additionally contained 10 mM HEPES (pH 7.4) and $NMDG^+$ at concentrations to reach similar osmolarity (10 Ca^{2+}: 125 mM NMDGCl, 10 Ca^{2+}/10 Na^+: 115 mM NMDGCl, 10 Na^+: 130 mM NMDGCl,). Oocytes had been injected with EGTA; 2 μM RFamide I was used for activation. Holding potential was -85 mV. *Right,* quantitative comparison of current amplitudes. ***, $p < 0.001$.

(From: Dürrnagel et al., 2012)

All Na^+ was replaced by the large monovalent cation $NMDG^+$ (but solution still contained 1 mM Ca^{2+}), which should abolish most of HyNaC inward currents. Under these conditions, HydraRFamide I still elicited a current with biphasic kinetics but of smaller amplitude. Peak current amplitudes were ~70% (n = 4, p = 0.14) and sustained currents ~30% (n = 4, $p <$ 0.001) of the currents measured in standard NaCl solution. In control experiments with a solution containing $NMDG^+$ nominally free of Ca^{2+}, no inward current was observed (n = 4;

Fig. 20A). These results are consistent with the idea that Ca^{2+} influx through HyNaCs secondarily activated CaCCs, greatly amplifying the HyNaC current.

To directly show Ca^{2+} influx through HyNaC, the channel was activated in the presence of Ca^{2+} (10 mM) as the exclusive extracellular cation and in EGTA-injected oocytes to prevent activation of the CaCC (Fig. 20B). Under these conditions, HydraRFamide I indeed induced a step-like inward current with an amplitude of 0.15 ± 0.01 mA (n = 11; Fig. 20B), directly demonstrating robust influx of Ca^{2+} through HyNaC. Addition of an equimolar concentration of Na^+ (10 mM) did only slightly increase the current amplitude to 0.16 ± 0.01 mA (n = 11, $p < 0.01$), whereas in the presence of Na^+ (10 mM) as the exclusive cation, peptide activated currents were increased ~3-fold (0.47 ± 0.04 μA, $n = 11$, $p < 0.001$; Fig. 20B). The smaller current amplitude with a higher total concentration of permeant cations (10 mM Ca^{2+}/10 mM Na^+ compared with 10 mM Na^+ alone) suggests that Ca^{2+} blocks HyNaC, in addition to permeating it. This behavior as a permeant blocker prohibits a direct quantitative comparison of the inward Na^+ and Ca^{2+} currents.

3.2.3 HyNaCs are unselective cation channels.

In Fig. 15A and in a previous report (Golubovic et al., 2007), an E_{rev} of sustained peptide-activated currents in HyNaC expressing oocytes of ~10 mV was reported indicative of an unselective ion channel. As the Cl^- currents through CaCCs contaminate the sustained peptide-activated currents, a re-evaluation of E_{rev} of HyNaC was necessary. HyNaCs were activated in oocytes for 50 s and stepped the holding potential from -70 mV to +30 mV in steps of 10 mV every 5 s. E_{rev} was determined in three different solutions: 1) standard bath, 2) standard bath with EGTA-injected oocytes, and 3) standard bath, in which Ca^{2+} had been replaced by Ba^{2+} (Fig. 21). Similar to the results in Fig. 15A and Fig. 18B, in standard bath, currents had an E_{rev} of 11.5 ± 2.5 mV ($n = 8$) and were characterized by strong inward rectification. In EGTA-injected oocytes, E_{rev} was shifted to more positive values (24.0 ± 3.7 mV, $n = 6$, $p < 0.05$) and currents were also inwardly rectifying. It should be noted that the strong inward rectification in these two conditions rendered the determination of E_{rev} imprecise. When Ca^{2+} was replaced by Ba^{2+}, two things changed: E_{rev} was shifted to 3.0 ± 1.9 mV ($n = 7$, $p < 0.05$) and current-voltage relations became linear. These results show, first, that HyNaCs indeed have an E_{rev} indicative of a relatively unselective cation channel and, second, that extracellular Ca^{2+} is the cause of their inward rectification, presumably by blocking HyNaCs at more positive voltages.

This Ca^{2+}-block could explain why currents were enhanced when Ca^{2+} was replaced by Ba^{2+} (Fig. 19C), why transient Cl^-- currents were smaller at more depolarized potentials in standard bath (Fig. 18B), and why Na^+ currents were strongly reduced by an equimolar amount of Ca^{2+} (Fig. 20B). It is concluded that Ca^{2+} is a permeant blocker of HyNaCs and that the block is voltage dependent. Ca^{2+} strongly blocks HyNaC already at -85 mV (Fig. 20B), but more strongly as the membrane potential becomes more depolarized, leading to an almost complete block of HyNaC at positive potentials (Fig. 21).

At present, a definite explanation for the shift of E_{rev} when Ca^{2+} had been replaced by Ba^{2+} (Fig. 21) is missing.

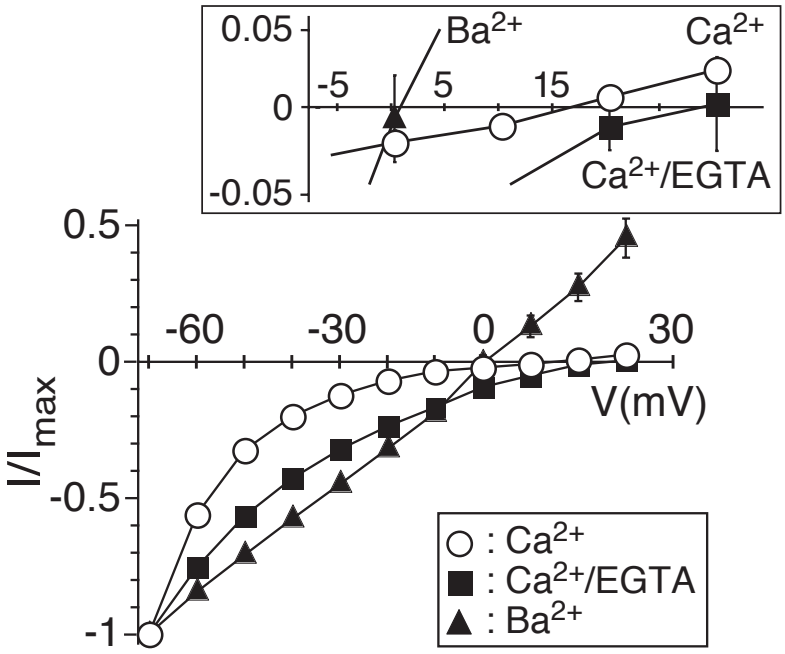

Fig. 21: Preventing a rise in $[Ca^{2+}]_i$ changes E_{rev} of sustained peptide-activated currents. *I/V* relations for HyNaC2/3/5 activated by 1 μM HydraRFamide I in standard bath (*open circles*), in standard bath after injection of EGTA (*filled squares*) and in standard bath, in which $CaCl_2$ had been replaced by $BaCl_2$ (*filled triangles*). Currents were normalized to the current measured at -70 mV, which had an amplitude of -4.4 ± 1.1 μA (Ca^{2+}), -1.4 ± 0.2 μA (Ca^{2+}/EGTA), or -6.0 ± 0.8 μA (Ba^{2+}) (*n* = 7 - 8), respectively. The inset shows the *I/V* relations close to the reversal potentials on an expanded scale.

(From Dürrnagel et al., 2012)

3.2.3 Ca^{2+} permeability of HyNaC is high.

Activation of CaCCs indirectly measures Ca^{2+} permeation through HyNaC. To directly measure Ca^{2+} permeation, we additionally performed photometric Ca^{2+} measurements using Fura-2 (this experiment was done in collaboration with Björn Falkenburger from the Department of Neurology, RWTH Aachen University). Application of HydraRFamide I to oocytes that expressed HyNaC and had been injected with Fura-2 led to a robust increase (Golubovic et al., 2007) in the F340/F380 ratio, indicating an increase in cytosolic Ca^{2+} (Fig. 22A). Simultaneous measurement of currents revealed that the $[Ca^{2+}]_i$ increase paralleled the opening of the HyNaC pore (Fig. 22A). $[Ca^{2+}]_i$ quickly rose after channel opening and remained high during channel activation. A similar rise in $[Ca^{2+}]_i$ was observed in all oocytes tested (n = 8, p < 0.001, paired t test; Fig. 22B). The robust signal in photometric Ca^{2+} measurements after opening of HyNaCs and the robust activation of CaCCs by HyNaC suggest a high Ca^{2+} permeability of HyNaCs.

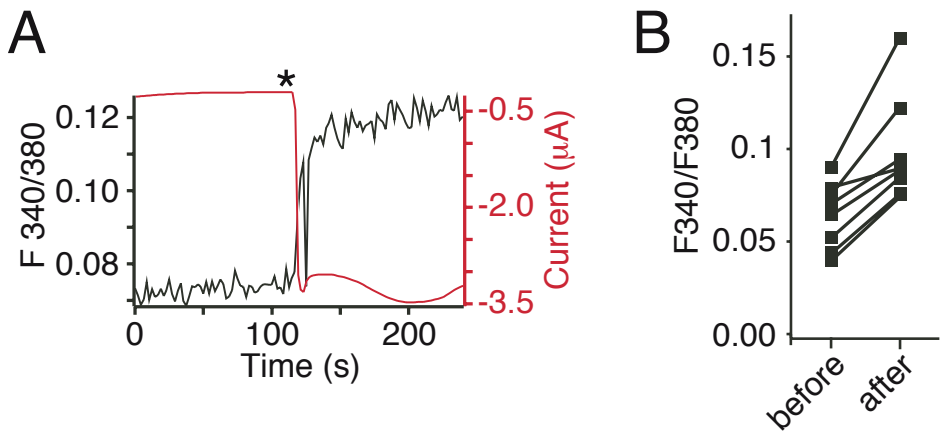

Fig. 22: Activation of HyNaC increases $[Ca^{2+}]_i$ in oocytes. (A) Representative trace (*black*) from photometric Ca^{2+} measurements illustrating the increase of the F340/380 ratio in a HyNaC2/3/5 expressing oocyte after application of RFamide I (*asterisk*). Oocytes had been injected with 50 nl Fura-2AM (1 mM) 30-120 min prior to the recording. Thus, the increased F340/380 ratio reflects an increase in $[Ca^{2+}]_i$. The red trace represents the current that paralleled the rise in $[Ca^{2+}]_i$. HyNaC was activated by pipetting HydraRFamide I into the bath to yield a final concentration of 1 µM RFamide I. (B) Changes of the F340/F380 ratio due to activation of HyNaC for individual measurements (n = 8).

(From: Dürrnagel et al., 2012)

To estimate the relative Ca^{2+} permeability of HyNaC, E_{rev} was determined in two different Ca^{2+} concentrations and with EGTA-injected oocytes. To increase the contribution of the

Ca^{2+} current to the total current, Na^+ was replaced by the larger, impermeant cation $NMDG^+$. In 1 mM Ca^{2+}, E_{rev} was -43 ± 1.5 mV (n = 9) while in 10 mM Ca^{2+} it was significantly shifted to -17 ± 2.6 mV (n = 10, p < 0.001; Fig. 23A). To assess these values, identical measurements were performed with P2X4, a purinergic ion channel of known high Ca^{2+} permeability (P_{Ca}/P_{mono} = 4.2; (Soto et al., 1996). In fact, E_{rev} of P2X4 in 1 mM and 10 mM Ca^{2+} were similar to previously published values for P2X4 (Soto et al., 1996) and to E_{rev} of HyNaC (Fig. 23B), suggesting that P_{Ca}/P_{mono} of HyNaC is on the same order as that of P2X4.

Finally, the relative Ca^{2+} permeability P_{Ca}/P_{Na} of HyNaC was calculated by determining the shift in E_{rev} when the solution contained either Ca^{2+} or Na^+ as the main permeant cation. As mentioned above, E_{rev} with 10 mM Ca^{2+} was -17 ± 2.6 mV and with 140 mM Na^+ it was shifted to 14 ± 2.5 mV (n = 8; Fig. 23A), allowing to calculate a permeability ratio P_{Ca}/P_{Na} = 3.85 (n = 8; see Methods 2.3.6), which is in good agreement with P_{Ca}/P_{mono} of P2X4.

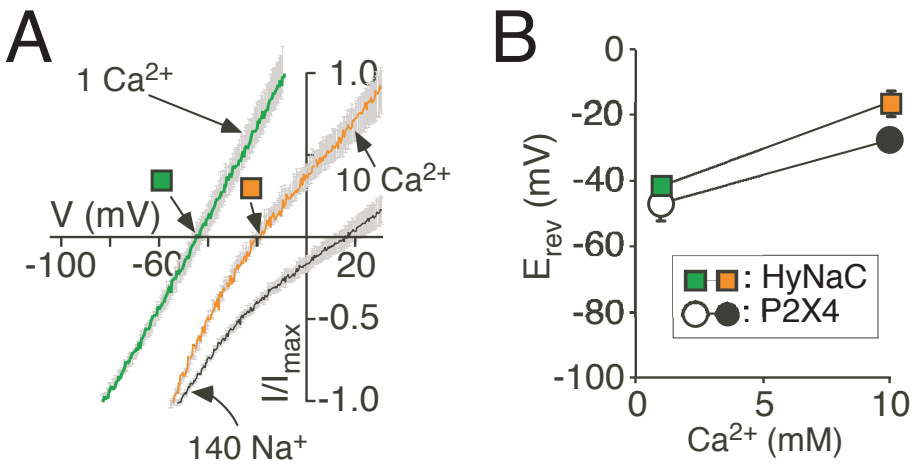

Fig. 23: Permeability ratio P_{Ca}/P_{Na} of HyNaC is comparable to P2X4. (A) *I/V* relations of HyNaC2/3/5 in solutions containing 1 or 10 mM $CaCl_2$ and no NaCl (which had been replaced by 140 or 126.5 mM NMDG-Cl, respectively) and in a solution containing 140 mM NaCl and 1 mM $CaCl_2$. Continuous voltage ramps were run with a speed of 0.46 ms per mV (thus, for example, 6 s per 130 mV). Different voltage ranges were chosen for different conditions. Currents were normalized to I_{max}. Lines are the sum of 8 - 10 individual measurements. S.E.M. is indicated by grey errors bars. 50 nl EGTA (20 mM) was injected prior to the recordings. Squares represent the reversal potentials that are plotted in (B). HyNaC was activated by 2 μM RFamide I. (B) Ca^{2+} dependent shifts of the reversal potential reveal a high Ca^{2+} permeability of HyNaC. Reversal potentials of the highly Ca^{2+}-permeable P2X4 receptor are shown for comparison and were similar to HyNaC. P2X4 was activated by 10 μM ATP.

(Adapted from: Dürrnagel et al., 2012)

To calculate the permeability ratio P_{Na}/P_K (see Methods 2.3.6) of HyNaC, E_{rev} was determined in solutions containing 140 mM of either Na^+ or K^+, yielding a relative permeability P_{Na}/P_K = 3.0 (n = 8; data not shown), which is in agreement with the results in Fig. 15B. The higher relative permeability for Na^+ over K^+ of HyNaC compared with P2X4 (P_{Na}/P_K ~1; (Soto et al., 1996) can explain the slightly more positive E_{rev} of HyNaC in 10 mM Ca^{2+} (-17 ± 2.6 mV compared with -27 ± 1 mV, $p < 0.01$) in the experiment shown in Fig. 23B.

In summary, these results provide consistent evidence for a high relative Ca^{2+} permeability of HyNaC.

3.2.3 Negative charges at the outer entrance to the ion pore are necessary for the high Ca^{2+}-permeability of HyNaC.

ASIC1a is a DEG/ENaC that is slightly permeable for Ca^{2+} (Waldmann et al., 1997b; Bässler et al., 2001; Samways et al., 2009) and at the same time blocked by Ca^{2+} (Paukert et al., 2008). A ring of conserved aspartates at the outer mouth of the ASIC1a pore is crucial for Ca^{2+} block, presumably by constituting a Ca^{2+} binding site (Paukert et al., 2008). These aspartates are conserved in HyNaC subunits 2, 3 and 5 (Fig. 24A). Therefore it was investigated, whether these residues contribute to Ca^{2+} permeability of HyNaCs. Substitution of the conserved aspartate by cysteine in all three HyNaC subunits (2/3/5; see Methods 2.2.4) resulted in functional channels (HyNaC_D-C). Activation of HyNaC_D-C in oocytes evoked currents similar to HyNaC wt (Fig. 24B), but the presence of a peak current component was more variable, suggesting reduced activation of CaCCs by HyNaC_D-C. Furthermore, current amplitudes were smaller than for HyNaC wt, as would be expected when CaCCs were less efficiently activated. To compensate for the smaller current amplitudes, a 20-fold greater amount of cRNA for HyNaC_D-C was injected. When Na^+ was replaced by $NMDG^+$ (keeping 1 mM Ca^{2+}) to abolish most of HyNaC_D-C inward currents, HydraRFamide I no longer elicited robust currents (Fig. 24C), whereas it elicited robust inward currents in standard bath (I = 1 ± 0.25 μA, n = 5; Fig. 24C).

As shown above, the currents in the absence of Na^+ are CaCC currents. These findings indicate that activation of HyNaC_D-C does not efficiently activate CaCCs and supports reduced Ca^{2+} influx through HyNaC_D-C. In standard bath, E_{rev} of HyNaC_D-C was +16 ± 2 mV (n = 6; Fig. 24D), indicative of a relatively unselective cation current, similar to HyNaC

wt. Of note, HyNaC_D-C currents were not inwardly rectifying (Fig. 24D), showing that the conserved Asp is necessary for inward rectification and in line with the requirement of Ca^{2+} for inward rectification. In EGTA-injected oocytes, HyNaC_D-C currents in the presence of 10 mM Ca^{2+} as the sole extracellular cation were tiny and ~7-fold smaller than in the presence of 10 mM Na^+ (0.01 ± 0.004 μA compared with 0.07 ± 0.01 μA, n = 11; Fig. 24E); the addition of Ca^{2+} (10 mM) to the Na^+ containing solution only slightly decreased the current amplitude by 29 ± 3 % (0.05 ± 0.01 μA, n = 11, $p < 0.001$; Fig. 24E), whereas for HyNaC wt, it decreased the current amplitude by 74 ± 2% ($p < 0.001$; Fig. 20B). These results are consistent with the interpretation that HyNaC_D-C had a lower Ca^{2+} permeability and was less blocked by Ca^{2+} than HyNaC wt.

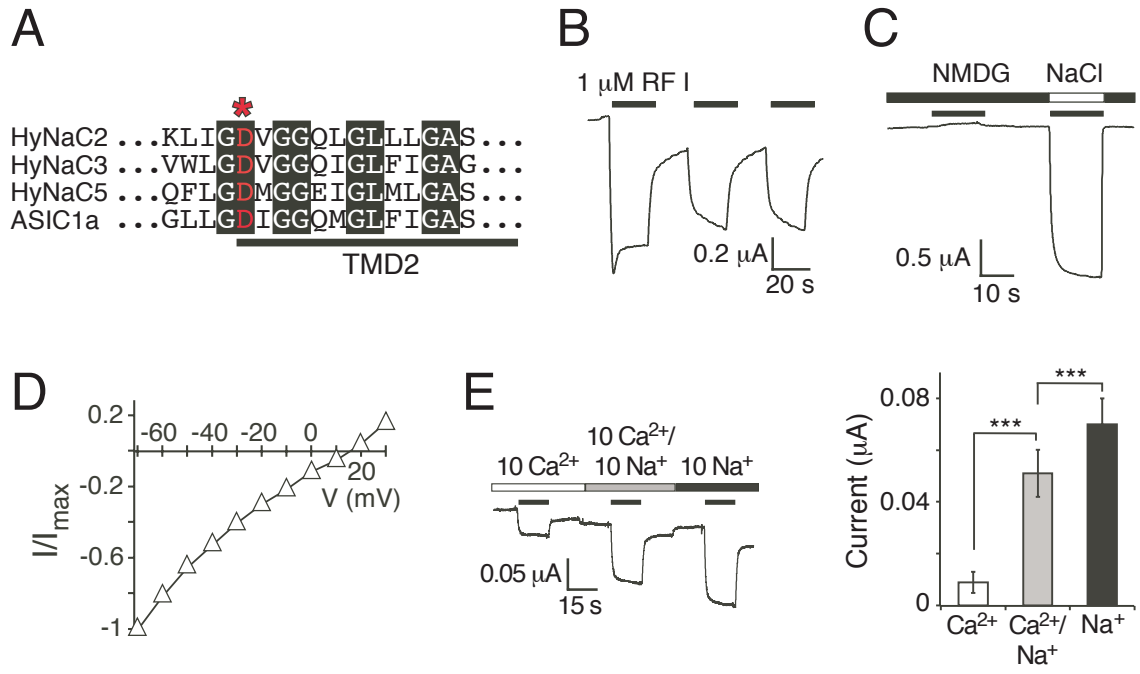

Fig. 24: A conserved aspartate is necessary for the high Ca^{2+} permeability of HyNaC. (A) Alignment of the amino acid sequences of HyNaC2, 3, and 5 and ASIC1a at the beginning of the second transmembrane domain TMD2 in the one-letter code. The crucial aspartate is indicated by an asterisk. Completely conserved amino acids are shown as white letters on black background. (B) Representative current trace for HyNaC_D-C activated by 1 μM RFamide I. The amplitude and shape of the transient current component was more variable than for the wt. Mean maximum current amplitudes were 3.45 ± 1.2 μA for the first activation (n = 5). (C) Representative current trace showing activation of HyNaC_D-C by 1 μM RFamide I in solutions containing 1 mM Ca^{2+} together with either 140 mM $NMDG^+$ or Na^+. No inward current was visible in $NMDG^+$ solutions. (D) *I/V* plot for HyNaC_D-C activated by 1 μM RFamide I in standard bath solution. Currents were normalized to the current measured at -70 mV, which had an amplitude of -1.1 ± 0.2 μA (n = 6). (E) *Left*, representative current trace for HyNaC_D-C in solutions containing 10 mM Ca^{2+}, 10 mM Ca^{2+} and 10 mM Na^+, or 10 mM Na^+ (nominally free of Ca^{2+}). Conditions were as in Fig. 3B. *Right,* quantitative comparison of current amplitudes. ***, $p < 0.001$.

(Adapted from: Dürrnagel et al., 2012)

With 1 and 10 mM Ca^{2+} in EGTA-injected oocytes, E_{rev} of HyNaC_D-C was significantly shifted to more negative potentials compared with HyNaC wt (n = 7 - 8, $p < 0.001$; Fig. 25A and Fig. 25B), confirming a reduced Ca^{2+} permeability of HyNaC_D-C.

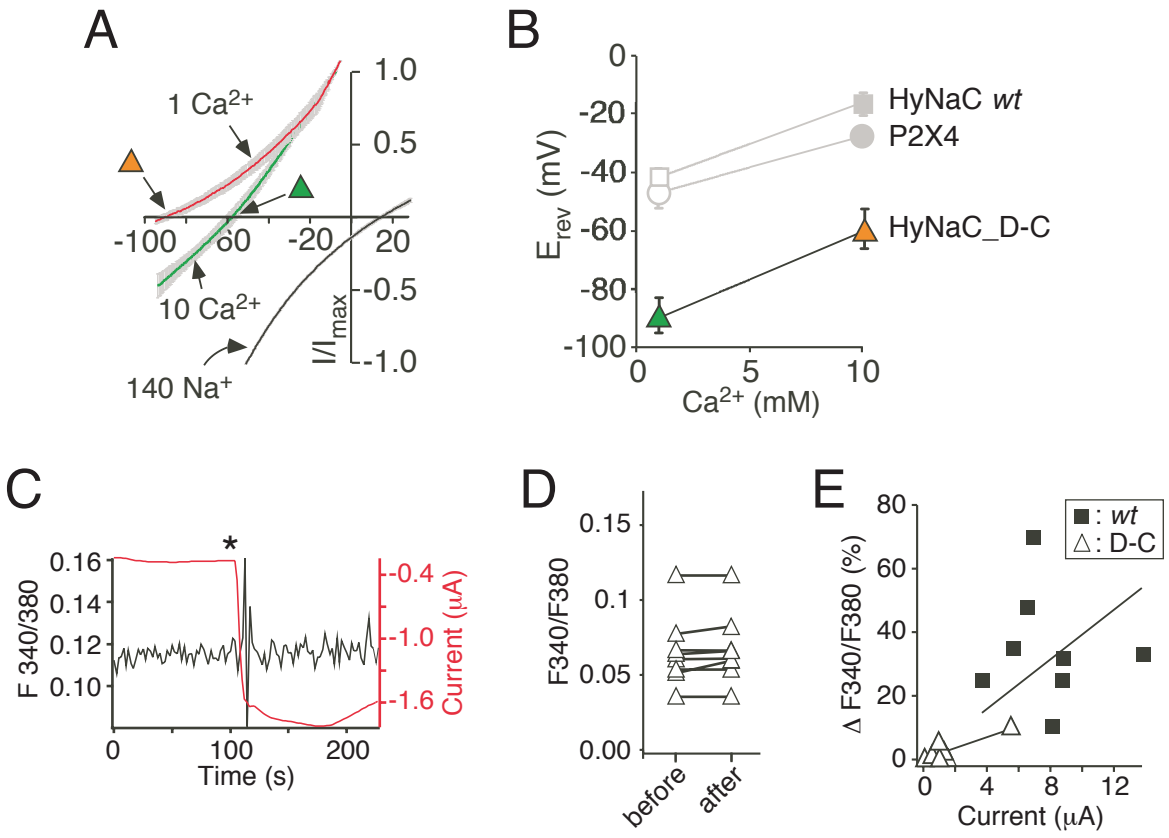

Fig. 25: A conserved aspartate is necessary for the high Ca^{2+} permeability of HyNaC. (A) *I/V* relations of HyNaC_D-C in solutions containing 1 or 10 mM $CaCl_2$ and no NaCl (which had been replaced by 140 or 126.5 mM NMDG-Cl, respectively) and in a solution containing 140 mM NaCl and 1 mM $CaCl_2$. Lines are the sum of 8 - 9 individual measurements. S.E.M. is indicated by grey errors bars. Experimental conditions were as in Fig. 23A. Triangles represent the reversal potentials that are plotted in (B). (B) Ca^{2+} dependent shifts of the reversal potential reveal a significantly lower Ca^{2+} permeability of HyNaC_D-C compared with HyNaC wt. Reversal potentials of HyNaC wt and P2X4 (*grey symbols*) are from Fig. 23B and shown for comparison. (C) Representative trace (*black*) from photometric Ca^{2+} measurements illustrating no change of the F340/380 ratio after application of RFamide I (1 µM; *asterisk*) in a oocyte expressing HyNaC_D-C. The deflections in the F340/380 ratio immediately after the peptide was added are due to movements of the solution and unspecific. Oocytes had been injected with 50 nl Fura-2AM (1 mM) 30-120 min prior to the recording. The red trace represents the current that robustly increased after peptide application. (D) F340/F380 before and after application of 1 µM RFamide I for HyNaC_D-C (n = 8). (E) Plot of the increase of the F340/380 ratio (in %) after application of RFamide I as a function of peptide-activated current amplitudes. Filled squares represent individual measurements for HyNaC wt and open triangles for HyNaC_D-C (n = 8). Current amplitudes were smaller for HyNaC_D-C than for HyNaC wt (n = 8, $p < 0.001$; Fig. 22B). Solid lines represent linear fits of the fluorescence/current ratio. Note that the slope of this line was larger for wt than for the D-C mutant, indicating a higher relative Ca^{2+} permeability of the wt.

(Adapted from: Dürrnagel et al., 2012)

The relative Ca^{2+} permeability of HyNaC_D-C, calculated by determining the shift in E_{rev} when the solution contained either Ca^{2+} or Na^{+} as the main permeant cation (Fig. 25A; see Methods 2.3.6), was P_{Ca}/P_{Na} = 0.44 (n = 8), thus 9-fold smaller than for HyNaC wt. In contrast, the permeability ratio for monovalent cations was comparable to HyNaC wt (P_{Na}/P_{K} = 2.9, n = 8; data not shown). These results suggest that the inefficient activation of CaCCs by HyNaC_D-C is caused by its strongly reduced Ca^{2+} permeability.

In photometric Ca^{2+} measurements, activation of HyNaC_D-C did not significantly increase the F340/F380 ratio (n = 8, p = 0.12, paired *t* test, Fig. 25D; example in Fig. 25C), consistent with a reduced Ca^{2+} influx in HyNaC_D-C expressing oocytes. As expected, the increase in F340/F380 ratio correlated with the current amplitude and could be fitted reasonably well with a line (Fig. 25E). This linear regression analysis for F340/F380 ratio change versus current showed a shallower slope for the D-C mutant than for HyNaC wt ($p < 0.01$; Fig. 25E), which is also consistent with a reduced Ca^{2+} permeability of HyNaC_D-C.

IV. Discussion

4.1 Part I: HyNaC2/3/5 forms a high affinity peptide receptor

4.1.3 HyNaC2/3/5 shows typical features of DEG/ENaC channels

The first part of this work describes the cloning and functional characterisation of HyNaC5, a novel DEG/ENaC subunit from *Hydra*. It is shown that the HydraRFamide I induced current amplitudes of HyNaC2/3 are potentiated ≈16-fold when HyNaC5 is coexpressed together with HyNaC2 and -3 (Fig. 13A). This finding, together with other results discussed below, strongly suggests that HyNaC2/3/5 forms a heteromeric peptide-gated ion channel. The identification of three homologous HyNaC subunits that together form a functional DEG/ENaC channel is similar to ENaC which is also composed of three (α,β,γ) subunits (Canessa et al., 1994). Reminiscent of the situation in HyNaCs, two ENaC subunits ($\alpha\beta$ or $\alpha\gamma$) are sufficient for generating small, constitutive currents and these currents are potentiated ≈25 to 50-fold by coexpression of the γ subunit (Canessa et al., 1994). In ENaC, the small currents reported for the $\alpha\beta$ or $\alpha\gamma$ subunits can be attributed to a poor incorporation of these subunits into the membrane and coinjection of the γ subunit enhances surface expression ≈20-fold (Firsov et al., 1996). In contrast to this, surface expression of the tagged HyNaC2-HA/3 channel was not altered by coinjection of HyNaC5 (Fig. 13C). In the case of HyNaC2/3/5, the larger current amplitudes most likely depend on an increased single channel amplitude or an increased open channel probability. We speculate that the HydraRFamides I and II are partial ligands for HyNaC2/3 i.e. they open the channel pore less effectively than the HyNaC2/3/5 pore which could explain the reduced whole cell currents.

The finding that three HyNaCs subunits concertedly form a high affinity receptor is also compatible with the crystal structure of ASIC1a, which revealed an homotrimeric assembly of this channel (Baconguis and Gouaux, 2012). As HyNaCs are closely related to ASICs, it is reasonable to assume that HyNaCs are also composed of three subunits. In the case of HyNaC2/3/5, this directly implicates a 1:1:1 ratio for the subunits in the functional channel

complex. Collectively, the findings suggest that a trimeric structure is an evolutionary conserved feature of all DEG/ENaCs.

Similar to HyNaC2/3, HyNaC2/3/5 is activated by the HydraRFamides I and II. Compared to HyNaC2/3, the apparent affinity for HyNaC2/3/5 is ≈100-fold increased and EC_{50} values for the HydraRFamides I and II were ≈5 μM and ≈0.35 μM, respectively (Fig. 14). For FaNaCs, the closely related peptide-gated ion channels, apparent affinities ranging from ≈2 μM for HaFaNaC (Lingueglia et al., 1995) to ≈70 μM for HtFaNaC (Jeziorski et al., 2000) were reported. Therefore, HyNaC2/3/5 has the highest apparent affinity of all known peptide-gated ion channels.

In the first part of this work, the permeability of HyNaCs for Ca^{2+} had not been noticed. The influx of Ca^{2+} through HyNaCs activates CaCCs, which are endogenously expressed in *Xenopus* oocytes (Miledi, 1982; Barish, 1983; Schroeder et al., 2008). Therefore, all current traces shown in this part are the sum of two individual currents. A HyNaC current, carried by Na^+ and Ca^{2+} and an additional Cl^- current due to secondary activation of CaCCs. Without block of contaminating Cl^- currents, the indicated EC_{50} values for the HydraRFamides I and II and the comparison of current amplitudes between HyNaC2/3 and 2/3/5 may be imprecise. However, as CaCCs are activated by HyNaCs, one might assume that the fraction of the CaCC current is roughly proportional to the HyNaC current. Indeed, concentration-response curves with oocytes that had been injected with EGTA to block contaminating CaCCs, yielded comparable EC_{50} values for HyNaC2/3/5 (Marc Assmann, personal communication). Fig. 19A shows that the CaCC current fraction of the total current in HyNaC2/3/5 injected oocytes is ≈4 times higher than the HyNaC2/3/5 current fraction. The CaCC current contributing to the total current for HyNaC2/3 injected oocytes was not determined but is likely in the same range. This implicates that the ≈16-fold increased current amplitude of HyNaC2/3/5 compared to HyNaC2/3 (Fig. 13A) is due to a larger charge flux through HyNaC2/3/5 and cannot be explained by an increased activation of CaCCs. However, an exact quantification of current amplitudes and apparent peptide affinities of HyNaC2/3 and HyNaC2/3/5 would demand additional measurements with EGTA injected oocytes.

HyNaC2/3 is equally permeable for Na^+, Li^+ and K^+ which is an unusual feature for a DEG/ENaC channel (Golubovic et al., 2007). In contrast to this, in an ion exchange assay HyNaC2/3/5 showed significantly higher currents in solutions containing Na^+ as main charge carrier than in K^+ containing solutions directly indicating an increased selectivity for

Na^+ (Fig. 15B). Controversially, the reversal potentials in standard bath Na^+ solution were not altered between both channels (Fig. 15A). One possible explanation for this is that the reversal potentials are affected by activation of CaCCs as they were measured without injection of EGTA. Assuming an intracellular Cl^- concentration of 33 mM (Barish, 1983) the calculated equilibrium potential of Cl^- in the used solution is ≈ -38 mV. This would cause a leftward shift of reversal potentials and the impact would depend on the magnitude of CaCC activation by HyNaCs. This could explain why the increased Na^+/K^+ current ratio of HyNaC2/3/5 measured in the ion exchange assay did not manifest in the voltage ramps. The reversal potentials of HyNaC2/3/5 under different ionic conditions were therefore re-evaluated in the second part of this work with a different experimental protocol and CaCCs were blocked by injection of EGTA (Fig. 21). In addition, the P_{Na}/P_K ratio was also determined in a new experiment with blocked CaCCs and yielded a P_{Na}/P_K value of ≈3 (see 3.2.3), which is in good agreement with the results obtained in the ion exchange assay confirming the slight selectivity of HyNaC2/3/5 for Na^+.

Similar to the selectivity for Na^+, the sensitivity for the inhibitor amiloride is a common feature of DEG/ENaCs (Kellenberger and Schild, 2002). Therefore, the relatively low apparent sensitivity of HyNaC2/3 for amiloride (IC_{50} ≈ 500 μM) (Fig. 16; see also (Golubovic et al., 2007) is exceptional. In contrast, HyNaC2/3/5 was shown to be ≈ 5-fold more sensitive for amiloride (Fig. 16). Similarly, the sensitivity for benzamil and phenamil is also enhanced. The sensitivity for amiloride did not depend on the applied HydraRFamide concentration, suggesting that both substances do not compete for the same binding site. Collectively, these findings implicate that sensitivity for amiloride is an evolutionary conserved feature of DEG/ENaCs. Since amiloride has been shown to act by blocking the open channel pore in other DEG/ENaCs (Brown et al., 2007), it is reasonable to assume a similar mechanism in HyNaCs. This would suggest the basic pore properties of DEG/ENaCs manifested itself early in evolution.

In summary, the following results suggest that HyNaC5 is incorporated into the HyNaC2/3 channel complex:

- The apparent affinity for both HydraRFamides increases ≈100-fold.
- The peptide-induced currents are potentiated ≈16-fold.
- The sensitivity for amiloride is ≈5-times increased.
- HyNaC2/3/5 is more Na^+ selective.

In addition, the selectivity for Na^+ and the increased sensitivity for amiloride strongly resemble other DEG/ENaC channels. It is therefore suggested that the channel complex containing HyNaC2/3/5 is more likely the physiologically relevant channel in *Hydra* than the complex formed byHyNaC2/3 only.

4.1.3 Physiological implications of HyNaCs

To investigate the physiological function of HyNaCs, we investigated the feeding reaction in *Hydra.* Interestingly, the GSH-induced feeding response, which includes movement of the tentacles, was significantly delayed when the animals were bathed in 100 *µ*M amiloride (Fig. 17). Moreover, the coordinated movement of the tentacles towards the hypostome was also impaired. The effect was reversible and did not affect general behaviour of the animals. Therefore, one might speculate that HyNaCs play an important role in generating the feeding reaction *of Hydra*. However, it is important to mention that an unspecific effect of amiloride cannot be excluded.

Consistent with the observed effect of amiloride in the feeding reaction, the whole mount *in situ* hybridization revealed the expression of *hynac2, -3, -4* and *-5* at the bases of the tentacles in adult animals, most likely in the epitheliomuscular cells (Fig. 11). Therefore, the specific expression of *hynac2-4* corresponds with a putative role of HyNaCs in generating coordinated movement of the tentacles during the feeding reaction. Subtle differences in the expression of *hynac4* and *hynac5* were observed in adult animals (Fig. 12). *hynac5* is predominantly expressed at the oral site of the tentacles, whereas *hynac4* expression is restricted to the aboral site. One might speculate that channels containing HyNaC5 or HyNaC4 have different physiological functions e.g. in regulating contraction or extension of the tentacles during feeding behaviour. In *Xenopus* oocytes, HyNaC4 did not show any currents after application of the HydraRFamides I-IV when HyNaC4 was expressed either alone or in combination with HyNaC2 and 3 (Golubovic et al., 2007). Only for HyNaC2/4/5 small currents were observed that were ≈10% of the size of the HyNaC2/3 (Fig 11A). Therefore, one might speculate that HyNaC4 associates with hitherto undiscovered subunits and forms an ion channel with different properties compared to the channel made of HyNaC2/3/5. Indeed, a BLAST search revealed that the genome of *Hydra magnipapillata* contains at least seven further genes related to the known HyNaCs indicating that more HyNaCs exist that may be gated by the HydraRFamidees III and VI.

The expression pattern of *hynac1-4* at the base of the tentacles and the expression of *hynac2*, *-3*, and *-5* during budding overlaps with the previously reported expression of the preprohormones A-C (Fig. 26). These preprohormones are precursor peptides that are cleaved to give rise to HydraRFamides (Hansen et al., 2000 Table 2). Especially the expression pattern of preprohormone A from which the HydraRFamides I-V are derived is very similar to the expression of the *hynac* genes. This strongly suggests that HydraRFamides are the natural ligands of HyNaCs *in vivo*. To date, the ligand binding site of the HydraRFamides I and II is not known. However, in a recent study the binding site of psalmotoxin, a small peptide toxin that acts as gating modifier of ASIC ion channels was identified (Baconguis and Gouaux, 2012). Psalmotoxin was shown to bind ASIC1 in in the acidic pocket, a region containing several negative charged residues that is formed by intersubunit contacts between the thumb, β-ball and finger domains together with residues from the palm domain (Jasti et al., 2007 Fig. 3). Further studies will show, whether the homologous region is also the peptide-binding site of HyNaCs.

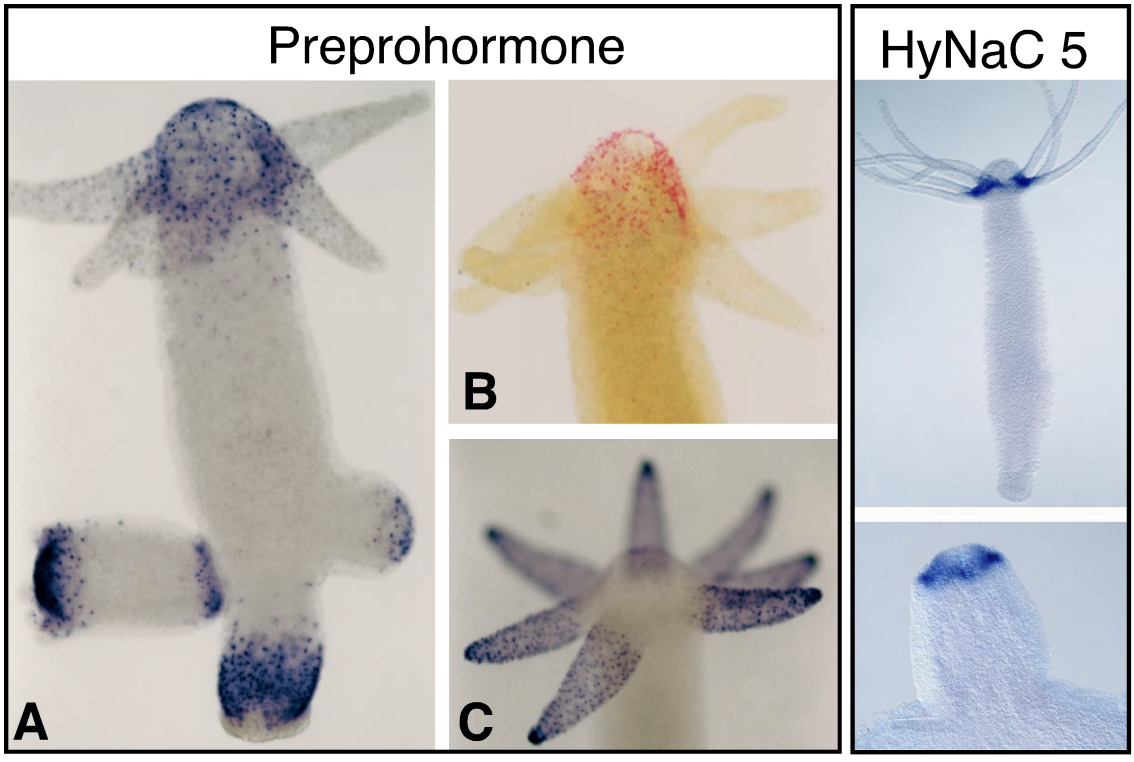

Fig. 26: (Left) Whole mount *in situ* staining with antibodys against the preprohormones A, B, C. (Adapted from: Hansen et al. 2000). (Right) *In situ* staining showing expression pattern of HyNaC5. (Adapted from: Dürrnagel et al., 2012)

4.2 Part II: HyNaC2/3/5 is highly permeable for Ca^{2+}

4.2.3 Several lines of evidence document the high Ca^{2+} permeability of HyNaC2/3/5

The first part this thesis describes the characterisation of HyNaC5, a novel DEG/ENaC subunit from *Hydra*. In the first part of this thesis and in a previous paper dealing with the characterisation of HyNaC2/3 (Golubovic et al., 2007), the biphasic currents after application of HydraRFamides were entirely attributed to currents flowing through the HyNaC pore. The results in the second part of this work now show that those previous conclusions were wrong. HyNaCs are highly Ca^{2+}-permeable members of the DEG/ENaC gene family. In *Xenopus* oocytes, this high Ca^{2+}-permeability leads to robust activation of the endogenous CaCC, and the Cl^- current adds to the cation current flowing through HyNaC itself. This secondary activation of the CaCC is entirely responsible for the biphasic appearance of peptide-activated currents in HyNaC expressing oocytes. This conclusion is based on several different observations. 1) E_{rev} of the transient current is Cl^- dependent; 2) intracellular chelation of Ca^{2+} abolishes the transient current and leads to step-like HyNaC currents; 3) HydraRFamides elicit biphasic inward currents also in the absence of permeant monovalent cations; 4) Ca^{2+} measurements reveal an increase in $[Ca^{2+}]_i$ that parallels the opening of the HyNaC pore; and 5) E_{rev} of HyNaC is Ca^{2+} dependent. These results consistently show that HyNaCs are Ca^{2+}-permeable. Moreover, it is shown that HyNaC currents have no strong time dependence; in the presence of the intracellular Ca^{2+} chelators EGTA or BAPTA, HydraRFamides elicit step-like currents that do not desensitize. The apparent biphasic HyNaC current and tachyphylaxis from first to second peptide application arise from the secondary activation of the CaCC. Consequently, tachyphylaxis was abolished in cells injected with EGTA (Fig. 19).

Several ligand-gated channels share a high Ca^{2+} permeability with HyNaCs and activate CaCCs when expressed in *Xenopus* oocytes, among them NMDA receptors (Leonard and Kelso, 1990), kainate receptor GluR6 (Egebjerg and Heinemann, 1993), α_7 and α_9 nicotinic acetylcholine receptors (Galzi et al., 1992; Vernino et al., 1992; Séguéla et al., 1993; Katz et al., 2000), and purinergic P2X4 receptors (Soto et al., 1996). The estimate of the Ca^{2+} permeability of HyNaCs, P_{Ca}/P_{Na} = 3.85, revealed a Ca^{2+} permeability similar to that of P2X4

(Soto et al., 1996), P_{Ca}/P_{mono} = 4.2, placing HyNaCs among the highly Ca^{2+} permeable ligand-gated ion channels. It should be mentioned, however, that P_{Ca}/P_{Na} ratios obtained by measurements of the shift in reversal potentials generally have to be regarded with caution as the GHK constant field voltage equation, which was used to calculate permeability ratios, requires that there is no interaction among permeating ions (Burnashev et al., 1995; Hille, 2001). Like for most ion channels, this is not the case for HyNaCs, implying that P_{Ca}/P_{Na} is not constant but depends in a complex manner on the voltage and the individual concentrations of divalent and monovalent ions on both sides of the membrane. For example, for HyNaC a ratio $P_{Ca}/P_{Na} \approx 10$ was estimated, when using E_{rev} in a solution containing 1 mM (instead of 10 mM) Ca^{2+} (Fig. 23A).

The FMRFamide-activated Na^+ channel, FaNaC, is another peptide-gated ion channel from the DEG/ENaC gene family (Lingueglia et al., 1995). When expressed in oocytes, FMRFamide elicits currents that develop comparatively slowly over a few seconds and that partially desensitize (Fig. 5). Moreover, FaNaC shows a reversal potential indicative of a highly Na^+ selective ion channel (Lingueglia et al., 1995). Thus, kinetics and ion selectivity are considerably different between the only two known peptide-gated ion channels, both from the DEG/ENaC gene family.

4.2.3 A conserved Asp confers high Ca^{2+}-permeability

In addition, the second part of this work identifies a conserved aspartate, necessary for the high Ca^{2+} permeability of HyNaCs. Again, this finding is based on several observations. 1) When the conserved aspartate was substituted by a cysteine (HyNaC_D-C), Hydra-RFamides elicit no strong inward currents in the absence of permeant monovalent cations; 2) E_{rev} with Ca^{2+} as main charge carrier was significantly shifted compared to wt; 3) the relative Ca^{2+} permeability was reduced to P_{Ca}/P_{Na} = 0.44; and 4) photometric Ca^{2+} measurements revealed no increase in $[Ca^{2+}]_i$ when channels opened. The aspartate is conserved in ASICs and is crucial for Ca^{2+} block of ASICs (Paukert et al., 2008) and for coordinating monovalent cations at the outer ASIC pore (Gonzales et al., 2009). Thus, likely these aspartates form a ring of negative charges at the outer entry of the HyNaC pore that attracts cations, in particular Ca^{2+}. Removing the aspartate abolished inward rectification (Fig. 24D), suggesting that the aspartate is a determinant of a Ca^{2+} binding site, which mediates Ca^{2+} block and thus inward rectification of HyNaC.

Since ASICs also have the crucial Asp but are impermeable for Ca^{2+}, with the exception of

ASIC1a that has a low Ca^{2+} permeability (Bässler et al., 2001; Samways et al., 2009), the Asp is necessary but not sufficient for Ca^{2+} permeability of HyNaCs. Reminiscent of this situation, for NMDA receptor channels it has been proposed that Ca^{2+} interacts with "external" and "deep" sites, corresponding to regions at the external mouth and central in the pore of the channel, respectively (Watanabe et al., 2002). The conserved aspartate of HyNaCs and ASICs could represent an external Ca^{2+} interaction site and the putative internal site would also be necessary for Ca^{2+} permeation. In fact, for ASIC1, amino acids at the intracellular N-terminus determine Ca^{2+} permeability (Bässler et al., 2001). Future experiments will show whether the high Ca^{2+} permeability of HyNaCs also depends on their intracellular N-termini or other regions along the axis of their pore.

Collectively, the results suggest the following scenario (Fig. 27): Ca^{2+} gets attracted to the outer mouth of the HyNaC pore by the negative charges of the conserved ring of aspartates. At positives potentials (for example, +30 mV), Ca^{2+} inefficiently permeates the channel and blocks the open pore, presumably by tightly binding to the aspartates. At more negative potentials (for example, -70 mV) Ca^{2+} more efficiently permeates the channel, liberating the pore for the passage also of monovalent cations.

Recently, the crystal structure of ASIC1 in complex with psalmotoxin revealed two different open channel conformations depending on the pH at which the crystals were derived (Baconguis and Gouaux, 2012). At acidic pH (5.5) the ASIC pore is selective for sodium. In this state, the pore has an asymmetric, elliptical structure with its narrowest constriction of ≈5-7 Å at about halfway of the membrane (Fig. 4B). In contrast to this, at neutral pH (7.25) the pore is unselective for monovalent cations and also permeable for the large $NMDG^{+}$ that has a radius of ≈4 Å. If the pore is also conductive for Ca^{2+} was not tested. In the unselective state (neutral pH), the ion pore has a threefold symmetric shape and is lined by the TM1 and TM2 helices of the three subunits (Fig. 4B). It would be interesting to investigate, if the unselective HyNaC pore has a similar structure as the ASIC1 pore at neutral pH.

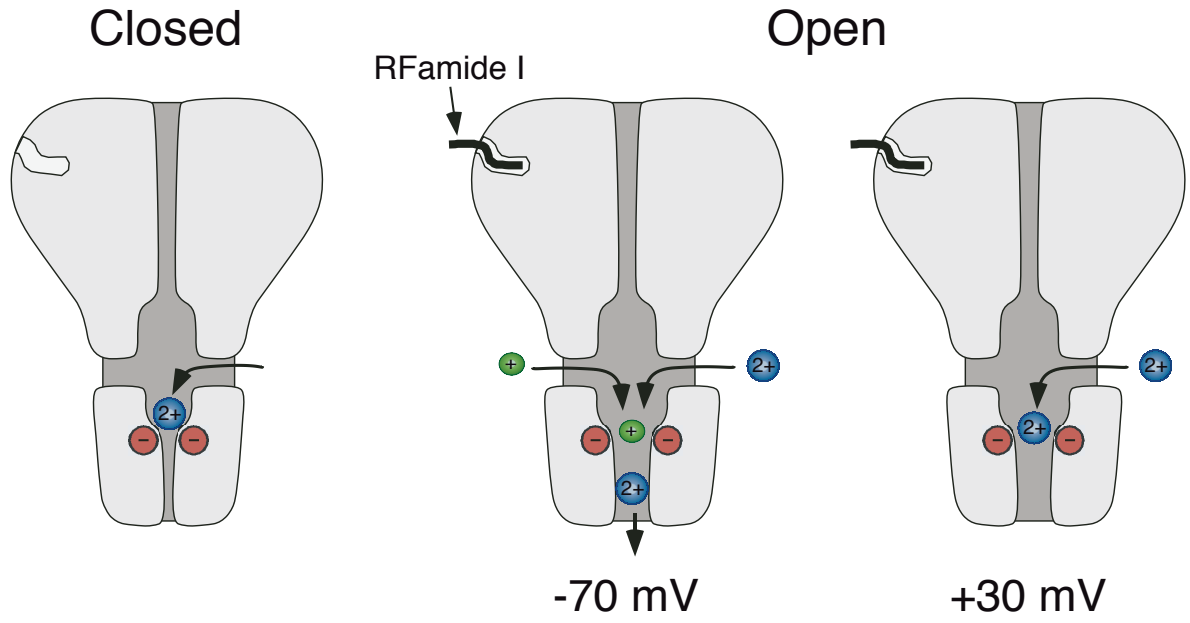

Fig. 27: In the closed conformation (left), Ca^{2+} can probably access the extracellular vestibule through three lateral fenestrations and bind to the conserved aspartates at the outer mouth of the ion pore. After binding of the ligand, HyNaC opens and, at negative membrane potentials, Ca^{2+} permeates the channel (–70 mV, middle), liberating the ion pore. At depolarized potentials (+30 mV, right), however, Ca^{2+} remains bound to the ring of negative charges and blocks the open pore. Based on the crystal structure of chicken ASIC1 (Jasti et al., 2007) (From: Dürrnagel et al.,2012)

4.2.3 HyNaCs are the first DEG/ENaC channels with a high Ca^{2+} permeability

So far, all DEG/ENaC channels have been found to be more or less Na^+ selective; in fact, Na^+ selectivity is a defining hallmark of these channels. In the few exceptions, where DEG/ENaC channels are associated with unselective ion pores, the unselective state co-exists with a Na^+-selective state, as in the case of some ASICs (Lingueglia et al., 1997; Springauf and Gründer, 2010) and rat brain liver intestine Na^+ channel (rBLINaC, now named bile acid-sensitive ion channel, BASIC) (Sakai et al., 1999; Wiemuth and Gründer, 2010; Wiemuth et al., 2012). In these cases, the Na^+ selective state probably carries most of the current under physiological conditions. MEC-4, a subunit of a mechanosensitive DEG/ENaC channel from *C. elegans* (Driscoll and Chalfie, 1991), can be constitutively activated by mutation (MEC-4(d)) and then carries a Ca^{2+} component with a permeability ratio of Ca^{2+} versus Na^+ (P_{Ca}/P_{Na}) of 0.22 (Bianchi et al., 2004), > 10-times lower than for

HyNaCs. Moreover, the physiologically relevant current carried by MEC-4 is a Na^+-current (Goodman et al., 2002; O'Hagan et al., 2005). Thus, HyNaCs are the first DEG/ENaC channels that are unselective cation channels with a high Ca^{2+} permeability.

At present, one can only speculate on the role of Ca^{2+} permeability for the physiological function of HyNaCs. HyNaCs are expressed at the base of the tentacles, perhaps in epitheliomuscular cells (Fig. 11), and the preprohormone gene that encodes their ligands Hydra-RFamides I and II, is expressed in adjacent nerve cells of the hypostome and upper gastric region (Hansen et al., 2000). Therefore, one can speculate that HyNaCs contribute to coordinate the Hydra feeding response. In agreement with this hypothesis, Antho-RFamide (pQGRF-NH2), a related RFamide peptide from anthozoans, another class within the phylum Cnidaria that contains sea anemones, has excitatory actions on sea anemone muscle preparations and increases the frequency of spontaneous tentacle contractions (McFarlane et al., 1991). Thus, the action of Antho-RFamide is compatible with the idea that HydraRFamides are transmitters at neuromuscular junctions and that HyNaCs are their postsynaptic receptors. Of note, another anthozoan neuropeptide, Antho-RWamide I (pQSLRW-NH_2), increases an inward Ca^{2+} current in endodermal myoepithelial cells of sea anemones (Cho and McFarlane, 1996). Whatever the exact physiological function of HyNaCs is, it is likely that Ca^{2+} influx through open HyNaCs supports their function. The block by Ca^{2+} of HyNaC will limit influx of Ca^{2+}, especially at more depolarized membrane potentials.

In summary, the results show that HyNaC has simple kinetics and does not desensitize in the prolonged presence of its ligands and that HyNaC is an unselective cation channel with a high Ca^{2+} permeability, which is an uncommon feature of DEG/ENaC channels. Therefore, it is possible that the highly selective Na^+ pore of DEG/ENaC channels that is a characterizing feature of these channels is in fact a feature that was not shared by the common ancestor and arose later in evolution.

V. References

Adams, C. M., Anderson, M. G., Motto, D. G., Price, M. P., Johnson, W. A., and Welsh, M. J. (1998). Ripped pocket and pickpocket, novel Drosophila DEG/ENaC subunits expressed in early development and in mechanosensory neurons. J. Cell Biol. *140*, 143–152.

Anctil, M. (2009). Chemical transmission in the sea anemone Nematostella vectensis: A genomic perspective. Comparative Biochemistry and Physiology - Part D: Genomics and Proteomics *4*, 268–289.

Anderson, P. A. V., and Trapido-Rosenthal, H. G. (2009). Physiological and chemical analysis of neurotransmitter candidates at a fast excitatory synapse in the jellyfish Cyanea capillata (Cnidaria, Scyphozoa). Invert Neurosci *9*, 167–173.

Askwith, C. C., Cheng, C., Ikuma, M., Benson, C., Price, M. P., and Welsh, M. J. (2000a). Neuropeptide FF and FMRFamide potentiate acid-evoked currents from sensory neurons and proton-gated DEG/ENaC channels. Neuron *26*, 133–141.

Askwith, C. C., Cheng, C., Ikuma, M., Benson, C., Price, M. P., and Welsh, M. J. (2000b). Neuropeptide FF and FMRFamide potentiate acid-evoked currents from sensory neurons and proton-gated DEG/ENaC channels. Neuron *26*, 133–141.

Baconguis, I., and Gouaux, E. (2012). Structural plasticity and dynamic selectivity of acid-sensing ion channel-spider toxin complexes. Nature.

Barish, M. E. (1983). A transient calcium-dependent chloride current in the immature Xenopus oocyte. J Physiol (Lond) *342*, 309–325.

Bässler, E. L., Ngo-Anh, T. J., Geisler, H. S., Ruppersberg, J. P., and Gründer, S. (2001). Molecular and functional characterization of acid-sensing ion channel (ASIC) 1b. J Biol Chem *276*, 33782–33787.

Ben-Shahar, Y. (2011). Sensory functions for degenerin/epithelial sodium channels (DEG/ENaC). Adv. Genet. *76*, 1–26.

Bianchi, L., Gerstbrein, B., Frøkjaer-Jensen, C., Royal, D. C., Mukherjee, G., Royal, M. A., Xue, J., Schafer, W. R., and Driscoll, M. (2004). The neurotoxic MEC-4(d) DEG/ENaC sodium channel conducts calcium: implications for necrosis initiation. Nat Neurosci *7*, 1337–1344.

Bode, H. R. (1992). Continuous conversion of neuron phenotype in hydra. Trends Genet. *8*, 279–284.

Boton, R., Singer, D., and Dascal, N. (1990). Inactivation of calcium-activated chloride conductance in Xenopus oocytes: roles of calcium and protein kinase C. Pflugers Arch *416*, 1–6.

Brown, A. L., Fernandez-Illescas, S. M., Liao, Z., and Goodman, M. B. (2007). Gain-of-Function Mutations in the MEC-4 DEG/ENaC Sensory Mechanotransduction Channel Alter Gating and Drug Blockade. The Journal of General Physiology *129*, 161–173.

Burnashev, N., Zhou, Z., Neher, E., and Sakmann, B. (1995). Fractional calcium currents through recombinant GluR channels of the NMDA, AMPA and kainate receptor subtypes. J Physiol (Lond) *485 (Pt 2)*, 403–418.

Canessa, C. M., Horisberger, J. D., and Rossier, B. C. (1993). Epithelial sodium channel related to proteins involved in neurodegeneration. Nature *361*, 467–470.

Canessa, C. M., Schild, L., Buell, G., Thorens, B., Gautschi, I., Horisberger, J. D., and Rossier, B. C. (1994). Amiloride-sensitive epithelial Na+ channel is made of three homologous subunits. Nature *367*, 463–467.

Chalfie, M., and Au, M. (1989). Genetic control of differentiation of the Caenorhabditis elegans touch receptor neurons. Science *243*, 1027–1033.

Chalfie, M., and Wolinsky, E. (1990). The identification and suppression of inherited neurodegeneration in Caenorhabditis elegans. Nature *345*, 410–416.

Chapman, J. A., Kirkness, E. F., Simakov, O., Hampson, S. E., Mitros, T., Weinmaier, T., Rattei, T., Balasubramanian, P. G., Borman, J., Busam, D., et al. (2010). The dynamic genome of Hydra. Nature *464*, 592–596.

Chen, C. C., England, S., Akopian, A. N., and Wood, J. N. (1998). A sensory neuron-specific, proton-gated ion channel. Proc Natl Acad Sci USA *95*, 10240–10245.

Chen, X., and Gründer, S. (2007). Permeating protons contribute to tachyphylaxis of the acid-sensing ion channel (ASIC) 1a. J Physiol (Lond) *579*, 657–670.

Chen, X., Kalbacher, H., and Gründer, S. (2006a). Interaction of acid-sensing ion channel (ASIC) 1 with the tarantula toxin psalmotoxin 1 is state dependent. The Journal of General Physiology *127*, 267–276.

Chen, X., Paukert, M., Kadurin, I., Pusch, M., and Gründer, S. (2006b). Strong modulation by RFamide neuropeptides of the ASIC1b/3 heteromer in competition with extracellular calcium. Neuropharmacology *50*, 964–974.

Cho, K., and McFarlane, I. D. (1996). The anthozoan neuropeptide Antho-RWamide I modulates Ca2+ current in sea anemone myoepithelial cells. Neurosci. Lett. *209*, 53–56.

Coscoy, S., Lingueglia, E., Lazdunski, M., and Barbry, P. (1998). The Phe-Met-Arg-Phe-amide-activated sodium channel is a tetramer. J Biol Chem *273*, 8317–8322.

Cottrell, G. A. (1997). The first peptide-gated ion channel. J. Exp. Biol. *200*, 2377–2386.

Cottrell, G. A., Green, K. A., and Davies, N. W. (1990). The neuropeptide Phe-Met-Arg-Phe-NH2 (FMRFamide) can activate a ligand-gated ion channel in Helix neurones. Pflugers Arch *416*, 612–614.

Cottrell, G. A., Jeziorski, M. C., and Green, K. A. (2001). Location of a ligand recognition site of FMRFamide-gated Na(+) channels. FEBS Letters *489*, 71–74.

Darmer, D., Hauser, F., Nothacker, H. P., Bosch, T. C., Williamson, M., and Grimmelikhuijzen, C. J. (1998). Three different prohormones yield a variety of Hydra-RFamide (Arg-Phe-NH2) neuropeptides in Hydra magnipapillata. Biochem J *332 (Pt 2)*, 403–412.

Davies, C. W. (1962). Ion association. Butterworth, London, 190.

Deval, E., Baron, A., Lingueglia, E., Mazarguil, H., Zajac, J.-M., and Lazdunski, M. (2003). Effects of neuropeptide SF and related peptides on acid sensing ion channel 3 and sensory neuron excitability. Neuropharmacology *44*, 662–671.

Dijkink, L., Hartog, A., van Os, C. H., and Bindels, R. J. M. (2002). The epithelial sodium channel (ENaC) is intracellularly located as a tetramer. Pflugers Arch *444*, 549–555.

Driscoll, M., and Chalfie, M. (1991). The mec-4 gene is a member of a family of Caenorhabditis elegans genes that can mutate to induce neuronal degeneration. Nature *349*, 588–593.

Dürrnagel, S., Kuhn, A., Tsiairis, C. D., Williamson, M., Kalbacher, H., Grimmelikhuijzen, C. J. P., Holstein, T. W., and Gründer, S. (2010). Three homologous subunits form a high affinity peptide-gated ion channel in Hydra. Journal of Biological Chemistry *285*, 11958–11965.

Egebjerg, J., and Heinemann, S. F. (1993). Ca2+ permeability of unedited and edited versions of the kainate selective glutamate receptor GluR6. Proc Natl Acad Sci USA *90*, 755–759.

Eppig, J. J., and Dumont, J. N. (1974). Oogenesis in Xenopus laevis (Daudin). II. The induction and subcellular localization of tyrosinase activity in developing oocytes. Dev. Biol. *36*, 330–342.

Escoubas, P., de Weille, J. R., Lecoq, A., Diochot, S., Waldmann, R., Champigny, G., Moinier, D., Ménez, A., and Lazdunski, M. (2000). Isolation of a tarantula toxin specific for a class of proton-gated Na+ channels. J Biol Chem *275*, 25116–25121.

Firsov, D., Gautschi, I., Mérillat, A. M., Rossier, B. C., and Schild, L. (1998). The heterotetrameric architecture of the epithelial sodium channel (ENaC). EMBO J *17*, 344–352.

Firsov, D., Schild, L., Gautschi, I., Mérillat, A. M., Schneeberger, E., and Rossier, B. C. (1996). Cell surface expression of the epithelial Na channel and a mutant causing Liddle syndrome: a quantitative approach. Proc Natl Acad Sci USA *93*, 15370–15375.

Frey, E. N., Culver, S. B., Ratti, M. A., and Askwith, C. C. (2012). A role for the extracellular domain of human ASIC1a in Big Dynorphin modulation. Characterisation of gating properties of a peptide-activated DEG/ENaC ion channel from Hydra magnipapillata, 1–4.

Fujisawa, T. (2008). Hydra peptide project 1993-2007. Dev. Growth Differ. *50 Suppl 1*, S257–68.

Fujisawa, T., and Hayakawa, E. (2012). Peptide signaling in Hydra. Int. J. Dev. Biol. *52*.

Furukawa, Y., Miyawaki, Y., and Abe, G. (2006). Molecular cloning and functional characterization of the Aplysia FMRFamide-gated Na+ channel. Pflugers Arch *451*, 646–656.

Galzi, J. L., Devillers-Thiéry, A., Hussy, N., Bertrand, S., Changeux, J. P., and Bertrand, D. (1992). Mutations in the channel domain of a neuronal nicotinic receptor convert ion selectivity from cationic to anionic. Nature *359*, 500–505.

Golubovic, A., Kuhn, A., Williamson, M., Kalbacher, H., Holstein, T. W., Grimmelikhuijzen, C. J. P., and Gründer, S. (2007). A peptide-gated ion channel from the freshwater polyp Hydra. J Biol Chem *282*, 35098–35103.

Gonzales, E. B., Kawate, T., and Gouaux, E. (2009). Pore architecture and ion sites in acid-sensing ion channels and P2X receptors. Nature *460*, 599–604.

Goodman, M. B., Ernstrom, G. G., Chelur, D. S., O'Hagan, R., Yao, C. A., and Chalfie, M. (2002). MEC-2 regulates C. elegans DEG/ENaC channels needed for mechanosensation. Nature *415*, 1039–1042.

Green, K. A., and Cottrell, G. A. (2002). Activity modes and modulation of the peptide-gated Na(+) channel of Helix neurones. Pflugers Arch *443*, 813–821.

Green, K. A., and Cottrell, G. A. (1999). Block of the helix FMRFamide-gated Na+ channel by FMRFamide and its analogues. J Physiol (Lond) *519 Pt 1*, 47–56.

Green, K. A., Falconer, S. W., and Cottrell, G. A. (1994). The neuropeptide Phe-Met-Arg-Phe-NH2 (FMRFamide) directly gates two ion channels in an identified Helix neurone. Pflugers Arch *428*, 232–240.

Grimmelikhuijzen, C. J. (1983). FMRFamide immunoreactivity is generally occurring in the nervous systems of coelenterates. Histochemistry *78*, 361–381.

Grimmelikhuijzen, C. J., and Westfall, J. A. (1995). The nervous systems of cnidarians. EXS *72*, 7–24.

Grimmelikhuijzen, C. J., Balfe, A., Emson, P. C., Powell, D., and Sundler, F. (1981a). Substance P-like immunoreactivity in the nervous system of hydra. Histochemistry *71*, 325–333.

Grimmelikhuijzen, C. J., Carraway, R. E., Rökaeus, A., and Sundler, F. (1981b). Neurotensin-like immunoreactivity in the nervous system of hydra. Histochemistry *72*, 199–209.

Grimmelikhuijzen, C. J., Dierickx, K., and Boer, G. J. (1982). Oxytocin/vasopressin-like immunoreactivity is present in the nervous system of hydra. Neuroscience *7*, 3191–3199.

Grimmelikhuijzen, C. J., Dockray, G. J., and Yanaihara, N. (1981c). Bombesin-like immunoreactivity in the nervous system of hydra. Histochemistry *73*, 171–180.

Grimmelikhuijzen, C. J., Leviev, I., and Carstensen, K. (1996). Peptides in the nervous systems of cnidarians: structure, function, and biosynthesis. Int. Rev. Cytol. *167*, 37–89.

Grunder, S., Geissler, H. S., Bässler, E. L., and Ruppersberg, J. P. (2000). A new member of acid-sensing ion channels from pituitary gland. Neuroreport *11*, 1607–1611.

Gründer, S., and Augustinowski, K. (2012). Toxin binding reveals two open state structures for one acid-sensing ion channel. channels *6*.

Gründer, S., and Chen, X. (2010). Structure, function, and pharmacology of acid-sensing ion channels (ASICs): focus on ASIC1a. Int J Physiol Pathophysiol Pharmacol *2*, 73–94.

Hansen, G. N., Williamson, M., and Grimmelikhuijzen, C. J. (2000). Two-color double-labeling in situ hybridization of whole-mount Hydra using RNA probes for five different Hydra neuropeptide preprohormones: evidence for colocalization. Cell Tissue Res *301*, 245–253.

Hansen, G. N., Williamson, M., and Grimmelikhuijzen, C. J. P. (2002). A new case of neuropeptide coexpression (RGamide and LWamides) in Hydra, found by whole-mount, two-color double-labeling in situ hybridization. Cell Tissue Res *308*, 157–165.

Hayakawa, E., Takahashi, T., Nishimiya-Fujisawa, C., and Fujisawa, T. (2007). A novel neuropeptide (FRamide) family identified by a peptidomic approach in Hydra magnipapillata. FEBS J. *274*, 5438–5448.

Heimfeld, S., and Bode, H. R. (1986). Growth regulation of the interstitial cell population in hydra. III. Interstitial cell density does not control stem cell proliferation. Dev. Biol. *116*, 51–58.

Hill, A. V. (1910). The possible effects of the aggregation of the moleculesof haemoglobin on its dissociation curves. J Physiol (Lond) *40*, 4–7.

Hille, B. (2001). Ion Channels Of Excitable Membranes, 3rd. Ed. Sinauer Associates, Inc., Sunderland, MA, 471–502.

Holstein, T. W. (2012). A view to kill. BMC Biol. *10*, 18.

Jasti, J., Furukawa, H., Gonzales, E. B., and Gouaux, E. (2007). Structure of acid-sensing ion channel 1 at 1.9 A resolution and low pH. Nature *449*, 316–323.

Jeziorski, M. C., Green, K. A., Sommerville, J., and Cottrell, G. A. (2000). Cloning and expression of a FMRFamide-gated Na(+) channel from Helisoma trivolvis and comparison with the native neuronal channel. J Physiol (Lond) *526 Pt 1*, 13–25.

Kass-Simon, G., and Pierobon, P. (2007). Cnidarian chemical neurotransmission, an updated overview. Comparative Biochemistry and Physiology - Part A: Molecular & Integrative Physiology *146*, 9–25.

Kass-Simon, G., Pannaccione, A., and Pierobon, P. (2003). GABA and glutamate receptors are involved in modulating pacemaker activity in hydra. Comparative Biochemistry and Physiology - Part A: Molecular & Integrative Physiology *136*, 329–342.

Katsukura, Y., Ando, H., David, C. N., Grimmelikhuijzen, C. J. P., and Sugiyama, T. (2004). Control of planula migration by LWamide and RFamide neuropeptides in Hydractinia echinata. J. Exp. Biol. *207*, 1803–1810.

Katsura, I., Kondo, K., Amano, T., Ishihara, T., and Kawakami, M. (1994). Isolation, characterization and epistasis of fluoride-resistant mutants of Caenorhabditis elegans. Genetics *136*, 145–154.

Katz, E., Verbitsky, M., Rothlin, C. V., Vetter, D. E., Heinemann, S. F., and Elgoyhen, A. B. (2000). High calcium permeability and calcium block of the alpha9 nicotinic acetylcholine receptor. Hear Res *141*, 117–128.

Kellenberger, S., and Schild, L. (2002). Epithelial sodium channel/degenerin family of ion channels: a variety of functions for a shared structure. Physiol. Rev. *82*, 735–767.

Kellenberger, S., Hoffmann-Pochon, N., Gautschi, I., Schneeberger, E., and Schild, L. (1999). On the molecular basis of ion permeation in the epithelial Na+ channel. The Journal of General Physiology *114*, 13–30.

Koizumi, O. (2007). Nerve ring of the hypostome in hydra: is it an origin of the central nervous system of bilaterian animals? Brain Behav. Evol. *69*, 151–159.

Koizumi, O., Wilson, J. D., Grimmelikhuijzen, C. J., and Westfall, J. A. (1989). Ultrastructural localization of RFamide-like peptides in neuronal dense-cored vesicles in the peduncle of Hydra. J. Exp. Zool. *249*, 17–22.

Krishtal, O. (2003). The ASICs: signaling molecules? Modulators? Trends Neurosci *26*, 477–483.

Leonard, J. P., and Kelso, S. R. (1990). Apparent desensitization of NMDA responses in Xenopus oocytes involves calcium-dependent chloride current. Neuron *4*, 53–60.

Leviev, I., Williamson, M., and Grimmelikhuijzen, C. J. (1997). Molecular cloning of a preprohormone from Hydra magnipapillata containing multiple copies of Hydra-L Wamide (Leu-Trp-NH2) neuropeptides: evidence for processing at Ser and Asn residues. J. Neurochem. *68*, 1319–1325.

Li, T., Yang, Y., and Canessa, C. M. (2009). Interaction of the aromatics Tyr-72/Trp-288 in the interface of the extracellular and transmembrane domains is essential for proton gating of acid-sensing ion channels. J Biol Chem *284*, 4689–4694.

Li, T., Yang, Y., and Canessa, C. M. (2011). Outlines of the pore in open and closed conformations describe the gating mechanism of ASIC1. Nature Communications *2*, 399.

Lin, H., Mann, K. J., Starostina, E., Kinser, R. D., and Pikielny, C. W. (2005). A Drosophila DEG/ENaC channel subunit is required for male response to female pheromones. Proc Natl Acad Sci USA *102*, 12831–12836.

Lingueglia, E., Champigny, G., Lazdunski, M., and Barbry, P. (1995). Cloning of the amiloride-sensitive FMRFamide peptide-gated sodium channel. Nature *378*, 730–733.

Lingueglia, E., de Weille, J. R., Bassilana, F., Heurteaux, C., Sakai, H., Waldmann, R., and Lazdunski, M. (1997). A modulatory subunit of acid sensing ion channels in brain and dorsal root ganglion cells. J Biol Chem *272*, 29778–29783.

Lingueglia, E., Deval, E., and Lazdunski, M. (2006). FMRFamide-gated sodium channel and ASIC channels: A new class of ionotropic receptors for FMRFamide and related peptides. Peptides *27*, 1138–1152.

Liu, L., Leonard, A. S., Motto, D. G., Feller, M. A., Price, M. P., Johnson, W. A., and Welsh, M. J. (2003). Contribution of Drosophila DEG/ENaC genes to salt taste. Neuron *39*, 133–146.

Loomis, W. F. (1955). Loomis. Ann. N. Y. Acad. Sci. *62*, 211–227.

Mahoney, J. L., Graugnard, E. M., Mire, P., and Watson, G. M. (2011). Evidence for involvement of TRPA1 in the detection of vibrations by hair bundle mechanoreceptors in sea anemones. J Comp Physiol A *197*, 729–742.

Mano, I., and Driscoll, M. (1999). DEG/ENaC channels: a touchy superfamily that watches its salt. Bioessays *21*, 568–578.

Martinez, D. E., Dirksen, M. L., Bode, P. M., Jamrich, M., Steele, R. E., and Bode, H. R. (1997). Budhead, a fork head/HNF-3 homologue, is expressed during axis formation and head specification in hydra. Dev. Biol. *192*, 523–536.

McFarlane, I. D., Anderson, P. A., and Grimmelikhuijzen, C. J. (1991). Effects of three anthozoan neuropeptides, Antho-RWamide I, Antho-RWamide II and Antho-RFamide, on slow muscles from sea anemones. J. Exp. Biol. *156*, 419–431.

McFarlane, I. D., Hudman, D., Nothacker, H. P., and Grimmelikhuijzen, C. J. (1993). The expansion behaviour of sea anemones may be coordinated by two inhibitory neuropeptides, Antho-KAamide and Antho-RIamide. Proc Biol Sci *253*, 183–188.

Miledi, R. (1982). A calcium-dependent transient outward current in Xenopus laevis oocytes. Proc. R. Soc. Lond., B, Biol. Sci. *215*, 491–497.

Mitgutsch, C., Hauser, F., and Grimmelikhuijzen, C. J. (1999). Expression and developmental regulation of the Hydra-RFamide and Hydra-LWamide preprohormone genes in Hydra: evidence for transient phases of head formation. Dev. Biol. *207*, 189–203.

Moosler, A., Rinehart, K. L., and Grimmelikhuijzen, C. J. (1996). Isolation of four novel neuropeptides, the hydra-RFamides I-IV, from Hydra magnipapillata. Biochem Biophys Res Commun *229*, 596–602.

O'Hagan, R., Chalfie, M., and Goodman, M. B. (2005). The MEC-4 DEG/ENaC channel of Caenorhabditis elegans touch receptor neurons transduces mechanical signals. Nat Neurosci *8*, 43–50.

Panula, P., Aarnisalo, A. A., and Wasowicz, K. (1996). Neuropeptide FF, a mammalian neuropeptide with multiple functions. Prog Neurobiol *48*, 461–487.

Panula, P., Kalso, E., Nieminen, M., Kontinen, V. K., Brandt, A., and Pertovaara, A. (1999). Neuropeptide FF and modulation of pain. Brain Res. *848*, 191–196.

Paukert, M., Babini, E., Pusch, M., and Gründer, S. (2004). Identification of the Ca2+ blocking site of acid-sensing ion channel (ASIC) 1: implications for channel gating. The Journal of General Physiology *124*, 383–394.

Paukert, M., Chen, X., Polleichtner, G., Schindelin, H., and Gründer, S. (2008). Candidate amino acids involved in H+ gating of acid-sensing ion channel 1a. J Biol Chem *283*, 572–581.

Perry, S. J., Straub, V. A., Schofield, M. G., Burke, J. F., and Benjamin, P. R. (2001). Neuronal expression of an FMRFamide-gated Na+ channel and its modulation by acid pH. Journal of Neuroscience *21*, 5559–5567.

Perry, S. J., Yi-Kung Huang, E., Cronk, D., Bagust, J., Sharma, R., Walker, R. J., Wilson, S., and Burke, J. F. (1997). A human gene encoding morphine modulating peptides related to NPFF and FMRFamide. FEBS Letters *409*, 426–430.

Pierobon, P. (2012). Coordinated modulation of cellular signaling through ligand-gated ion channels in Hydra vulgaris (Cnidaria, Hydrozoa). Int. J. Dev. Biol. *56*, 551–565.

Pierobon, P., Concas, A., Santoro, G., Marino, G., Minei, R., Pannaccione, A., Mostallino, M. C., and Biggio, G. (1995). Biochemical and functional identification of GABA receptors in Hydra vulgaris. Life Sci. *56*, 1485–1497.

Price, M. P., Snyder, P. M., and Welsh, M. J. (1996). Cloning and expression of a novel human brain Na+ channel. J Biol Chem *271*, 7879–7882.

Putnam, N. H., Srivastava, M., Hellsten, U., Dirks, B., Chapman, J., Salamov, A., Terry, A., Shapiro, H., Lindquist, E., Kapitonov, V. V., et al. (2007). Sea anemone genome reveals ancestral eumetazoan gene repertoire and genomic organization. Science *317*, 86–94.

Roumy, M., and Zajac, J.-M. (1998). Neuropeptide FF, pain and analgesia. Eur. J. Pharmacol. *345*, 1–11.

Sakai, H., Lingueglia, E., Champigny, G., Mattei, M. G., and Lazdunski, M. (1999). Cloning and functional expression of a novel degenerin-like Na+ channel gene in mammals. J Physiol (Lond) *519 Pt 2*, 323–333.

Samways, D. S. K., Harkins, A. B., and Egan, T. M. (2009). Native and recombinant ASIC1a receptors conduct negligible Ca2+ entry. Cell Calcium *45*, 319–325.

Samways, D. S. K., Khakh, B. S., and Egan, T. M. (2012). Allosteric Modulation of Ca2+ flux in Ligand-gated Cation Channel (P2X4) by Actions on Lateral Portals. Journal of Biological Chemistry *287*, 7594–7602.

Scappaticci, A. A., and Kass-Simon, G. (2008). NMDA and GABA B receptors are involved in controlling nematocyst discharge in hydra. Comparative Biochemistry and Physiology - Part A: Molecular & Integrative Physiology *150*, 415–422.

Scappaticci, A. A., Jacques, R., Carroll, J. E., Hufnagel, L. A., and Kass-Simon, G. (2004). Immunocytochemical evidence for an NMDA1 receptor subunit in dissociated cells of Hydra vulgaris. Cell Tissue Res *316*, 263–270.

Schaefer, L., Sakai, H., Mattei, M., Lazdunski, M., and Lingueglia, E. (2000). Molecular cloning, functional expression and chromosomal localization of an amiloride-sensitive Na(+) channel from human small intestine. FEBS Letters *471*, 205–210.

Schroeder, B. C., Cheng, T., Jan, Y. N., and Jan, L. Y. (2008). Expression cloning of TMEM16A as a calcium-activated chloride channel subunit. Cell *134*, 1019–1029.

Séguéla, P., Wadiche, J., Dineley-Miller, K., Dani, J. A., and Patrick, J. W. (1993). Molecular cloning, functional properties, and distribution of rat brain alpha 7: a nicotinic cation channel highly permeable to calcium. J. Neurosci. *13*, 596–604.

Sherwood, T. W., and Askwith, C. C. (2009). Dynorphin opioid peptides enhance acid-sensing ion channel 1a activity and acidosis-induced neuronal death. Journal of Neuroscience *29*, 14371–14380.

Snyder, P. M., Cheng, C., Prince, L. S., Rogers, J. C., and Welsh, M. J. (1998). Electrophysiological and biochemical evidence that DEG/ENaC cation channels are composed of nine subunits. J Biol Chem *273*, 681–684.

Soto, F., Garcia-Guzman, M., Gomez-Hernandez, J. M., Hollmann, M., Karschin, C., and Stühmer, W. (1996). P2X4: an ATP-activated ionotropic receptor cloned from rat brain. Proc Natl Acad Sci USA *93*, 3684–3688.

Springauf, A., and Gründer, S. (2010). An acid-sensing ion channel from shark (Squalus acanthias) mediates transient and sustained responses to protons. J Physiol (Lond) *588*, 809–820.

Takahashi, T., Hatta, M., Yum, S., Gee, L., Ohtani, M., Fujisawa, T., and Bode, H. R. (2005). Hym-301, a novel peptide, regulates the number of tentacles formed in hydra. Development *132*, 2225–2234.

Takahashi, T., Koizumi, O., Ariura, Y., Romanovitch, A., Bosch, T. C., Kobayakawa, Y., Mohri, S., Bode, H. R., Yum, S., Hatta, M., et al. (2000). A novel neuropeptide, Hym-355, positively regulates neuron differentiation in Hydra. Development *127*, 997–1005.

Take-Uchi, M., Kawakami, M., Ishihara, T., Amano, T., Kondo, K., and Katsura, I. (1998). An ion channel of the degenerin/epithelial sodium channel superfamily controls the defecation rhythm in Caenorhabditis elegans. Proc Natl Acad Sci USA *95*, 11775–11780.

Vernino, S., Amador, M., Luetje, C. W., Patrick, J., and Dani, J. A. (1992). Calcium modulation and high calcium permeability of neuronal nicotinic acetylcholine receptors. Neuron *8*, 127–134.

Vilim, F. S., Aarnisalo, A. A., Nieminen, M. L., Lintunen, M., Karlstedt, K., Kontinen, V. K., Kalso, E., States, B., Panula, P., and Ziff, E. (1999). Gene for pain modulatory neuropeptide NPFF: induction in spinal cord by noxious stimuli. Molecular Pharmacology *55*, 804–811.

Waldmann, R., and Lazdunski, M. (1998). H(+)-gated cation channels: neuronal acid sensors in the NaC/DEG family of ion channels. Curr. Opin. Neurobiol. *8*, 418–424.

Waldmann, R., Bassilana, F., de Weille, J., Champigny, G., Heurteaux, C., and Lazdunski, M. (1997a). Molecular cloning of a non-inactivating proton-gated Na+ channel specific for sensory neurons. J Biol Chem *272*, 20975–20978.

Waldmann, R., Champigny, G., Bassilana, F., Heurteaux, C., and Lazdunski, M. (1997b). A proton-gated cation channel involved in acid-sensing. Nature *386*, 173–177.

Watanabe, J., Beck, C., Kuner, T., Premkumar, L. S., and Wollmuth, L. P. (2002). DRPEER: a motif in the extracellular vestibule conferring high Ca2+ flux rates in NMDA receptor channels. Journal of Neuroscience *22*, 10209–10216.

Wemmie, J. A., Chen, J., Askwith, C. C., Hruska-Hageman, A. M., Price, M. P., Nolan, B. C., Yoder, P. G., Lamani, E., Hoshi, T., Freeman, J. H., et al. (2002). The acid-activated ion channel ASIC contributes to synaptic plasticity, learning, and memory. Neuron *34*, 463–477.

White, M. M., and Aylwin, M. (1990). Niflumic and flufenamic acids are potent reversible blockers of Ca2(+)-activated Cl- channels in Xenopus oocytes. Molecular Pharmacology *37*, 720–724.

Wiemuth, D., and Gründer, S. (2010). A single amino acid tunes Ca2+ inhibition of brain liver intestine Na+ channel (BLINaC). Journal of Biological Chemistry *285*, 30404–30410.

Wiemuth, D., Sahin, H., Falkenburger, B. H., Lefèvre, C. M. T., Wasmuth, H. E., and Gründer, S. (2012). BASIC--a bile acid-sensitive ion channel highly expressed in bile ducts. FASEB J.

Wu, G., and Hamill, O. P. (1992). NPPB block of Ca(++)-activated Cl- currents in Xenopus oocytes. Pflugers Arch *420*, 227–229.

Xiong, Z.-G., Zhu, X.-M., Chu, X.-P., Minami, M., Hey, J., Wei, W.-L., Macdonald, J. F., Wemmie, J. A., Price, M. P., Welsh, M. J., et al. (2004). Neuroprotection in ischemia: blocking calcium-permeable acid-sensing ion channels. Cell *118*, 687–698.

Zhong, L., Hwang, R. Y., and Tracey, W. D. (2010). Pickpocket is a DEG/ENaC protein required for mechanical nociception in Drosophila larvae. Curr. Biol. *20*, 429–434.

VI. Appendix

6.1 List of experimental procedures performed by other researchers

The experimental protocols listed below were performed by other researches. Prof. Stefan Gründer performed cloning of HyNaC5. The in *situ* hybridization and the analysis of the feeding behaviour of *Hydra* were done in collaboration with the lab of Prof. Thomas Holstein, at the Institute of Zoology, Heidelberg. Anne Kuhn did the *in situ* hybridisation staining; the analysis of feeding behaviour was performed by Dr. Charisos Tsiairis.

6.1.3 Cloning of HyNaC5

Several partial sequences for a protein showing sequence homology to HyNaCs were identified from the on-line *Hydra* expressed sequence tag data base and used to design primers for rapid amplification of 3´-cDNA ends (RACE). Using the Smart RACE cDNA amplification kit (Clontech), two rounds of 3-RACE were performed with cDNA prepared from poly(A)$^+$ RNA, isolated from adult one-day starved budding stage *Hydra magnipapillata* (strain 105). Full-length HyNaC5 was assembled from expressed sequence tags and 3-RACE products. For expression studies in *Xenopus* oocytes, the entire coding sequence of HyNaC5 was amplified by PCR from cDNA of whole *Hydras* and subcloned. The clone was entirely sequenced to exclude PCR errors. The consensus sequence of HyNaC5 was assembled from the expressed sequence tags and several independent PCR products. This sequence data has been submitted to the DDBJ/EMBL/GenBank^{TM} databases under accession number FN257513.

6.1.2 *In Situ* Hybridization of *Hydra*

A1435-bp fragment from the coding part of HyNaC5 cDNA was subcloned in the vector pBluescript KS. Whole mount ISH was carried out as described previously (Martinez et al., 1997) by using BMP Purple as substrate for the antibody-conjugated alkaline phosphatase, except that blocking of the animals was performed in monoclonal antibody/1x blocking

reagent (Roche Applied Science) and that the alkaline phosphatase-conjugated anti-digoxygenin Fab fragments (Roche Applied Science) were diluted 1:4000. Two different antisense probes of 810 and 1435 bp, respectively, were used at concentrations of 0.08–0.16 ng/µl for 60 h. Both probes applied alone or together resulted in the same localization pattern, a combination of both probes yielding a stronger signal than the single probes. Performing ISH with the corresponding sense riboprobes did not display any staining.

6.1.3 Analysis of the Feeding Reaction of *Hydra*

Five animals of the species *H. magnipapillata* (wild-type strain 105) were placed in 10 ml of *Hydra* medium (1.0 mM Tris-HCl, 1.0 mM $NaHCO_3$, 0.1 mM KCl, 0.1 mM $MgCl_2$, and 1.0 mM $CaCl_2$) or *Hydra* medium supplemented with 100 µM amiloride. Once they were relaxed in the new medium, glutathione was added to a final concentration of 10 µM at time 0. Every 30 s, we recorded the number of animals moving their tentacles as a response to the application of glutathione. The experiments were repeated four times. Additional experiments were performed with *Hydra oligactis* without finding any differences (data not shown).

List of abbrevations

°C	degree celsius
5-HT	serotonine
A	ampere
Å	angström
ACH	acetylcholine
AMPA	2-amino-3-(3-hydroxy-5-methyl-isoxazol-4-yl)propanoic acid
approx.	approximal
Arg	arginin
Asp	aspartate
ATP	adenosine triphosphate
Ba^{2+}	barium
BAPTA	1,2-bis(o-aminophenoxy)etahne- N,N,N',N'-tetraacetic acid
BASIC	bile acid sensing ion channel
BLINaC	brain-liver-intestine sodium channel
bp	baise pair
BSA	bovine serum albumin
C-	carboxy
Ca^{2+}	calcium ion
CACC	calcium-activated chloride channel
cDNA	complement DNA
cfu	colony forming unit
Cl^-	chloride
CNS	central nervous system
Cs	caesium
Da	dalton
DEG	degenerin
DEPC	diethylpyrocarbonate
DNA	deoxyribonucleic acid
E	epinephrine
e.g.	lat.: exempli gratia
EC_{50}	ligand concentration evoking 50% of the maximal activation
ECD	extracellular domain

EDTA	ethylenediaminetetraacetic acid
EGTA	ethylene glycol tetraacetic acid
ENaC	epithelial sodium channel
EPSP	excitatory postsynaptic potential
E_{rev}	reversal potential
EtOH	ethanol
FaNaC	FMRFamide-gated sodium channel
fig.	figure
FLR	fluoride resistant mutant
FMRFamide	phenylalanine-methionine-arginine-phenylalanine-amide
g	gram
g	standard gravity
GABA	gamma-aminobutyric acid
GluR	glutamate receptor
GPCR	G-protein coupled receptor
GSH	gluthatione
h	hour
H^+	proton
HA	hemaglutinine
HaFaNaC	FaNaC from *Helix aspersa*
HEPES	4-(2-hydroxyethyl)-1-piperazineethanesulfonic acid
HG-motif	histidine-glycine-motif
His	histidine
HtFaNaC	FaNaC from *Heliosoma trivolis*
HyNaC	*Hydra* sodium channel
Hz	herz
I	electric current
i.e.	lat. : id est
IC_{50}	inhibitor concentration evoking 50% of the maximal inhibition
IgG	immunoglobuline G
I_{max}	maximal electric current
INaC	human intestine sodium channel
ISH	*in situ* hybridisation
k	kilo

K^+	potassium ion
kB	kilobase
l	litre
lat.	Latin
Li^+	lithium ion
M	molar
MCS	multiple cloning site
MEC	mechanosensitive mutants
Met	methionine
mg	milligram
Mg^{2+}	magnesium ion
ml	milliliter
mmol	millimol
mRNA	messenger ribonucleic acid
mV	millivolt
MΩ	megaohm
n	count of samples
N-	amino
NA	numerical apperture
Na^+	sodium ion
NaAc	sodium actetate
Na_e	extracellular sodium
NaGluc	sodium gluconate
NE	norepinephrine
ng	nanogram
NH_2	amide
nl	nanolitre
nm	nanometer
NMDA	*N*-Methyl-D-aspartic acid
NMDG	N-methyl-D-glucamine
nmol	nanomol
NO	nitric oxide
NPFF	neuropetide FF
NPPB	5-nitro-2-(3-phenylpropylamino)-benzoate

NPSF	neuropeptide SF
OR-2	oocyte-ringer solution 2
p	probability
p	pyro
PCR	polymerase chain reaction
Phe	phenylalanine
pmol	picomole
PPK	pickpocket
Pro	proline
PVP	polyvinylpyrrolidone
RACE	rapid amplification of 5´and 3´-cDNA ends
RLU	relative light units
RPK	ripped pocket
rpm	rotations per minute
s	second
S.D.	standard deviation
S.E.	standard error
S.E.M.	standard error of the mean
Tab.	table
TEA	tris acetate EDTA buffer
TEVC	two electrode voltage clamp
T_m	melting temperature
TM	transmembrane domain
TRP	transient receptor potential channel
Trp	tryptophan
Tyr	thyrosine
U	enzyme unit
UV	ultraviolett light
v/v	volume/volume
V_{hold}	holding potential
V_m	membrane potential
w/w	weight/weight
wt	wildtype
μ:	micro

Danksagung

Ich danke Prof. Dr. Stefan Gründer für die ausgezeichnete Betreuung und stetige Unterstützung in den letzten Jahren. Seine herrausragende fachliche Kompetenz, seine Großzügigkeit und motivierende Art haben maßgeblich zum Erfolg dieser Arbeit beigetragen. Danke für die spannende, abwechslungsreiche und lehrreiche Zeit an Deinem Institut!

Prof. Dr. Peter Bräunig danke ich für die freundliche Übernahme der Zweitbetreuung und die unkomplizierte Zusammenarbeit.

Mein besonderer Dank gilt dem alten Würzburger Team, Dominik, Andi und Georg, die mir den Start in Aachen leicht gemacht haben. Jumper, vielen Dank für die lustige Zeit am Drehteller und Deine große Hilfsbereitschaft. Ganz besonders möchte ich mich bei Dominik für den Spaß, die große Unterstützung bei schwierigen Fragen sowie der Hilfe bei der Korrektur dieser Arbeit bedanken. Allen Doktorranden, Katrin, Heike, Marc und Cathérine, vielen Dank für die schöne Zeit. Danke Pia, für die Korrektur dieser Arbeit, die Geduld mit dem Schlüssel und die schöne Zeit!

An alle TAs und Mitarbeiter: Hilde, Barbara, Rosi, Adrienne, Monika, Birgit, Marion, Malu und Hans-Jürgen. Vielen Dank für Eure Unterstützung beim Klonieren, RNA synthetisieren, Bestellen und Verwalten. Hannelore, vielen Dank für Deinen stetigen Einsatz bei den patch-clamp Messungen und den zahlreichen anderen Baustellen.

Danke liebe Eltern, für Eure Unterstützung und Euer Vertrauen, und natürlich Markus, dass Du immer auf den kleinen Bruder aufpasst.

Besonders bedanken möchte ich mich außerdem bei meinen Freunden, Simon, Linus Steffen und Georg, dass Ihr meine Freunde seid.

Und Danke Hanna für Deine Liebe, Unterstützung und Geduld in den letzten Jahren!

Curriculum vitae

PERSONAL DETAILS:

Name:	Stefan Dürrnagel
Date of birth:	09.06.1980 in Würzburg
Address:	Metzgerstrasse 49; 52070 Aachen
Phone:	+491736661254
Mail:	stefanduerrnagel@gmx.de

EDUCATION:

2000:	Abitur at Riemenschneider-Gymnasium Würzburg
2001-2002:	Study of electrical engeneering, Friedrich-Alexander-Universität, Erlangen
2002-2004:	Study of biology, Johannes Guttenberg Universität, Mainz
2004-2008	Study of biology, Julius-Maximilians-Universität, Würzburg.
	Degree: Diplom Biologe
Since 2008:	Doctoral thesis in the group of Prof. Stefan Gründer at the Institute of Physiology, RWTH Aachen University

PUBLICATIONS:

Dürrnagel, S., Falkenburger, B. H., and Gründer, S. (2012).
High Ca^{2+} permeability of a peptide-gated DEG/ENaC from *Hydra*. *The Journal of General Physiology 140*, 391–402.

Chen, X., Qiu, L., Li, M., **Dürrnagel, S.,** Orser, B. A., Xiong, Z.-G., and Macdonald, J. F. (2010).
Diarylamidines: high potency inhibitors of acid-sensing ion channels. *Neuropharmacology 58*, 1045–1053.

Dürrnagel, S., Kuhn, A., Tsiairis, C. D., Williamson, M., Kalbacher, H., Grimmelikhuijzen, C. J. P., Holstein, T. W., and Gründer, S. (2010).
Three homologous subunits form a high affinity peptide-gated ion channel in *Hydra*. *Journal of Biological Chemistry 285*, 11958–11965.

Yarali, A., Niewalda, T., Chen,Y-C., Tanimoto, H., **Dürrnagel, S.**, and Gerber, B. (2008). Pain-relief learning in fruit flies. *Animal Behaviour* 76, 1173-85.

Dürrnagel, S., Pusch, M., Golubovic, A., and Gründer, S.
Inhibition of peptide-gated HyNaCs by Ca^{2+}: evidence for an allosteric mechanism. *Manuscript in preparation.*

POSTER:

Dürrnagel S., Falkenburger B., Gründer S.
"Peptide-Gated DEG/ENaC Channels from *Hydra magnipapillata* are Highly Permeable for Calcium". Presented at: 8th Fens Forum of Neuroscience; 2012 Jul 14-18, Barcelona, Spain.

Assmann M.C., **Dürrnagel S.**, Kuhn A., Schultz M.B., Holstein T.W., Gründer S.
„Three New Subunits Expand Our Understanding of the Functions and Biophysical Properties of the Peptide-Gated *Hydra* Sodium Channel (HyNaC)". Presented at: 8th Fens Forum of Neuroscience; 2012 Jul 14-18, Barcelona, Spain.

Dürrnagel S., Falkenburger B., Gründer S.,
„Peptide-Gated DEG/ENaC Channels from *Hydra magnipapillata* are Highly Permeable for Calcium". Presented at: 56th Annual Meeting of the Biophysical Society; 2012 Feb 25-29; San Diego, CA, USA.

Dürrnagel S., Golubovic A., Gründer S.
„Characterisation of Gating Properties of a Peptide-Activated DEG/ENaC Ion Channel from *Hydra magnipapillata*". Presented at: 7th Fens Forum of Neuroscience; 2010 Jul 3-7, Amsterdam, Netherlands.

Dürrnagel S., Golubovic A., Gründer S.
"Peptide-gating of HyNaCs Shares Features with Proton-Gating of ASICs". Presented at: 54th Annual Meeting of the Biophysical Society, 2010 Feb 20-24; San Francisco, CA, USA.

Dürrnagel S., Kuhn A., Williamson M., Grimmelikhuijzen C.J.P., Holstein T.W., Gründer S.
„The Peptide-Gated Ion Channel from *Hydra magnipapillata* is Made of Three Homologous Subunits". Presented at: 8th Meeting of the German Neuroscience Society; 2009 Mar 25-29; Göttingen, Germany.

AWARD:

Travel grant from the „German Neuroscience Society" for participation at the 8th Fens Neuroscience Meeting 2012 in Barcelona, Spain.